DOCTOR OF PHILOSOPHY

Particle separation via the hybrid application of optical and acoustic forces

O'Mahoney, Paul

Award date:
2015

Awarding institution:
University of Dundee

Particle separation via the hybrid application of optical and acoustic forces

Paul O'Mahoney

A thesis submitted for the degree of

Doctor of Philosophy (PhD)

University of Dundee

August 2015

CONTENTS

LIST OF FIGURES

LIST OF TABLES

LIST OF ABBREVIATIONS

RBC	Red blood cell
VCSEL	Vertical cavity surface emitting laser
TiO_2	Titanium dioxide
AOD	Acousto optic deflector
DOE	Diffractive optical element
LCD	Liquid crystal display
SLM	Spatial light modulator
GPC	Generalised phase contrast
MOPA	Master oscillator power amplifier
Nd:YAG	Neodymium-doped yttrium aluminium garnet
DNA	Deoxyribonucleic acid
FACS	Fluorescence activated cell sorting
MACS	Magnetically activated cell sorting
DLD	Deterministic lateral displacement
DEP	Dielectrophoresis
CTC	Circulating tumour cell
WBC	White blood cell
FFA	Free flow acoustophoresis
PC-3	Human prostate cancer cell line
NA	Numerical aperture
ITO	Indium tin oxide
LNO	Lithium niobate
IR	Infrared
SAW	Surface acoustic wave
LWD	Long working distance
PBS	Polarising beam splitter
QWP	Quarter wave plate
DM	Dichroic mirror

FOM	Figure of merit
ASP	Aspheric lens
b.c.t	Body centred tetragonal
CMOS	Complementary metal oxide semiconductor
SD	Standard deviation

ACKNOWLEDGEMENTS

I would firstly like to thank my supervisor, Mike MacDonald. Throughout my PhD he has given me a lot of support and guidance, and I am truly grateful to him for giving me the opportunity of realising my childhood dream of becoming a scientist.

I also extend thanks to several members of staff at IMSaT: Sandy Cochran, Paul Prentice, Christine Démoré, Sheila Smith and our visiting academic Gabe Spalding to name a few. Each has contributed towards making the department an enjoyable and productive place to conduct research. Thanks are extended to Peter Glynne-Jones of Southampton University and Alan McGuinn of Heriot Watt University for their efforts and assistance with simulations.

Many thanks are given to my lab partners over the years: Graham Brodie for showing me the ropes of the optics lab and putting up with all the questions from the new guy, and Craig McDougall for his invaluable support in the lab, and always reassuring me that 'it'll all be sweet, dude'. I would also like to thank Han Wang and Yongqiang Qiu for their expertise and assistance with the acoustics, and the newer members of the group, Daniel and Sascha for their 'encouragement' and general comedic value. Thanks are also owed to Craig MacDonald, not only for many useful discussions, but primarily for convincing me through much experimentation that in fact, beer doesn't all taste the same.

I also owe a great deal of thanks to my parents, John and Shona, not only for their constant encouragement and support throughout my PhD, but also from the very beginning. I have no doubts that my love for science was crafted during my childhood years, probably due to the massive amounts of books, science kits and programmes we have shared over the years, for which I am incredibly grateful.

Credit is also due to my oldest friends, James and Gavin, who honoured me by standing as best men at my wedding. Though distance has often limited the time we can all spend together in these past years, it has done nothing to diminish the bonds of friendship that hold us together. Being able to call upon friends such as you guys no matter what lies ahead is a great comfort and gives me courage that even should I fail spectacularly, we'd all be able to have a good laugh about it after.

Lastly, the most thanks are due to my wife, Katie, who somehow gave me the encouragement I needed to make the unlikely jump from 'studying' at Music College to studying engineering at university. Although I sometimes wonder what life would be like touring the world as the rock star I was destined to become, I can't help but be immeasurably happy at the life we have made for ourselves. As much as I know you love all the science non-sense I come out with sometimes, this thesis is for you.

DECLARATION

I hereby declare that I am the author of this thesis, entitled 'Optical and Acoustic Particle Separation Methods'. It has been prepared by me under the direct guidance of Dr. Mike MacDonald as part of my study for the award of PhD Degree at the University of Dundee, Dundee, Scotland. All references, unless otherwise stated, have been consulted by me. I have not submitted this dissertation previously for the award of any degree or diploma at any other institution.

Signature Date

This is to certify that the candidate has fulfilled the conditions of the Regulations appropriate of the degree of Doctor of Philosophy in the University of Dundee and that the candidate is qualified to submit this thesis in application for that degree.

Signature Date

ABSTRACT

Non-contact manipulation technologies present a useful and powerful means of handling particles or cells. Such techniques are of interest in regenerative medicine applications, and in particular the scalability of these techniques is an area of active research.

Optical trapping is a precise and dextrous method of manipulating particles with the forces exerted by a laser beam, while acoustic trapping is a scalable technique capable of exerting a force on particles through standing wave resonance. These complimentary modalities can be utilised in a hybrid system to give a resultant technique that borrows from the strengths of each individual method. In this thesis, methods of force balancing, using optics and acoustics, are explored, both independently and in combination with each other.

A technique for 3D acoustic trapping in glass capillaries is shown, utilising the two pairs of opposing channel walls and the air-water interfaces of two air bubbles as acoustic reflectors. Standing waves set up between these surfaces show discrete acoustic trapping sites for varying lengths of fluid cavity.

A method of optical radiation force balancing is observed in a 3D potential energy landscape, using similar principles as seen in particle trapping with counter-propagating beams. Tuning of the radiation force balance in this system allows particles to, instead of being pinned to the surface by the radiation force from the optical pattern, become localised at discrete planes of trapping sites throughout the fluid volume.

A hybrid force balance separation method using the optical and acoustic forces is devised using a single laser beam as the primary deflection mechanism with acoustic trapping providing both localisation and a force balance with the optics. Separation of different sized particles is observed, with larger scale optical deflection mechanisms and their resultant thermal effects demonstrated.

1 INTRODUCTION

Non-contact manipulation is the act of moving an object without applying physical contact. This has seen numerous developments over the last few decades, and the integration of such processes with lab on a chip devices has opened the door to many biological applications such as cell manipulation, sorting and analysis[1–4]. Such methods of manipulating particles or cells with as minimal contact as possible has helped to overcome problems such as contamination and mechanical damage. It is with real biological challenges in mind that these techniques are actively being developed.

Specifically, interest in scalable label-free sorting – the ability to differentiate cells or particles without the need for e.g. fluorescent or magnetic labels - is present in the industrial scale manufacture of blood. Such a project aims to exist alongside current blood transfusion services, and aims to help alleviate strain on the current donor-based system. Strain is brought upon the current system due to an unpredictable supply, as well as difficulties in maintaining adequate supplies of different blood types, particularly the 'universal donor' type O^- (Figure 1-1). Successful execution of the overall aims of the project could also benefit patients who are required to undergo regular blood transfusion, e.g. those suffering from Thalassaemia.

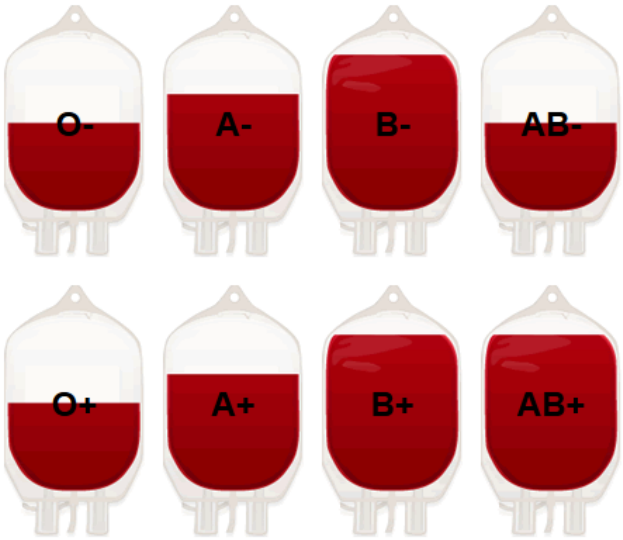

Figure 1-1. Relative stock levels of blood available for transfusion in Scotland as of 12/11/15. The 'universal donor' type O^- is reported as having 6.2 days of stock according to predicted use. The recommended minimum stock level for O^- is 6 days for average use in Scotland. Information provided by Scottish National Blood Transfusion Service via www.scotblood.co.uk on 12/11/15.

In the production of red blood cells (RBCs), the cells undergo a differentiation cycle, from stem cells to RBCs. Although such a protocol is first devised *in* vitro, bringing an *in vitro* process into an industrial scale process requires careful replication of the necessary conditions for full cell differentiation. For use *in vivo*, the quality of the end product must be assured, and to that end a means of cell sorting is required. Sorting is achieved by spatially separating one or more of the constituents in a colloidal solution such that recovery of the separated species is possible at defined channel outlets. Many different sorting modalities exist, and in this thesis focus is placed on optical sorting and acoustic sorting as two differing yet complimentary techniques.

Optical trapping, pioneered by Ashkin in 1970, describes the manipulation of small objects using only the momentum imparted by an incident laser beam[5]. Since then, optical

trapping has evolved into many different configurations. Of particular interest is optical sorting, where objects in the micron size scale can be sorted based on inherent characteristics, such as size, shape, refractive index and polarisability[1]. The sorting of objects by optical forces is primarily driven by either the radiation or the gradient force. Different designs of optical systems take advantage of these forces in different ways, with each showcasing various strengths.

Another popular non-contact manipulation technique, acoustic trapping, uses acoustic standing waves to localise objects within a sample geometry, with the objects responding to the acoustic field based on their acoustic contrast factor, compressibility and density[6]. The large area over which acoustic trapping can act is a very desirable feature for bulk manipulation of a sample, with current devices reaching very high throughputs[7].

Optical and acoustic sorting each have their own strengths, and combining the two into a hybrid sorting technique, utilising the specificity of optics and the large area manipulation of acoustics, could go further towards realising a potentially powerful sorting method. In particular, it is of interest to investigate how the force balance differs between using the optical radiation and gradient forces as the primary separation forces, independently or when combined with acoustic confinement.

The field of regenerative medicine requires sorting techniques that are sterile, non-destructive, and boast a high efficiency and throughput. Alongside these necessities, a wide range of sorting parameters is desirable given the often similar physical composition of cells. This is particularly applicable to the industrial scale manufacture of stem cell derived blood. In this context, the hybridisation of optical and acoustic sorting and the creation of new sorting modalities could lend itself to the scale up and efficiencies demanded from such an application. This thesis will explore the force balance of optical and/or acoustic techniques for particle separation.

In Chapter 2, the theories of optical and acoustic trapping will be discussed, outlining some of their key developments in particle manipulation. Other sorting techniques will be detailed and compared to each other, outlining some of the benefits and drawbacks to each. Although a relatively niche field, hybrid manipulation techniques will be explored, drawing on some of the recent literature to contextualise the work presented in this thesis.

Chapter 3 will lay the foundations for our use of acoustic manipulation, detailing the process of our microfluidic chip design with integrated acoustic trapping capabilities. A novel phenomenon, 'bubble-bounded resonance', will be described, adding another dimension to acoustic trapping in glass capillaries.

All-optical force balance will be the focus of Chapter 4, where the optical gradient force in complex potential energy landscapes will be used to achieve particle separation. An investigation into the potential for particle manipulation throughout the volume of the potential energy landscape will be considered, utilising principles from counter-propagating optical tweezers.

Chapter 5 will explore the balance of optical and acoustic forces, achieving particle separation in a hybrid system. The experiment is designed such that the balance of the optical radiation and acoustic gradient forces is exploited to give particle separation with acoustic enhancement. The application of the optical radiation force over a large area will also be investigated, including a discussion of the effects of heating in the sample due to laser absorption.

Chapter 6 will draw together the discussions and conclusions from the work carried out in this thesis, highlighting the successes and challenges of the work and discussing future directions for this research.

2 LITERATURE REVIEW: LABEL-FREE SORTING

2.1 Introduction

The need for a high throughput, label-free and non-contact method of sorting cells is apparent in the field of regenerative medicine, in particular the industrial scale production of stem cell derived RBCs. Many sorting methods exist, and each has their own advantages and disadvantages in specific applications. Factors in individual systems such as contamination, pre-processing or cell viability can often immediately rule out possible techniques. It is for this reason that hybrid solutions, where two or more techniques can complement each other, hold promise. This chapter will discuss the development of non-contact manipulation techniques and how they compare to other forms of micro manipulation, a more in-depth review of the theory and applications of optical and acoustic trapping, and the development of a hybrid approach to sorting.

2.2 Sorting

The ability to manipulate small particles with optical, acoustic, magnetic, electric or hydrodynamic forces allows for many forms cell sorting. Sorting techniques can generally be divided into two categories – active and passive. Techniques that are defined as *active* rely on an external decision making process to selectively choose which particles or cells

to sort, while *passive* techniques sort based on the cells response to an inertial or externally applied field. Another useful categorisation, particularly where the cells are required *in vivo* post-processing, is whether the technique requires the tagging of cells prior to sorting. Techniques also differ in their throughput, scalability, dexterity and parameters with which they can sort by. A categorisation of common sorting techniques is shown in Table 2-A.

Technique	Passive	Label-free	Sorting Parameters	Scalability	Dexterity	Throughput
Optical Sorting[8]	Yes	Yes	Size, polarisability, shape, RI	Low	High	Low
Acoustic Sorting[9]	Yes	Yes	Density, compressibility, size	High	Low	Medium
FACS[10]	No	No	Fluorescence	Low	Medium	High
MACS[10]	Yes	No	Magnetic susceptibility	High	Low	High
DEP[11]	Yes	Yes	Polarisability	High	Medium	Medium
DLD[12]	Yes	Yes	Size, shape, deformability	High	Low	Medium
Hydro-dynamic[13]	Yes	Yes	Size, shape, density, deformability	High	Low	High

Table 2-A. A classification of common sorting techniques.

Choosing a sorting technique requires consideration of all aspects of available modalities, and in some cases, innovation on previous methods. These techniques will be discussed in greater detail in the following sections.

2.2.1 Active and Labelling

Fluorescent activated cell sorting[14] (FACS) requires either an innate fluorescence in the cell, or more commonly for the cells to be tagged with fluorescent markers. FACS is considered an active sorting mechanism as the fluorescence of the cells are 'observed' by detectors, and based on this information a decision is then made on how to process each cell. The cells themselves are typically hydrodynamically focused, and in some cases this can also be assisted by acoustic focusing (Invitrogen™ Attune™ Flow Cytometer). They are then separated into individual droplets via a vibrating mechanism in the device, and are then given a charge by a charging ring depending on the prior fluorescence based decision. The droplets then pass through an electrostatic deflection field, which displaces droplets into receptacles according to their electrostatic charge (Figure 2-1).

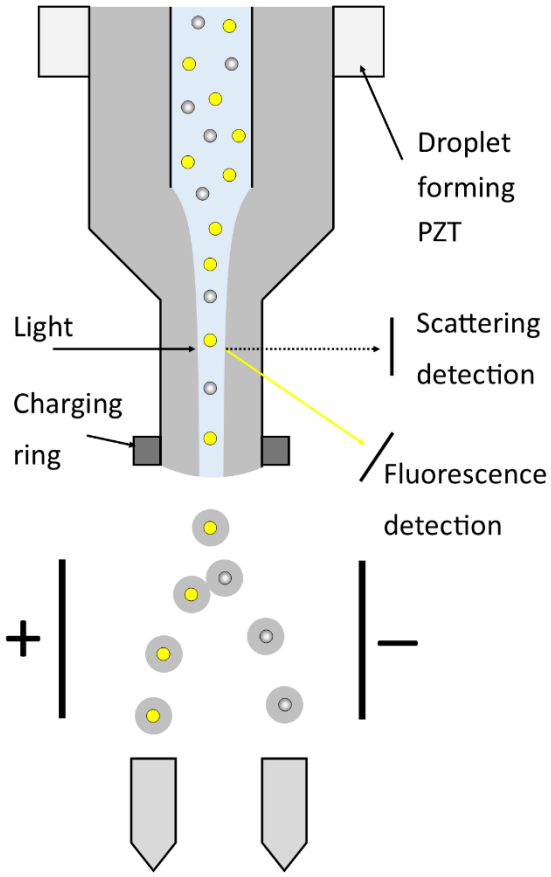

Figure 2-1. Schematic of a FACS machine. The cells are hydrodynamically focused, and the fluorescence of each cell analysed. A decision is then made to charge the droplets such that the electric field sorts out the cells with fluorescent tags from those without. Adapted from Dholakia *et al*[15].

FACS is used routinely in life sciences and medicine for a variety of purposes, including cell cycle[16] and viability analysis[17]. Commercial systems can offer throughputs anywhere in the region of tens of thousands to millions of cells per second, which makes the technique largely unparalleled in terms of processing speeds[18]. However, FACS is largely an expensive method of sorting, with a high initial equipment cost and the recurring costs of reagents.

Integrating FACS into lab on a chip devices presents some differences to standard FACS. The closed environment in the μFACS devices reduces the risk of contamination from

aerosolisation, which is particularly useful when the cells are required to be re-cultured, or used for an *in vivo* procedure. However, scaling down to a microfluidic level whilst maintaining a high efficiency usually results in a loss of throughput[19]. As the cells are no longer held in self-contained droplets, attention is focused on developing new switching mechanisms for μFACS devices in order to increase the throughput. Wang *et al.* developed an all optical force switching mechanism for integrating into μFACS, which enables fast and active control of cell deflection while reducing the complexity of the microfluidic chip[20]. A detection system is in place similar to a standard FACS setup, however the deflection is carried out by scanning a laser spot firstly where the cell is, and then guiding the cell towards the appropriate outlet. With this method they were able to report cell sorting at a rate of 106 cells per second, and cell viability was verified by an analysis of the expression of cellular stress indicators.

An alternative method of switching in μFACS was developed by Wu *et al*[19]. In this system, a pulsed laser is used to induce cavitation and create a bubble in a chamber next to the flow chamber. The system is synchronised such that when a cell of interest is detected, a bubble is created as the cell passes a small nozzle between the two chambers. This nozzle carries the shockwave into the flow region, and subsequently diverts the cell into the appropriate outlet as shown in Figure 2-2. Using this switching method, the authors were able to report sorting speed of up to 1500 cells per second, while retaining a purity of >90%.

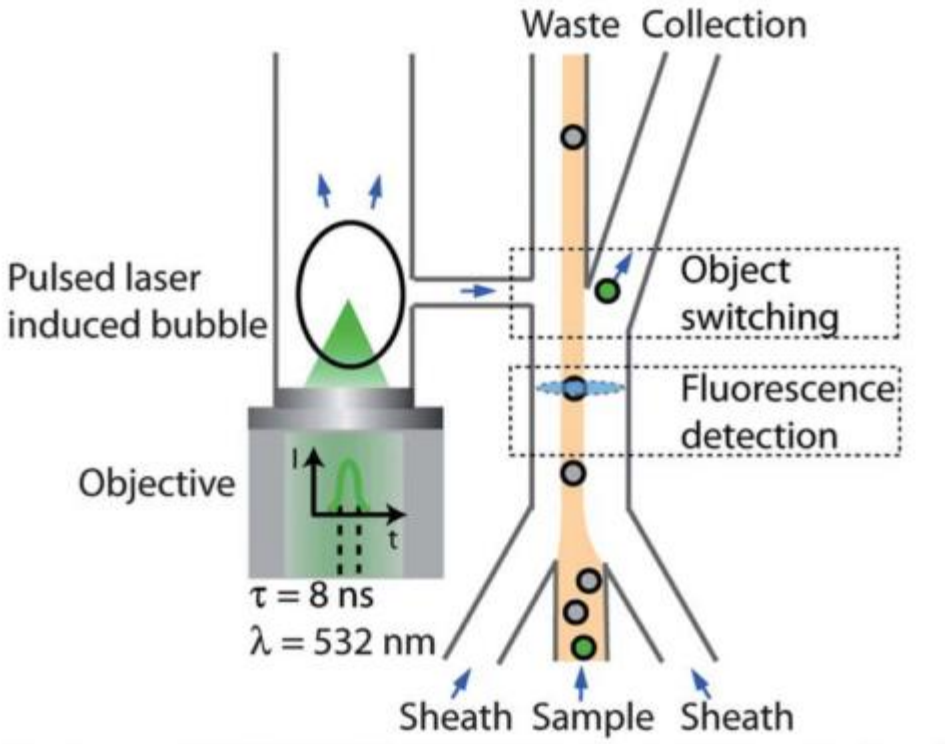

Figure 2-2. The shockwave from a pulsed laser induced bubble acts as the method for force switching. This allows the cells to remain in the fluid flow, as opposed to being aerosolised like in a typical FACS system. Image sourced from Wu *et al*[19].

Though FACS can offer high throughput sorting, the active element of sorting means that it still remains a serial process, sorting one cell at a time, while the need for tagging in most applications limits its usefulness in areas such as regenerative medicine.

2.2.2 Passive and Labelling

In terms of techniques that rely on tagging and yet are passive, there is an alternative to the single file nature of FACS. Magnetic activated cell sorting (MACS) relies on the antigens expressed by a cell to attach to a corresponding antibody during incubation, which is coated with magnetic nanoparticles. The cells are then exposed to a magnetic

field, whereby the tagged cells will be separated from the untagged cells. This is particularly useful for bulk separation of two species. The main advantage of MACS over FACS is that sorting can be carried out in parallel. This has led to development of microfluidic devices that have been shown, for example, to separate magnetically tagged live *E.coli* from RBCs[21], and leukocytes from whole blood[22]. Throughputs in these microfluidic MACS devices have reached upwards of 10,000 cells per second.

While this does offer a higher throughput and a more parallel sorting process than μFACS, it does require tagging of cells during incubation which can be unsuitable depending on the application, particularly in regenerative medicine. It also only allows binary separation of samples, whereas FACS can sort via as many as 12 different fluorescent signals and 2 scattering parameters[14].

2.2.3 Passive and Label-free

Label-free sorting techniques do not require tagging, so are of great interest in the life sciences in cases where tagging is either unsuitable, or too costly. One of the greater challenges with passive, label-free sorting is the reduction in throughput compared to active, or tag-based techniques. Passive techniques in general will be discussed, and their potential for scaling will be considered.

Inertial forces

Centrifugation remains one of the most common sorting techniques used in laboratories. Centrifugation relies on inherent differences in cell densities in a heterogeneous mixture

for sorting. The mixture is spun about a central axis, resulting in the cells of larger densities moving further away from the central axis than those of lower density. In order to achieve sorting, the supernate is usually removed manually with a syringe, leaving the pellet of high density cells at the bottom of the tube. The involvement of a manual stage in the sorting process introduces a factor of human error into the process, as the volume of supernate aspirated from the tube is usually judged by eye, which will not be entirely accurate. Still, the simplicity and relatively low cost of the method means that it is used extensively in the life sciences. It is observed however, that centrifugation is known to induce haemolysis[23], and so depending on the parameters may be unsuitable for work where erythrocyte viability is desired.

Efforts have been made to miniaturise centrifugation, and integrate the principles into lab on a chip devices. Mach *et al.* created a chip which separates cells based purely on a fluid dynamic phenomenon where cells selectively move to micro-scale vortices in the chip geometry[24]. This device offers the benefits of continuous and sequential sorting that typical bench top centrifuge systems cannot offer, and at a much lower cost. Such a device also poses benefits over optical and acoustic methods for example by not relying on an external field for sorting to occur, and sorting parameters can be controlled solely by varying the fluid flow.

Using controlled laminar flow or physical microstructures can be a low-cost and simple means of achieving cell separation. Size discrimination filters have been used by several groups, in particular for the separation of constituents in whole blood. Such a device was developed by Mohamed *et al.*[25], in order to separate cancer cells from peripheral blood for subsequent downstream genetic analysis. The device features a two dimensional array of columns, through which the blood was flowed. The arrays feature a gradual decrease

in column spacing. The design allowed sorting of cells by size, as smaller cells could flow through the spaces between the columns, whereas larger cells were retained. Deformability of the cells eventually allowed larger cells to pass through the small gaps at a much slower rate than smaller cells, however this method does not laterally displace cells in a manner that would allow continuous separation at the outlets.

Another style of filtration, termed deterministic lateral displacement (DLD), is illustrated in Figure 2-3.

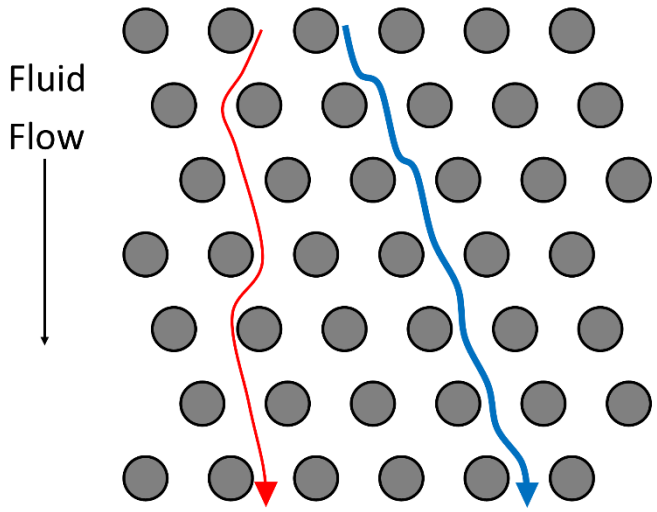

Figure 2-3. Smaller particles (red) find a different path through the array of columns than the larger particle (blue), which cannot fit through the same gaps. The pattern can extend as far as separation is required. Adapted from Inglis[26].

In this arrangement, a repeating array of cylindrical columns is used in a regular pattern throughout the interaction area. Smaller cells or particles will be able to navigate through narrower gaps, and in this instance will effectively travel in the same direction as the fluid flow. Larger particles however must follow the path made available by the array, and are

forced to flow at an angle to direction of fluid flow. Allowing all cells to pass through the obstructions, as opposed to the pattern used by Mohammed *et al.*, facilitates collection of sorted species at independent outlets. Using the distance between the individual columns and the distance between rows of columns, it is perfectly possible to tailor a DLD device not just for sorting species by size, but also sorting cells by deformability and shape. Beech *et al.* demonstrated the effects that different channel geometries have on the pre-focusing, and subsequent response of RBCs to the same DLD obstacles[27]. DLD in general has been used extensively in blood filtration, such as isolating circulating tumour cells (CTCs) from blood[28], removal of parasites from blood[29], and the separation of healthy RBCs from nucleated red blood cells (nRBCs) and white blood cells (WBCs)[30].

Due to cells interacting with a physical obstacle, problems can arise with blockages and contamination[31]. Also, imperfections in the fabrication of DLD devices can have a major impact on the performance of the device, with no dynamic, reconfigurable means to fix such defects.

Applied field

The electrical polarisation or inherent charge of a cell can be used for fractionation of bulk samples in flow. Dielectrophoresis (DEP), first described by Pohl[32], uses electrodes on either side of a channel to create a non-uniform electric field across it, in which the particles or cells will experience a time-averaged ponderomotive DEP force. This is shown in Equation 2.1[11], where ε_m is the absolute permittivity of the surrounding medium, R is the particle radius and E is the amplitude of the electric field. The Claussius-Mossotti factor, CM, which is dependent on the polarisability of the particle and its surrounding

fluid is shown separately in Equation 2.2[11], where $\mathcal{E}^*_p$ and $\mathcal{E}^*_m$ are the complex permittivities of the particle and fluid respectively.

$$F_{DEP} = 2\pi\varepsilon_m R^3 CM(\nabla E^2) \tag{2.1}$$

$$CM = \frac{\varepsilon_p^* - \varepsilon_m^*}{\varepsilon_p^* + 2\varepsilon_m^*} \tag{2.2}$$

Intrinsic differences in the dielectric properties of cells have been exploited to separate healthy erythrocytes from those infected by the malaria pathogen[33]. Changes to the membrane of the erythrocytes following infection result in a changed response to electrical fields, resulting in the healthy erythrocytes being trapped at the high field regions, while the infected erythrocytes were repelled to the low field regions. The infected cells being repelled allows for them to be carried away by flow, while the healthy cells are still retained. The large area over which DEP can act shares familiarity with MACS, however as shown in this case, the absence of tagging greatly simplifies the process whilst still allowing for massively parallel sorting.

The ability to affect particles based purely on their dielectric properties is a useful tool, however it can become more challenging if the particle types' dielectric properties do not differ greatly. In such instances, the effects of DEP can be enhanced by the use of dielectric tagging[34]. Although this does add another step to the process and places limits on the *in vivo* use of processed cells, it does greatly increase the throughput, and also allows for sorting of cells whose dielectric properties are very similar. These developments bring DEP a lot closer to the capabilities of techniques such as MACS.

Using optical forces as a primary sorting mechanism offers many benefits. By exploiting the inherent response of particles to an optical field, it is possible to elicit a varying response based purely on characteristics such as size, shape and refractive index – without the need for tagging. Selectivity based on these parameters has allowed the sorting of many different types of particulate, and choosing the geometry of ones optics can further improve the overall efficiency of the sorting.

Perhaps the first real demonstration of optical sorting was by Imasaka *et al.* in 1995, with the development of optical chromatography[35]. In this technique, a laser beam is focused transversely down a capillary, against a counter-flowing solution of particles. The radiation pressure from the laser pushes particles against the drag force from the fluid flow, which will then reach a balance at a certain distance away from the beam focus, while the gradient force from the beam will localise particles in the centre of the beam intensity profile.

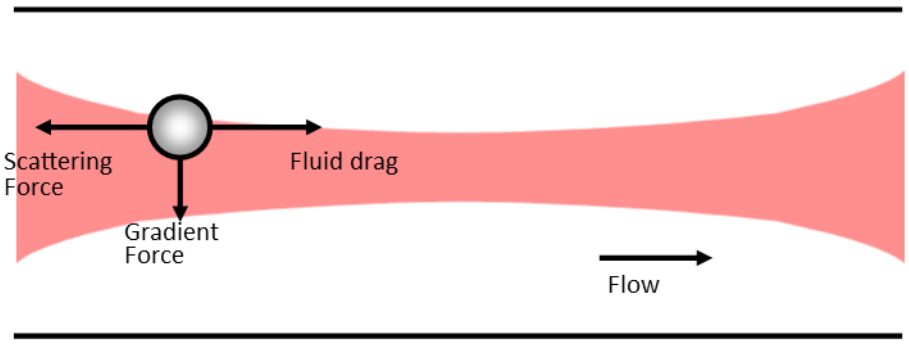

Figure 2-4. The particle experiences a gradient force from the laser beam, drawing it into the central axis of the beam. The scattering force balances out against the Stokes drag resulting in different species of particles resting at different points in the stream. In general, larger particles will be pushed further from the beam focus by the scattering force than smaller particles. Adapted from Imasaka[36].

Smaller particles will experience a different radiation force from larger particles, and as such will reach a balance at a different distance away from the beam focus. Although optical chromatography initially did not have any means of separating samples at the outlet, 'cascade optical chromatography' was later developed[37], which uses multiple laser beams to create a sequential sorting system where different particles are sorted out of the sample at separate outlets along the channel.

In 2002, Korda *et al.* developed a technique whereby particles are transported through an array of optical traps created using a DOE[38]. As discussed in Chapter 2.3.2, a DOE is a diffractive grating that allows a laser beam to be split into multiple parts. In these experiments, a 10x10 array of optical traps is produced at the sample plane. 1.5 μm spheres are flowed through this array, and are shown to follow discrete channels along the direction of the array. When the array is rotated with respect to the direction of fluid flow, particles are seen to follow defined paths through the array, however with an angle of rotation past 11° the particles no longer follow clearly defined trajectories through the array of traps. This does however demonstrate the potential for particle displacement along an optical potential.

The use of optical potential energy landscapes as a means of sorting between different species of particles was pioneered by MacDonald *et al*[1]. A DOE was used to split the laser beam into five separate beams – four beams diverging from the centre beam at 4.6° in a cross shape. These beams were collimated, and then focused and interfered through an aspheric lens to produce a three-dimensional optical lattice at the sample plane. The optical landscape takes the form of a body centred tetragonal (b.c.t) lattice structure, with strongly interlinked local intensity maxima along the desired direction of particle displacement. By placing and rotating a coverslip in the path of each beam, individual control over the phase of each beam in the collimated infinity space is possible, allowing

for fine tuning of the optical structure. Separation of 2 μm polymer and silica spheres by refractive index is shown at flow speeds in excess of 35 μms^{-1} at deflection angles of 45°. The technique is also used to sort by size 2 μm protein microcapsules from a polydisperse particle stream. A typical flow system for sorting in this manner is described in Figure 2-5.

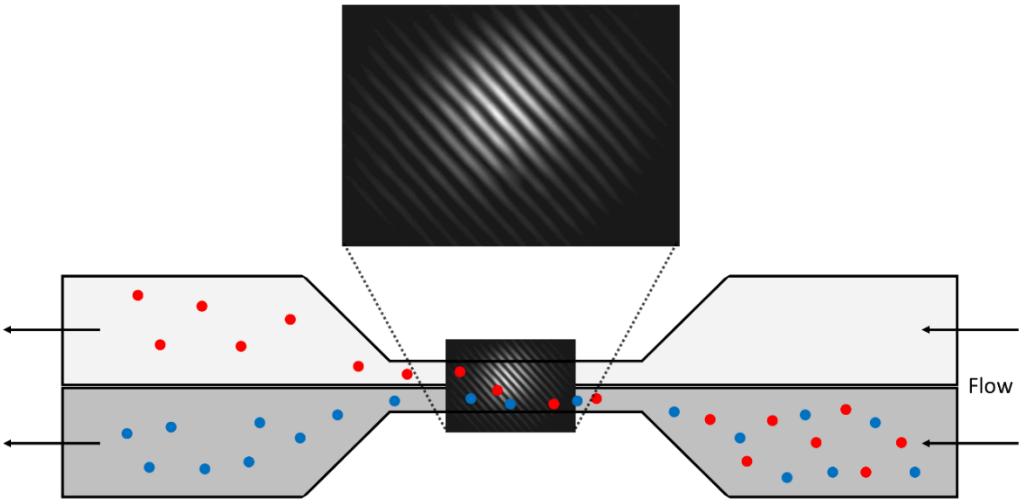

Figure 2-5. Schematic for a potential energy landscape sorter. The colloidal solution flows into the optical interaction area, where it runs parallel to a buffer flow. The particles that are affected by the potential landscape (red) are deflected into the buffer flow, and out into a separate outlet from the unaffected particles (blue). Adapted from MacDonald *et al* [1].

Other means of displacing particles using optical methods have been demonstrated. Optical peristalsis, for example, uses a spatially symmetric optical ratchet to trap particles in a low potential energy well, and transport them by cycling the pattern continuously[39].

The principles of acoustic trapping, discussed in more detail in Chapter 2.4, can be applied to continuous flow systems, constituting another contactless manipulation technique. Termed acoustophoresis, Petersson *et al.* utilised the standing waves created between two cavity walls to sort RBCs and lipid particles[40], the motivation being blood-wash for the removal of lipids during open heart surgery. Their device relied on the differing response of the two components to the acoustic field: due to their differing compressibility and density, the RBCs move towards the pressure node, while the lipids move towards the anti-nodes at the edge of the channel. Three outlets at the end of the channel, one in the centre and two at the edges, allows for the separated erythrocytes and lipids to be separately collected. Efficiencies close to 100% were observed using this method, and to further increase the throughput, a parallel design was conceived[41]. The eight channel design presented allows for the single transducer to drive multiple channels at once, which greatly increases the throughput of the system.

For particles with more similar acoustic properties, separation can be achieved during flow based on parameters such as acoustic power and flow rate. In many designs, the colloidal solution of particles will enter the acoustic manipulation area of the channel via an inlet that runs alongside a buffer inlet, as shown in Figure 2-6. When the particles enter the acoustic field, the particles that experience a greater force will be moved to the node much quicker than the less affected particles. Although all the particles are drawn to the node in this case, the difference in migration time allows for a form of acoustic fractionation, and the individual particle species are then separated at the outlets.

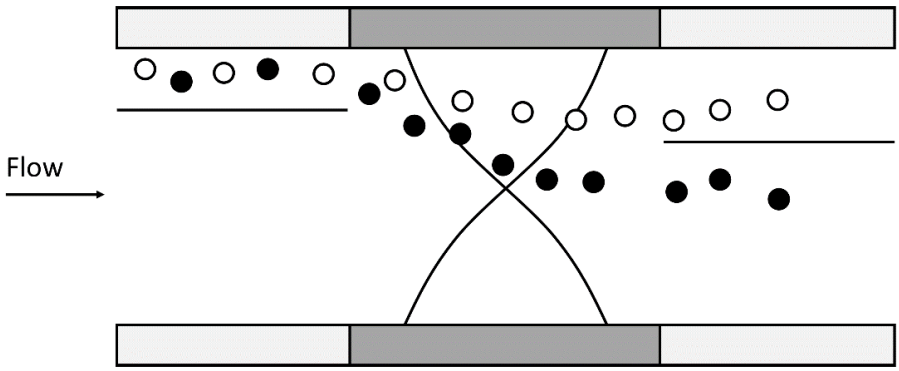

Figure 2-6. Split flow design of an acoustic sorter. The particles are fractionated along the acoustic manipulation zone, with control over the acoustic power and flow rates determining where the particle species end up in the stream due to their respective migration times towards the acoustic node. Adapted from Kumar *et al*[42].

This method of acoustophoresis, free flow acoustophoresis (FFA), was demonstrated by Kumar *et al.* as a means of sorting hybridoma and *Lactobacillus rhamnosus* cells[42]. The group also modelled the system, and predicted the necessary parameters for acoustic power and flow speed necessary to achieve well defined separation. The authors also consider the scalability of the process, with the possibility of multiple chips stacked together being driven by a single transducer. Many other groups have used FFA, and it remains a powerful technique for bulk sorting of biological matter. Some examples include the sorting of CTCs[7] and cells at different phases of the cell cycle[43].

2.3 Optical trapping

The notion of moving physical objects with light was first recorded by Johannes Kepler in the early 17th century[44]. His belief stemmed from his observation that the tails of comets always pointed away from the sun, leading to the hypothesis of an outward solar radiation

force. Many experiments in the following centuries attempted to prove the existence of this force, with one of the key developments being Maxwell's theory of electromagnetism, which required a resultant pressure from the absorption or reflection of light from a surface[45]. Although now a verified property of light, it wasn't until the invention of the laser in the mid-20th century that the pressure from an electromagnetic wave was fully exploited. Specifically, the work of Arthur Ashkin and his colleagues at Bell Laboratories pioneered optical trapping, which became a widely used non-contact particle manipulation technique.

2.3.1 Optical trapping theory

The invention of the laser allowed Ashkin to trap particles in a stable optical potential well for the first time[5], with his first paper published on the subject describing two methods of optical trapping: single beam trapping, where the radiation pressure from a loosely focused beam accelerates a particle along the axis of beam propagation and pins it against a side wall of the chamber; and a counter-propagating trap, where two opposing loosely focused beams accelerate a particle into a stable potential well between the two beams. Ashkin and Dziedzic also demonstrated optical levitation, by balancing a 20 μm glass sphere in a potential well as a result of the force balance between a vertically directed laser beam and gravity[46]. Using a ray optics model, it was evident that there would be a transverse force acting on the spheres in conjunction with the axial scattering force. This transverse force arises due to the intensity profile of a Gaussian beam, where the centre of the beam is more intense than the surrounding profile. As rays from the centre and elsewhere in the beam refract through a transparent sphere, there will be a net momentum pull towards the central axis of the beam profile, as depicted in Figure 2-7. The more

intense rays will produce a greater change in momentum within the sphere, causing a net momentum pull in that direction until the particle is trapped in the most intense part of the beam. In a Gaussian beam, this is the centre of the beam profile. This force is commonly known as the optical gradient force, while the scattering force is also commonly referred to as the optical radiation force. Ashkin *et al.* later developed optical trapping into three dimensions, a technique which would be known as 'optical tweezers'[47]. By using a high numerical aperture objective (NA=1.25), they were able to produce a backwards radiation force that could overcome the radiation pressure in the direction of beam propagation on the surface, which brings the particle to rest just beyond the focus of the beam, demonstrating fully 3D trapping of particles up to 10 μm in size using 100 mW of laser light.

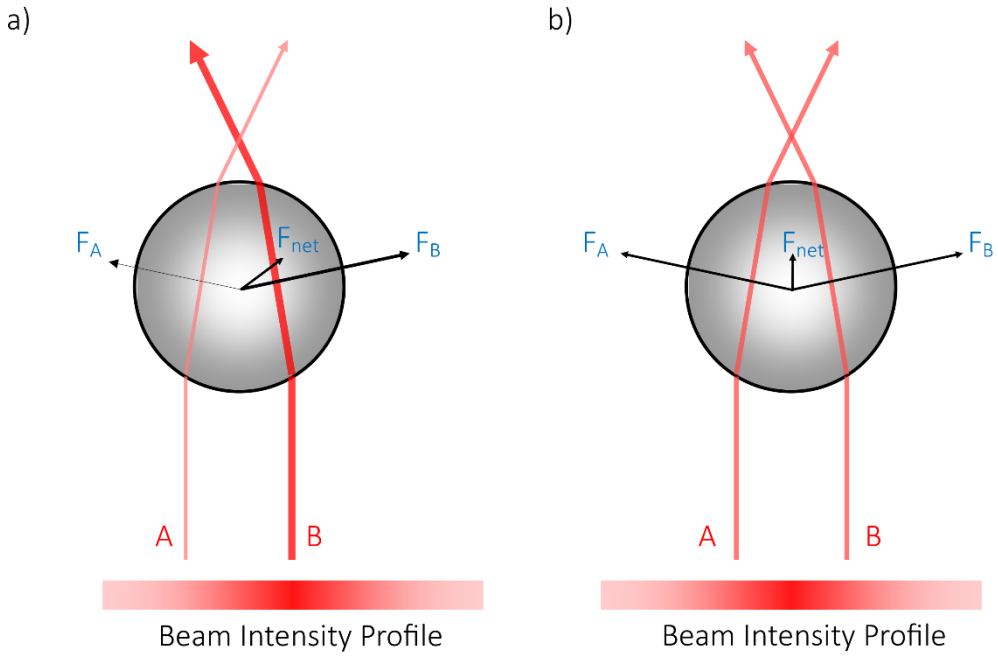

Figure 2-7. Ray trace model of optical tweezers. In a), the more intense ray B produces a greater force than A by refraction, with the resultant particle motion towards B. In b), the rays A and B are of equal intensity, however there is still a net gradient force towards the focus of the beam. Adapted from principles set out by Ashkin *et al*[47].

This ray optics approach to optical trapping theory presented is appropriate for particles whose radius is larger than the wavelength of the trapping laser. Such particles are said to be in the Mie regime. In this case, Mie scattering on the surface of the particle contributes towards the radiation force, where an equal and opposite reaction is observed due to the momentum transfer from the incident photons, in accordance with Newton's third law. Photons that are scattered away from the central axis of the particle will also contribute towards the axial forces. In the Mie regime, the gradient force arises from refraction of the light through the particle, and serves to exert a net force in the direction of the intensity gradient as shown in Figure 2-7, when the index of refraction of the particle is greater than that of its surrounding medium. Inversely, when the index of refraction of the particle is less than that of the surrounding medium, the net force is in the opposite direction. These two forces, arising from the same source, act to bring a particle to rest at the focus of the laser beam.

For spheres whose radius is much smaller than the wavelength of the trapping laser, these particles are said to be in the Rayleigh regime, and the ray-optics model no longer applies, so a particle must be treated as a point dipole. In this regime, the radiation and gradient forces can be completely separated, and treated as two separate entities. The radiation, or scattering force, is the result of the particle absorbing and reradiating the incident light, and can be expressed as Equation 2.3[47], where I_0 is the intensity of the incident light, c is the speed of light, r is the particle radius, λ is the wavelength of the incident light, m is the ratio of refractive indices of the particle to the surrounding medium, n_b.

$$F_s = \frac{I_0}{c}\frac{128\pi^5 r^6}{3\lambda^4}\left(\frac{m^2-1}{m^2+2}\right)^2 n_b \tag{2.3}$$

The gradient force is the result of the time-averaged interaction of the particle with an inhomogeneous field, and can be expressed as in Equation 2.4 and 2.5, where α is the polarisability of the sphere[47].

$$F_g = -\frac{n_b \alpha}{2} \nabla {I_0}^2 \tag{2.4}$$

$$\alpha = n_b^2 r^3 \left(\frac{m^2 - 1}{m^2 - 2} \right) \tag{2.5}$$

It is observed through Equations 2.3 and 2.4, that the scattering force acts in the direction of beam propagation, and the gradient force draws up the intensity gradient when m>1.

Although most applications (particularly in cell sorting) fall into the Mie regime, an analysis of Rayleigh regime trapping is particularly important for trapping in the nano-scale, for example trapping gold nanoparticles[48]. For the work in this thesis, work will be carried out only in the Mie regime.

A phenomenon observed in optical trapping, known as 'optical binding', can occur when more than one particle is trapped in the laser beam(s). The effect occurs via the mutual interaction of the scattered light from nearby particles, that can then affect other close by particles[49,50]. These inter-particle forces can hold particles in place relative to each other, and chains or arrays of particles have been observed due to optical binding[51]. Some of the work on optical binding has led to innovations in multiple particle trapping, in particular the arrayed organisation of particles in an optical field, and subsequent methods used to create large potential energy landscapes for particle manipulation, discussed further in the next section.

2.3.2 Array optical tweezers

For scale up of optical techniques, as could be required in high throughput cell sorting methods, a functional evolution of single beam optical tweezers is to realise an array of optical tweezers, or a potential energy landscape, in which many particles can be manipulated simultaneously. It is for this reason that a study into the parallelisation of optical trapping is necessary to set the foundations for the work presented.

Since their conception, optical tweezers have been used by many groups for a plethora of applications and have been utilised in many different modalities such as molecular force sensing[4] and nanoparticle injection into single cells[52]. A fairly intuitive step in the development of optical tweezers is to have multiple traps in the one system. In particular, this is a useful step in considering the scale up of optical technologies.

Perhaps one of the more obvious implementations is to employ multiple laser sources. Although usually impractical in most cases, Ogura *et al.* achieved trapping of particles in multiple discrete traps by developing a vertical cavity surface-emitting laser (VCSEL) array[53]. The VCSEL contains an individually addressable 8x8 array of semi-conductor laser sources, with an optical output power of up to 5 mW per laser source, with which they successfully demonstrated transporting 6 and 10 μm particles along a series of traps from the VCSEL array by switching on one trap at a time.

Time-shared traps

Sasaki *et al.* demonstrated the trapping of multiple latex and TiO_2 particles in a laser-scanning system, based on computer controlled galvano mirrors[54]. This works by having

a steering mirror in a Fourier plane corresponding to the sample plane, such that any angular movement of the mirror produces a lateral displacement of the beam in the sample plane. The trapping laser is scanned at a rate of 13-50 Hz to produce a pattern of optical traps in the sample plane. The technique was later used to move all of the trapped particles along the pattern at a constant velocity[55]. Laser-scanning can also be achieved by the use of an acousto-optic deflector (AOD). The AOD consists of a crystal, in which a density grating is created by driving a travelling acoustic wave through the crystal. The first order optical beam is deflected by an angle defined by Equation 2.6, where λ, f and v are the wavelength, frequency and speed of the applied acoustic wave respectively.

$$\theta = \frac{\lambda f}{v} \tag{2.6}$$

Time-shared optical traps can only maintain multiple trapping sites if the beam revisits each site before the particle can diffuse away, as a result of Brownian motion, gravity or other influences. AODs can typically scan at rates in the region of 100 MHz, and can create very large arrays of optical traps by rapidly scanning between multiple points in the sample plane[56]. Such capabilities have facilitated large scale 2D patterning of colloids on a surface[57], and 3D patterning in colloidal dispersions combined with confocal imaging[56]. The 3D patterning is achieved by splitting the laser beam in to two, and changing the divergence of one beam relative to the other, such that when recombined and focussed in to the same objective, the position of one of the trapping planes will be shifted relative to the other.

Compared to scanning mirrors, which are typically limited to scanning rates of a few kHz, AODs pose a significant advantage in terms of number of possible traps. In terms of producing a number of stable traps, AODs also have the advantage of being ultimately limited by available laser power, whereas scanning mirrors tend to be limited by scanning speeds.

Holographic trapping

Multiple optical traps can also be created by splitting a single laser beam into multiple parts using a diffractive optical element (DOE). A DOE is essentially a diffraction grating, with a specifically designed pattern etched periodically into its surface. In practice, this means that any arbitrary pattern of optical traps can be produced from a specifically designed DOE. This was used by Dufresne *et al.* to create the 'hexadeca tweezer' consisting of a 4x4 array of optical tweezers, where each trap was shown to individually trap 0.5 μm silica spheres[58].

To expand upon the holographic approach to trapping seen in DOEs, Reicherter *et al.* developed a method for multiple particle trapping in which computer generated holograms are sent to an LCD, which then generates arbitrary light fields in the Fourier plane of the LCD[59]. The LCD screen formed the basis for an addressable spatial light modulator (SLM). This allows for dynamic, independent manipulation of individual optical traps, leading to a highly customisable and dextrous beam shaping system, compared to the static nature of the DOEs. The SLM was shown to not only produce multiple traps, but also the capability to dynamically modify the wavefront of each individual trap, thus allowing a vast array of different modes of light[60]. The technique is

now commonly known as 'holographic optical tweezers'. Holographic optical tweezers, and SLMs in general, have been used in a wide range of applications, including holographic microscopy, particle sorting, and beam shaping[61–64].

Another way of utilising holography for optical tweezing is the Generalised Phase-Contrast (GPC) method[65]. In standard holographic optical tweezers, the SLM is placed in the Fourier plane such that it forms the diffraction grating of the desired pattern. However in the GPC method, the SLM is placed in the imaging plane. This allows almost all of the incident light to be transferred into the sample plane, and as the kinoform is simply an image of the pattern desired in the sample plane, this method is much less computationally intensive. This method typically only allows 2D trapping, however increasingly complex optical systems can allow for 3D trapping by the use of counter-propagating beams[66].

Holography also allows for the creation of complex 3D optical landscapes. By splitting the laser beam into multiple parts either with a DOE or an SLM for example, this allows one to re-combine the beams at the sample plane, creating complex potential energy landscapes via the interference of the multiple beams. The resultant structure is primarily determined by the number of beams, and the arrangement in which the beams interfere. MacDonald *et al.* demonstrated the resultant structures produced by several configurations of interfering beams[67], with further complex patterns observed and analysed by Jákl *et al*[68].

These resultant optical landscapes can allow for a potentially large area of effects when considering optical sorting, and are of great interest where the dexterity of optical manipulation is desired to be integrated in to a scalable sorting system.

2.3.3 Optical tweezers in biology

Applying optical tweezers to biological problems was posited by Ashkin as he developed optical tweezers. The ability to produce forces on the pN scale is ideal for dealing with small objects like cells or bacteria. Ashkin and Dziedzic reported trapping of bacteria and viruses[69], whole cells[70] and intra cellular components[71]. They noted that as most biological matter absorbs weakly in the near infrared region, lasers in this range (e.g. 1064 nm) are quite well suited to interaction with biological matter. This was further analysed by Neuman *et al.*, who studied the photodamage to *Escherichia coli* in optical traps[72]. They used tuneable Ti:sapphire (780-970 nm), MOPA diode (991 nm) and Nd:YAG (1064 nm) lasers to examine photodamage as a function of wavelength, and also as a function of laser power. In their findings, they conclude that wavelengths on either side of 850-950 nm cause the least photodamage (Figure 2-8), and result in a higher subsequent cell viability. Sensitivity in this case is defined as the reciprocal of the time it takes for the rotation rate of a cells to drop below 50% of its initial rate. The authors also compared the wavelength dependent photodamage of *E. coli* and Chinese Hamster Ovary cells, finding a similar response suggesting common chromophores between cell species.

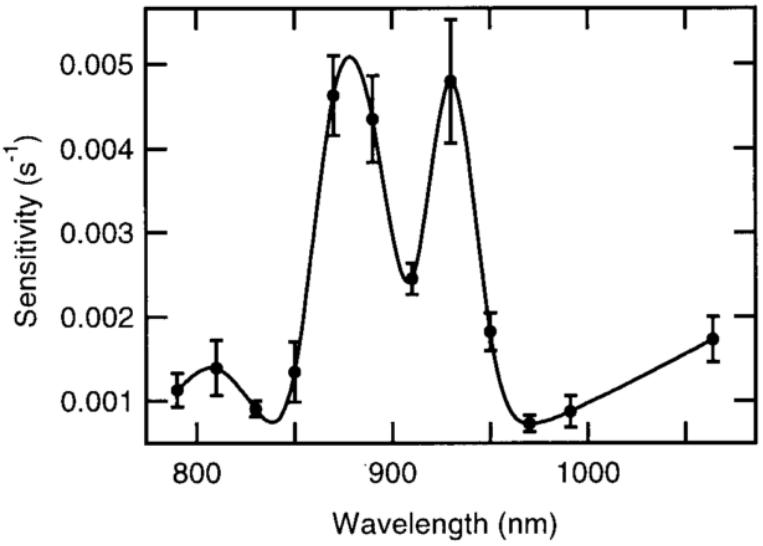

Figure 2-8. The wavelength dependent sensitivity of *E.coli*, showing peak sensitivities around 870-930 nm, with relatively low sensitivity at 1064 nm. From Neuman *et al*[72].

It is worth noting that in these tests, and in recent analysis of photodamage to red blood cells[73], the interaction time of the cells with the laser to produce such results is in the order of hundreds of seconds. In the work carried out in this thesis, the interaction time of particles with the laser is typically in the order of <1s for the work in Chapter 5 and a few seconds in Chapter 4. Therefore, although consideration of photodamage must be taken in to account when transferring such systems from particle to cell sorting, it is anticipated that, due to the previous literature cited, that little effect will occur.

One of the more important applications of optical tweezers in biology, and where the technique has gained the most recognition, is that of a force measurement device. As the trapping strength of optical tweezers is in the order of pN forces, it is an ideal complement to the scale of forces in the cellular regime, in particular to sense molecular forces. Using optical tweezers, Kuo and Sheetz measured the force of single kinesin molecules on a microtubule[4]. They did this by first characterising the escape force of a

bead from a single beam optical tweezers. To calibrate the escape force, a particle of known size is held in an optical trap against fluid flow. As the laser power is lowered, the stiffness of the trap will decrease. When the laser power is low enough, the particle will be carried out of the optical trap, and it can be said that the Stokes drag (Equation 2.7) acting on the particle at that laser power is equal to the stiffness of the optical trap, with the intensity of the trapping laser being proportional to the trap stiffness[74], where η is the fluid viscosity, r is the particle radius and U is the object speed.

$$F_D = 6\pi\eta r U \tag{2.7}$$

After the escape force has been calibrated as detailed above, a particle that is attached to a microtubule is held in the optical trap, with the microtubule itself attached to an immobilised kinesin molecule. As the laser power is lowered, the trapped microsphere begins to move away from its initial position, pulled by the kinesin, as the balance between mechanical, biological and optical forces shifts. In this manner, the forces of the kinesin molecule can be characterised and is calculated to be 1.9 ± 0.4 pN. Various other groups have used optical trapping for the measurement of a wide range of biological forces[75–79].

The dexterity of optical tweezers in this regard makes it a very useful tool, particularly when dealing with sub-cellular structures. The main drawback is the scale over which optical tweezers can act, and the resultant issues with parallelisation of such techniques. One could envisage a scenario where a reading of a particular cellular force is required, but in the region of hundreds or thousands of readings simultaneously in order to provide a higher degree of statistical significance. It is here that optical tweezers becomes limited in its applicability.

2.4 Acoustic trapping

While optical manipulation offers great dexterity and flexibility, it is often limited by the scale with which it can manipulate particles. Acoustic trapping is another non-contact manipulation modality where an applied acoustic field exerts forces on a particle, and can often compliment optical trapping by providing a technique that while less dextrous, is inherently scalable.

2.4.1 Acoustic manipulation theory

Acoustic radiation pressure was first described towards the end of the 19th century[80] as a means of measuring the speed of sound in various gases, and was further understood by Lord Rayleigh in 1902[81]. Particles experience non-zero time averaged forces in acoustic standing waves due to the energy density gradient in the acoustic field. This has been theoretically described in detail by King[82], Gor'kov[83] and Doinikov[84]. In general, the time averaged acoustic force can be expressed as the gradients of the kinetic and potential energy densities, shown in Equation 2.8 and further expanded upon in Equations 2.9 and 2.10, where V is the volume of the particle, ϱ_p and ϱ_f are the densities of the particle and fluid respectively, c_p and c_f are the speeds of sound in the particle and fluid respectively, u is the acoustic velocity and p is the acoustic pressure[85].

$$\langle F \rangle = \nabla V \left(\frac{3(\rho_p - \rho_f)}{2\rho_p + \rho_f} \langle E_{kin} \rangle - \left(1 - \frac{\rho_f c_f^2}{\rho_p c_p^2} \right) \langle E_{pot} \rangle \right) \tag{2.8}$$

$$\langle E_{kin} \rangle = \frac{1}{2} \rho_f u^2 \tag{2.9}$$

$$\langle E_{pot} \rangle = \frac{1}{2\rho_f c_f^2} p^2 \tag{2.10}$$

In general, particles with a high acoustic contrast compared to their surrounding medium will elicit a greater response to the acoustic field. It is also true that particles of low compressibility and high density compared to the surrounding fluid will become trapped at the nodes of the standing wave, with the inverse also true for trapping at the antinodes.

Alongside the primary forces, the interaction between the ultrasonic standing wave and the particles, there are also secondary forces, experienced via particle-particle interactions. These particle-particle interactions are the result of the acoustic waves scattering off of particles, and generating an acoustic force when particles are close together, also known as Bjerknes forces[86]. The strength of the secondary forces is highly dependent on the distance between particles, and is generally negligible until particles have been confined to a common plane.

As the primary acoustic force scales with the cube of the particle radius, acoustic manipulation becomes less effective on smaller particles, in the 1-2 μm region, where the forces generated by acoustic streaming become larger than those from the standing wave pattern, and begin to dictate particle motion[87]. Although the acoustic force on a particle scales with its radius cubed, larger particles are more subject to sedimentation depending on their buoyancy in the surrounding fluid.

The optical forces exerted by a light beam can broadly be defined as the radiation force, from the scattering of incident light on the surface of a particle, and the gradient force which acts to draw a particle into the area of least potential. When considering the behaviour of a particle in a standing wave acoustic field, in particular when thinking of an analogue to optical trapping, it becomes clear that the effect observed is that of a gradient force. This also fits with Equation 2.8, which describes the motion of a particle in an acoustic field in terms of its response to the gradients of the kinetic and potential energies. In the literature, the acoustic forces in such a system are commonly referred to as radiation forces. However, this definition makes the conceptualisation of a hybrid optical and acoustic manipulation system unclear, and as such the acoustic forces generated in a standing wave design will be referred to as a gradient force.

2.4.2 Applications of acoustic trapping

Acoustic trapping has proven a useful tool in non-contact particle manipulation. Some of the earlier examples of acoustic trapping were using a resonant plate and a reflector to trap droplets in air[88–90]. It was noted that acoustic levitation is particularly well suited to use in the field of microanalysis, as it is a convenient way to work with small sample volumes, and reduces sample composition as the sample is not in contact with a surface.

The majority of acoustic trapping applications rely on the geometry of the sample chamber to shape the acoustic field. Typically a transducer serves as one face of the channel geometry, while another channel wall some distance away facilitates the role of an acoustic reflector, such that driving the transducer at a resonant frequency corresponding to the distance between it and the reflector layer will produce a standing wave, as depicted in Figure 2-9.

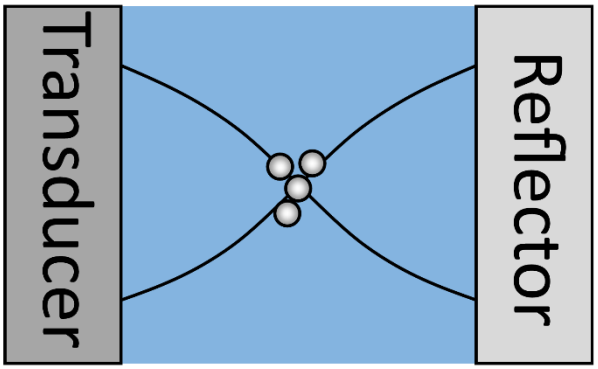

Figure 2-9. A standing wave set up between a transducer and a reflector. Particles of high acoustic contrast relative to the surrounding medium will migrate towards the nodes of the standing wave (pictured). Adapted from principles set out by Gor'kov[83].

The resulting landscape shows that in general acoustic forces are best implemented where bulk manipulation of particles is required, and typically not where fine single particle manipulation is needed. This is due to the standing wave being created across the channel, and as such it lacks the specificity to pick out individual particles in the way that a technique like optical tweezers can. Such studies using acoustic trapping have investigated the viability of cells exposed to acoustic forces, by manipulating a large number of cells, and then observing their doubling time in culture[91]. However, array type designs can also facilitate the bulk manipulation of particles or cells in a different manner. By driving a 100 well array with a single transducer, Vanherberghen *et al.* were able to trap cells at the centre of each of the wells[92]. An observed behaviour of the cells to maintain viability by continuing to divide whilst under the influence of the acoustic field facilitates the long-term microscopy of cell-cell interactions, such as studying the response of natural killer cells[93]. Standing wave acoustic traps can also greatly assist in the formation of 3D cell cultures, which more closely resemble *in vivo* conditions than conventional monolayer cultures[94,95].

Advanced transducer arrangements, such as those developed by Glynne-Jones, Démoré *et al.*[85,96], can allow for more localised trapping in the typical standing wave cavity by having a 1D array of individually addressable active elements along the length of the cavity and switching the elements off or on. This provides a far more dextrous system than typical standing wave designs, however the manipulation of single cells is still not typically within the realms of acoustic trapping in this case.

Oberti *et al.* used an ultrasonic transducer to manipulate particles in a droplet on the surface of the transducer[97]. In this configuration the standing waves are set up at the fluid-air interfaces. Alongside the many trapping geometries presented, this also allows direct access to the material inside the droplets, opening up new possibilities for the probing of cells which is not usually possible in cavity type designs.

As mentioned previously, optical trapping can be used as a molecular force sensing tool, however it can become limited by scalability. As acoustic trapping can exert forces across a sample volume, it follows that this scalability could be exploited in a force sensing method. Sitters *et al.* demonstrated such a device, exerting forces on thousands of biomolecules simultaneously[98]. A DNA molecule is attached by one end to the top of a microfluidic chamber, and to a microsphere on the other end. When a standing wave is generated across the chamber, the microsphere is attracted to the node, and stretches the DNA molecule. The degree of defocusing of the microsphere gives information on how much the DNA molecule is stretched, and hence the forces present. This technique demonstrates well the scalability of acoustic trapping, and how it differs in, yet compliments the limitations present in optical trapping.

2.5 Hybrid manipulation

The integration of two or more manipulation techniques is often hindered by the difference in experimental requirements of the respective techniques. In recent years, novel developments have made the hybridisation of trapping techniques much more feasible, for example, the development of optically transparent ultrasound transducers[99].

When dealing with the term 'hybrid', it is first prudent to define exactly what is meant be a 'hybrid' system. The first issue to consider is serial and parallel processes. A serial process would have each sorting technique one after the other, whereas a parallel process would have the different techniques acting on the particle at the same time. A serial hybrid system should not be considered, as it becomes a trivial matter to place one sorting technique after the other.

Simply defining it as 'a combination of two parallel sorting modalities' is somewhat misleading. With such a definition, when used in flow, many manipulation methods could be considered hybrid modalities as one must deal with the drag and gravitational forces present in all microfluidic systems. This definition of a hybrid system to include inertial forces is unhelpful, therefore a more specific definition is required. For the purposes of this work, a hybrid system shall be defined as '*a system comprising two or more externally applied fields working in parallel to manipulate an object*'.

Although not a hybrid technique as such, the technique described by Chiou *et al.,* 'optoelectronic tweezers'[100], has led to some hybrid technique development (Figure 2-10). Optoelectronic tweezers relies on the dielectrophoresis being triggered by selective illumination of a photoconductive layer. When the photoconductive layer is illuminated by the incident light, virtual electrodes are turned on, enabling particle manipulation via

the resulting non-uniform electric fields. The group demonstrated the creation of 15,000 particle traps, a virtual conveyer belt, and the selective trapping of live and dead cells. One of the great advantages to this technique, aside from the vast reconfigurability of the trapping geometries, is that the incident light used can be as low as 100,000 times less than that needed for optical tweezers. The use of a low magnification objective to relay the light pattern on to the photoconductive layer allows for a very large manipulation area compared to optical tweezers.

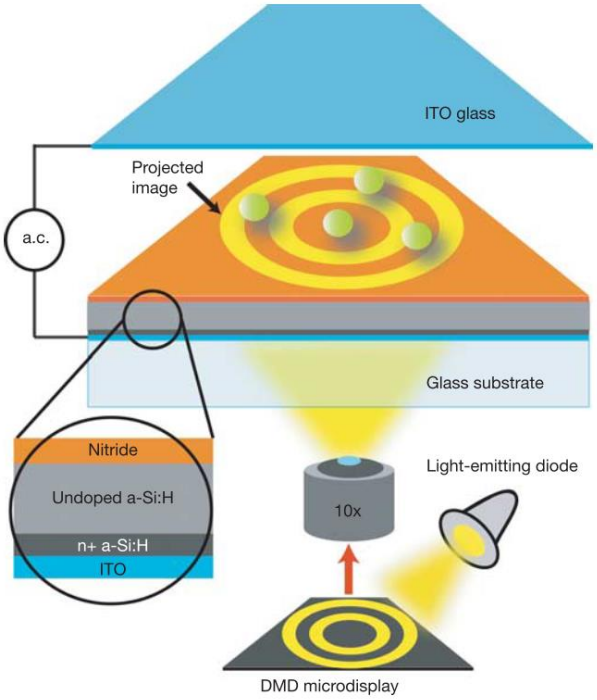

Figure 2-10. The photoconductive layer is illuminated by the light pattern, and creates dielectric traps in the sample corresponding to the input light pattern. Image sourced from Chiou *et al* [100]

A similar method has been used to separate PC-3 cells from leukocytes, by scanning a bar of light across the photoconductive layer[101]. The difference in size between the cells prompted a different response in the resultant electric field experienced. The light bar

was first scanned to one side of the channel at a velocity of 67.3 μms^{-1} to drag all of the cells to one side of the chamber. The bar was then scanned to the other side of the chamber at a faster rate, 150.8 μms^{-1}, such that only the PC-3 cells experienced enough force in the smaller exposure time to move with the bar.

Optoelectronic tweezers have also been used for selective cell lysis[102]. The method relies on the 'electrical shadow' cast by the cells, which affects the electrical potential beneath it. This was demonstrated with RBCs and WBCs, where their differing shapes caused a change in the electrical field concentration around them. RBCs were shown to cause wide deflections of the electric field, and subsequently increase the electrical field at their edges resulting in cell lysis, whereas the effect of increasing the electrical field around the WBCs was less pronounced. Like the design in Figure 2-10, this method was shown to work over a large field of view, allowing the processing of thousands of cells simultaneously.

In the context of a hybrid system, selective cell lysis by optoelectronic tweezers has been enhanced by the addition of acoustic trapping[103]. The mechanics of lysis remain the same, however the cells are flowed through a microfluidic channel, where acoustic trapping confines the cells to a single stream in the centre of the channel. This allows all of the cells in the flow to be affected by the optoelectronic tweezers, while under the influence of the acoustic forces. The method is shown to achieve a lysing efficiency of >99% for sample concentrations of 10^6 cells/ml.

Acoustic trapping has also been used in combination with DEP, where DEP can produce trapping in directions not easily possible in standard half wave resonance designs. Neale *et al.*[104] used DEP to hold 10 μm particles in a line orthogonal to the channel walls against fluid flow, and then used acoustic trapping to move the particles to the acoustic node in the centre of the channel, thus forming a dense aggregate at a precisely located node. As

both DEP and acoustic trapping are dependent on particle size (Equations 2.1 & 2.8), it is possible to use this method to sort between differently sized particles.

Thalhammar *et al.* demonstrated the combination of acoustic and optical trapping, utilising the large scale trapping abilities of acoustic trapping and the precision, selectivity and flexibility of optical tweezers[105]. The setup involved using 'optical macro-tweezers', a technique that allows greater field of view and working distance than conventional high NA optical trapping. The trap is formed by reflecting a loosely focused beam off of a mirror, back into the sample chamber, effectively forming a counter-propagating trap, but with only one beam. Acoustic trapping is achieved by fixing a ceramic piezo transducer to the top of the chamber, as the opposing face of the chamber is no longer needed for beam access, as in typical dual beam setups.

Using this system, they were able to acoustically confine a sample of micro-organisms to a common plane, and then selectively optically trap an individual organism and move it laterally across the levitation plane. The large field of view allowed for a relatively large displacement (1 mm) of the micro-organism compared to many high NA optical systems.

The group also demonstrate active particle sorting. In this application, polystyrene beads in flow are trapped acoustically in a single plane in the centre of the capillary, and subsequently reach a point in the capillary where a separate transducer is driven to create three nodal planes. The particles can then be selectively deflected between the nodes from the radiation force of a loosely focused optical trap.

2.6 Synopsis

Methods of non-contact manipulation have been discussed, highlighting applications where the specific traits of each technique have provided a solution to a problem. It is proposed that using a hybrid system of parallel applied fields, more flexible systems can be engineered. Such hybrid systems have been discussed, with some key methods having only been developed in the past few years.

The design of a system to ultimately handle the sorting of blood cells requires consideration of all facets of the techniques available. Tagging techniques are ruled out due to subsequent *in vivo* use, as are active techniques due to the inherent lack of scalability. Techniques based on the inertial forces of the fluid itself often do not offer as reconfigurable a toolbox as techniques using applied fields, and can suffer from a lack of selectivity. Therefore sorting techniques using applied fields are of primary interest here. Sorting based on a wide range of parameters is desirable, and as such optical and acoustic sorting are chosen as two techniques that offer: a wide range of sorting parameters; the possibility of hybridisation; scalability; and a contrasting approach of both large area manipulation and specificity when used in a hybrid configuration.

The two contrasting yet complimentary techniques, optical and acoustic trapping, have been discussed in detail, highlighting key areas in which the two techniques could work together in a hybrid system. The work in this thesis will investigate the application of optical and acoustic trapping into different separation techniques, focusing on the balancing of radiation and gradient forces in such methods. The intention here is to devise a technique whereby the sorting parameters are much less dependent on fluid drag, and therefore are controlled by forces, e.g. optical or acoustic, which will lend itself better towards scale up of the process for large scale sorting applications.

3 ACOUSTIC MANIPULATION

3.1 Introduction

An important factor when considering hybrid optical and acoustic sorting is the environment in which the sorting will take place. This environment will affect how well sorting techniques can be integrated together, the efficacy of each sorting technique, and how well any sorting can be observed and quantified for example. For this, it is necessary to design a microfluidic chip which accommodates the simultaneous use of both optical and acoustic manipulation.

This chapter will detail the fabrication process for the microfluidic chip used throughout the work in this thesis, and will also demonstrate the acoustic manipulation capabilities of the chip. This is expanded in to a novel approach to acoustic trapping in glass capillaries, whereby air bubbles in the fluid cavity can act as acoustic reflectors thus providing discrete 3D acoustic trapping.

3.2 Chip design

Many different configurations of manipulation environments exist. The design of such an environment for the work carried out in this thesis consisted of the following fundamental principles: the chip must have all planes of optical access, such that optical manipulation and imaging could be achieved in whichever axis required; the chip must incorporate acoustic manipulation without obstruction to optical accessibility, in order to

perform simultaneous optical and acoustic manipulation if desired; the chip must accommodate fluid flow; and the chip should leave a small footprint, such that it is simple to integrate into existing optical systems with little to no need for re-adjustment.

With these principles in mind a disposable chip was constructed, similar in design to that demonstrated by Hammarstrom *et al*[106], schematically shown in Figure 3-1, Figure 3-2 and pictured in Figure 3-3.

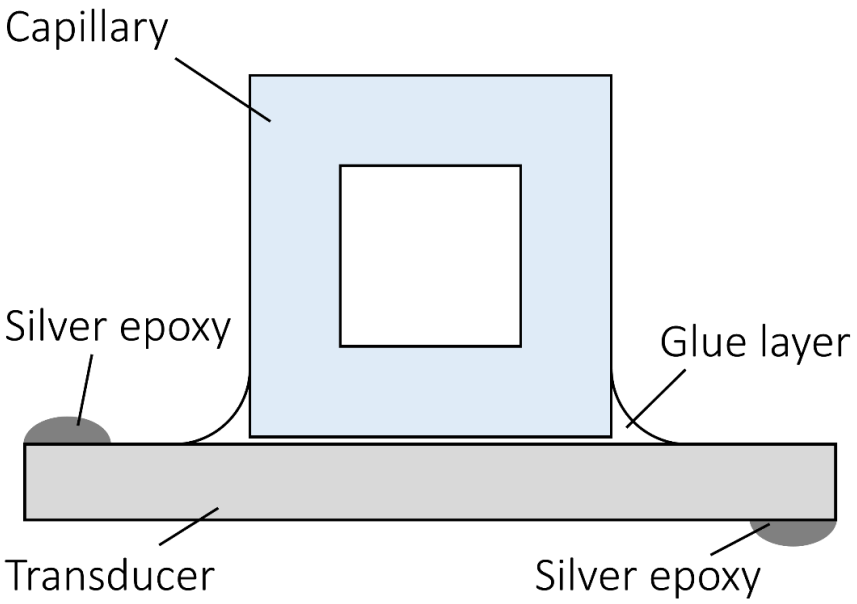

Figure 3-1. The capillary is glued flat to the transducer, while the silver epoxy is used to connect wires to drive the transducer.

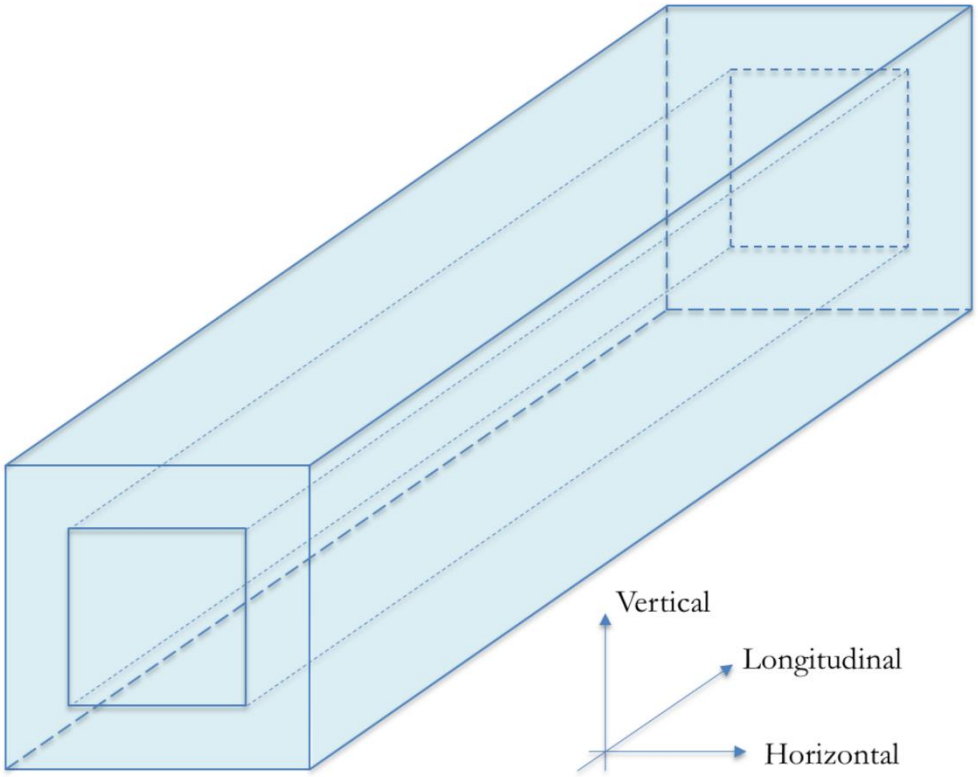

Figure 3-2. Axis system defining directions corresponding to the capillary as referenced in the text.

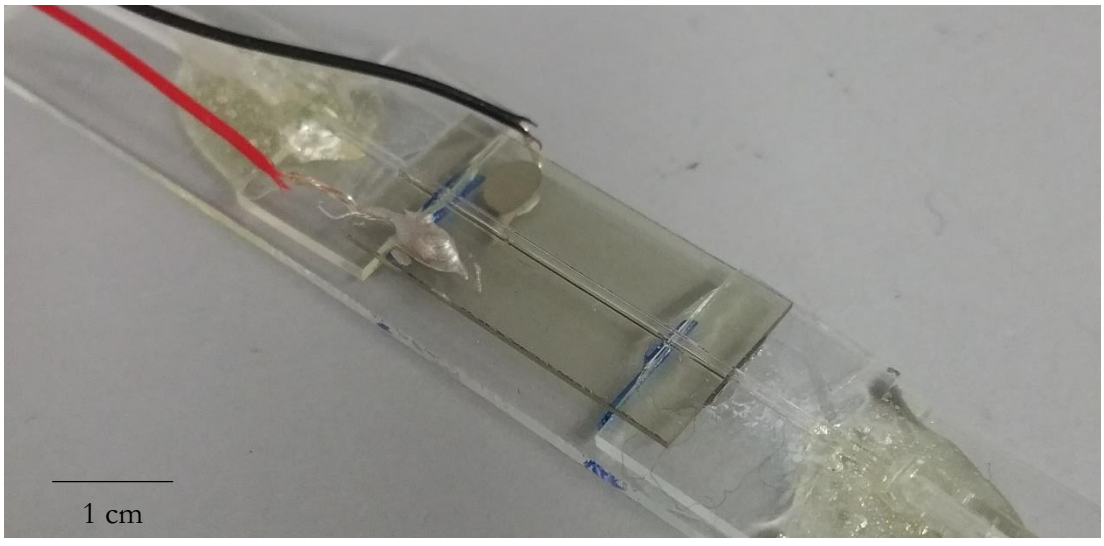

Figure 3-3. A photograph of the resultant chip. The glass capillary can be seen across the centre of the transducer, glued to the transducer to fix it in position and to conduct the acoustic waves. The red and black wires are fixed with silver epoxy to opposing sides of the transducer, and the whole design is structured around a glass scaffold.

The transducer is glued on to a glass scaffold with an air backing to dampen unwanted acoustic resonance. Wires are fixed to either face of the transducer with a two part silver epoxy (Agar Scientific, AGG3349). This is achieved by mixing equal parts of the two part silver epoxy, and placing a blob of this mix on either side of the transducer, as shown in Figure 3-3. The wires are then inserted in to each blob of the silver epoxy and taped in place such that movement is restricted during curing. To cure the silver epoxy, the device is placed on a hot plate set to 50°C, and is left to cure for 20 minutes as per the manufacturer guidelines. A glass capillary is then glued to the surface of the transducer. The glue serves a dual purpose by acting as an adhesive and as a conductor for the acoustic waves. Lengths of 0.8 mm inner diameter tubing (Tygon® E-3603, Saint-Gobain) are glued into place around the ends of the capillary such that a sealed flow chamber is created. The individual constituents of the chip will be discussed in more detail in the following sections.

3.2.1 Optical properties of the chip

Optical access is an important factor in a chip that is designed to be integrated in to optical manipulation systems. To better integrate this feature into the design of a microfluidic chip with acoustic capabilities, a transparent transducer developed by Brodie *et al*[99] will be used. This Indium Tin Oxide (ITO)-coated Lithium Niobate (LNO) transducer was developed specifically with optical manipulation in mind, whilst still allowing all planes of optical access and facilitating simultaneous optical and acoustic manipulation.

The transducer has been shown to have comparable optical transmission compared to uncoated LNO, as shown in Figure 3-4[99]. The range of optical transparency not only allows imaging through the transducer, but also facilitates optical manipulation at IR wavelengths e.g. 1064 nm.

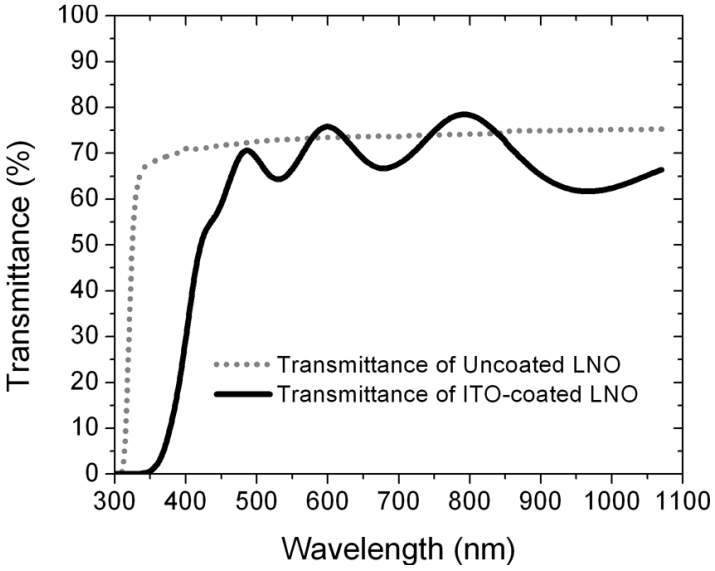

Figure 3-4. The transmittance of the LNO-ITO transducer compared to uncoated LNO over a range of wavelengths, as measured by Brodie. Image sourced from Brodie *et al* [99].

The transmission of 1064 nm through the LNO-ITO transducers was tested firstly to verify the results found by Brodie *et al* for the transmission of 1064 nm laser through the LNO-ITO transducer, and also to investigate any effects the transmission of a laser beam of increasing power may cause. It can be seen in Figure 3-4 that there is an apparent fluctuation in transmittance with increasing wavelength, and while of little significance when using only a single wavelength laser beam, it is of interest to verify whether or not this fluctuating pattern is also present when dealing with a laser power dependence as opposed to a wavelength dependence. At least some of the energy lost in transmission will be converted to heat, and the concern is that any change in temperature of the

transducer may affect the transmittance. A laser beam is increased in power from 10 mW up to 100 mW in 10 mW increments, and the power of the laser recorded both with and without a LNO-ITO transducer in the path. Our results, Figure 3-5, show agreement with the previous results, with a transmission of approximately 67% which is also consistent for a range of increasing laser powers. This is significant as the transmittance must be taken into account if performing optical manipulation through the transducer, and also helps to show that there is no change in transmittance due to laser absorption in this power range, and any subsequent heating of the transducer. Laser powers higher than 100 mW were experimentally observed to cause structural degradation of the glue used to bond the transducer and capillary, hence only powers up to 100 mW were tested and it is recommended that if one is applying larger laser powers that the chip be oriented such that the laser does not pass through the transducer, as in Chapter 5.2.

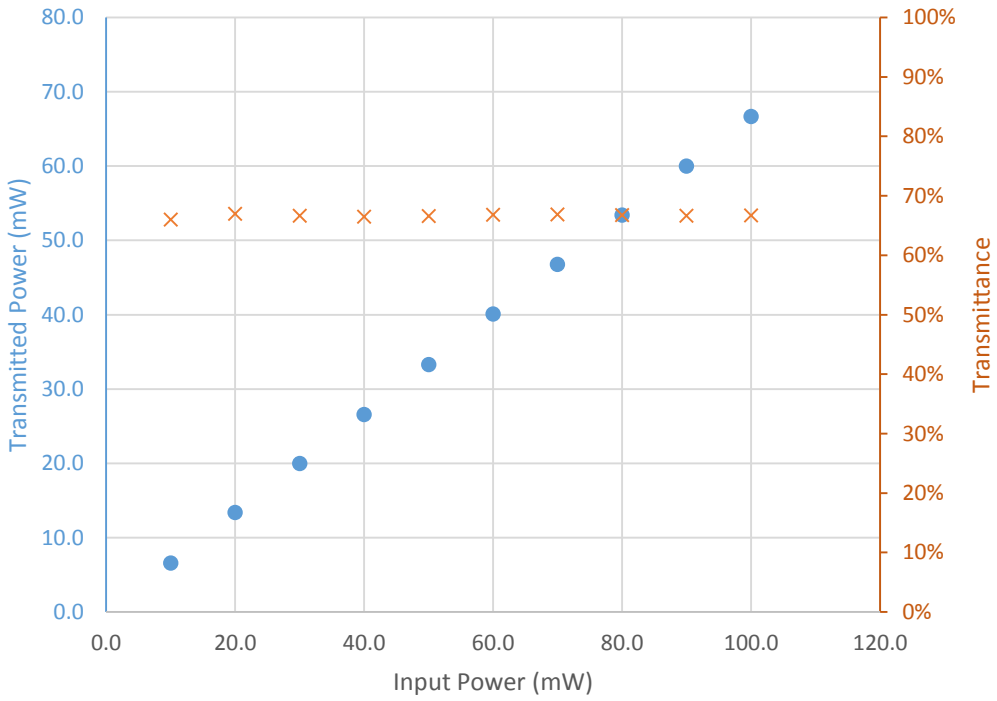

Figure 3-5. The optical transmission of the LNO-ITO transducer is shown to be constant at 66% for laser input powers up to 100 mW.

3.2.2 Acoustic resonance in the chip

In the simplest case, the frequency at which a standing wave can be produced in a channel is dictated by the speed of sound in water v, and the wavelength λ of the acoustic wave (Equation 3.1).

$$f = \frac{v}{\lambda} \tag{3.1}$$

The wavelength of the fundamental mode is equal to twice the distance between channel walls. Driving the transducer at the fundamental frequency related to the channel dimensions will produce a single node at the centre of the channel. Thus it is important to choose the dimensions of the channel to match the properties of the chosen transducer. For the ITO-LNO transducers, Brodie *et al.* recorded a peak acoustic resonance at 6.498 MHz, corresponding to a half wave resonance, or inner channel dimensions, of (114x114) μm.

Glass capillaries are easily fixed to a transducer, and suit the design of a small, simple chip[106]. When fabricating the chips, it was found that glass capillaries with an inner dimension of (100x100) μm (close to the peak resonance of the transducer) were susceptible to breakage during the fabrication process, and the glue used to bond it to the transducer would be drawn up the sides of the capillary due to surface tension, obscuring access from the side. (300x300) μm inner dimension capillaries were found to be a good compromise between durability in the fabrication process, and the ability to produce a range of resonant modes within the operating range of the transducer. In order to achieve acoustic trapping for such a capillary at the fundamental mode, the system would need to

be driven at 2.47 MHz. Although outwith the peak resonance of the transducer, trapping is still possible, and it leaves room to investigate higher harmonics.

The wall thickness of the (300x300) μm capillary is 150 μm. It is possible in these capillaries to create a standing wave not only between the inner walls, but also between any combination of inner and outer walls, as illustrated in Figure 3-6.

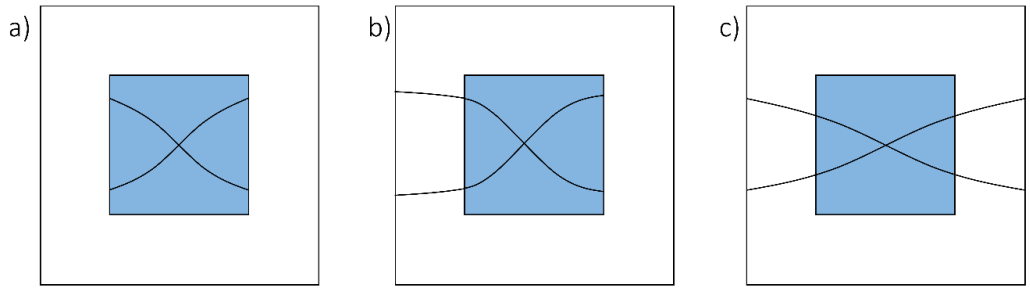

Figure 3-6. Illustrated here are the possible configurations for creating a standing wave between the opposing pairs of reflective surfaces, with a) between the inner channel walls, b) between an outer and inner wall, and c) between the two outer walls.

In practice, this means that to achieve trapping or confinement in a desired number of nodes, there are several frequencies one could drive the system at. This is calculated by Equation 3.2, where $d_{f,w}$ is the distance the wave must travel in each medium, and $v_{f,w}$ is the velocity of the wave in the fluid cavity and channel wall respectively, and shown for the 1st, 2nd and 3rd harmonics in Table 3-A.

$$f = \frac{1}{\left(\frac{d_f}{v_f} + \frac{d_w}{v_w}\right)} \tag{3.2}$$

Harmonic	Resonant frequency between inner walls (MHz)	Resonant frequency between inner/outer wall (MHz)	Resonant frequency between outer walls (MHz)
1st	2.47	2.21	1.97
2nd	4.94	4.41	3.95
3rd	7.41	6.62	5.92

Table 3-A. This table gives an approximate numerical solution to the frequencies that one might expect to produce the associated harmonic, based on Equation 3.2 for the different possible pairs of reflective surfaces.

Table 3-A is calculated using Equation 3.2. The speed of sound in the fluid and capillary walls are constant at 1482 ms^{-1} and 5640 ms^{-1} respectively. The distance the acoustic wave must travel through in the fluid is equal to the width of the inner dimensions, 300 μm, and the in the channel walls is equal to the channel wall thickness, 150 μm. The three examples in Table 3-A represent the three examples pictured in Figure 3-6, firstly when the resonance is achieved only in the fluid volume, secondly when resonance occurs throughout the fluid volume and one of the channel walls, and lastly when resonance occurs throughout both channels walls and the fluid.

One result of setting up the standing wave trap between an inner and outer surface, is that the positions of the nodes will shift, relative to if resonance was achieved between the two inner channel walls. As illustrated in Figure 3-6b, if part of the standing wave is travelling faster through the glass, the whole standing wave is shifted, and becomes asymmetrical in that axis. If the standing wave is created between the two outer walls, then the node will remain at the centre of the channel.

In an acoustic resonator, the nodal position is defined as the position the sound wave reaches at t/2, between the reflective surfaces for the fundamental resonance. The position of the node from the inner channel wall in this case can be calculated using Equation 3.3, where d is the distance of the node from the inner channel wall, $d_{f,w}$ and the widths of the fluid cavity and the channel walls respectively.

$$d = \frac{v_f}{2}\left(\frac{d_f}{v_f} + \frac{d_w}{v_w}\right) \tag{3.3}$$

In the case of first harmonic resonance between an inner and outer wall, as shown in Figure 3-6b, the node will sit 170 μm from the inner channel wall, or 20 μm off centre. As this is dependent on the speed of sound in the chosen fluid, the position of the node in this case will shift towards the centre of the channel if the speed of sound in the fluid is lower than water, and vice versa for a higher speed of sound in the fluid.

3.2.3 Thermal analysis

As shown by Brodie *et al.*, the resonant frequency of the LNO-ITO transducers we are using is found to be 6.498 MHz. In achieving first or second harmonic resonance in the (300x300) μm capillaries (Table 3-A) that have been proposed previously, the transducer will be driven at frequencies out with its peak efficiency. Although this means that more of the power input from the function generator will be dissipated as heat, it is necessary to drive the transducer at these frequencies to achieve stable and useful acoustic resonances for sorting. Although general rises in temperature are manageable, by using a refrigerated chamber for example, localised thermal gradients in the capillary could cause problems with the stability of the acoustic trapping. Thermal analysis of the chip is also prudent when considering potential implication with blood cells. It has been reported that haemolysis is induced in RBCs at temperatures of 48-50°C[107]. It is thus important to analyse one of our chips as a whole, and find where any localised hot-spots or thermal gradients may occur, and if heating of the chip has potential to impact upon RBC survival rate.

To measure the heat distribution, a combination of thermal imaging and thermocouples is used. A chip is spray painted matt black as it allows calibration of the thermal camera (FLIR i7) with a known emissivity. Five thermocouples (Type T, Omega) are also fixed in position on the surface of the chip to measure the surface temperatures at various points, as shown in Figure 3-7. Type T thermocouples typically are used for differential temperature measurements, like the work presented here, and have a known relationship between voltage and temperature of 43 μV °C^{-1}.

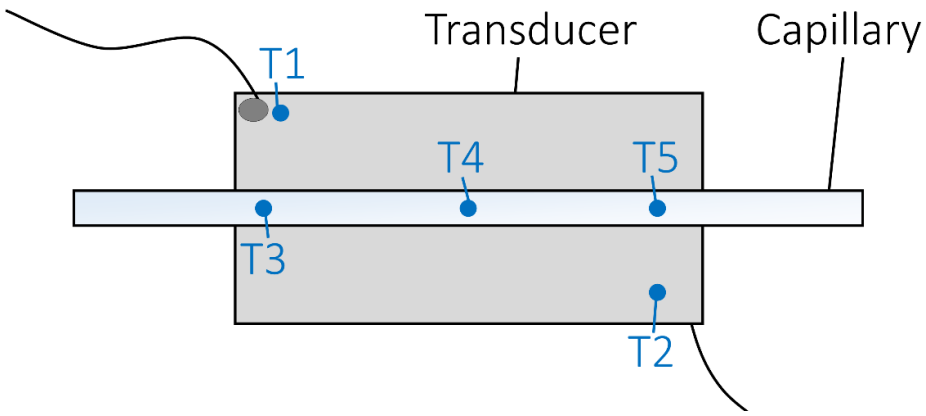

Figure 3-7. Thermocouples are fixed at points T1-5 on the chip to give the temperatures at various points on the chip as it is driven with increasing powers.

A custom LabView program is written to acquire temperature readings from each of the thermocouples in real time. A sixth thermocouple is added to measure the ambient air temperature. In practice, acoustic resonances are most conveniently found by scanning around a theoretical value of the frequency until particle trapping is observed. Throughout the acoustic experiments carried out, 2.15 MHz was often found to give a strong fundamental resonance. For this reason, a signal generator (Rigol DG4102) is run at 2.15 MHz, and initially at 2 Vpp. Although other resonances are found in the course of this work, this low frequency value will give the strongest contrast in terms of power lost to heat to driving the transducer at its peak resonance. The temperatures are allowed to settle, and readings taken for each thermocouple. There is an inherent error of ±0.5°C in each thermocouple reading as stated by the manufacturers. The amplitude is then increased to 4 Vpp, and the process repeated. This is carried out for 2 Vpp to 20 Vpp in 2 Vpp intervals.

The same procedure is carried out on the same chip for a driving frequency of 6.489 MHz, the peak resonance of the transducer. The expectation is that driving the transducer at the peak resonance will produce less heat than driving at 2.15 MHz.

The thermal camera does not have a high enough resolution to read radiometric data for individual points, however it can give a reading for the maximum surface temperature of the chip at each acoustic power and frequency.

As the thermocouples only read the surface temperature by conduction, it is reasonable to assume that due to heat losses there is a significant error in the readings compared to the actual surface temperature, and that this error will be proportional to the difference between the ambient and measured temperature. The thermal camera shows that the temperature across the surface of the chip is reasonably uniform, so to give a more accurate result the readings are stretched out under the assumption that the thermocouple with the highest readings will be close to, if not the same as the peak reading on the thermal camera. The thermal camera has a much lower margin for error as it is reading the infrared radiation from the surface using a known emissivity (0.98) for the black paint on the chip. The resultant temperature rise for each data point is calculated using as shown in Equation 3.4, where T_n is the temperature of the numbered data point, T_{amb} is the ambient temperature, T_{cam} is the temperature measured from the thermal camera, and T_{max} is the maximum temperature recorded from the thermocouples $T_{1\text{-}5}$. As the interest lies in measuring temperature differences and interpolating the results with respect to the data from the IR camera, further calibration is not necessary. The results for each frequency are plotted in Figure 3-8 and Figure 3-9. The error in each measurement is also adjusted for this data manipulation. Full data is given in Appendix A.

$$(T_n - T_{amb})\frac{T_{cam}}{T_{max}} \tag{3.4}$$

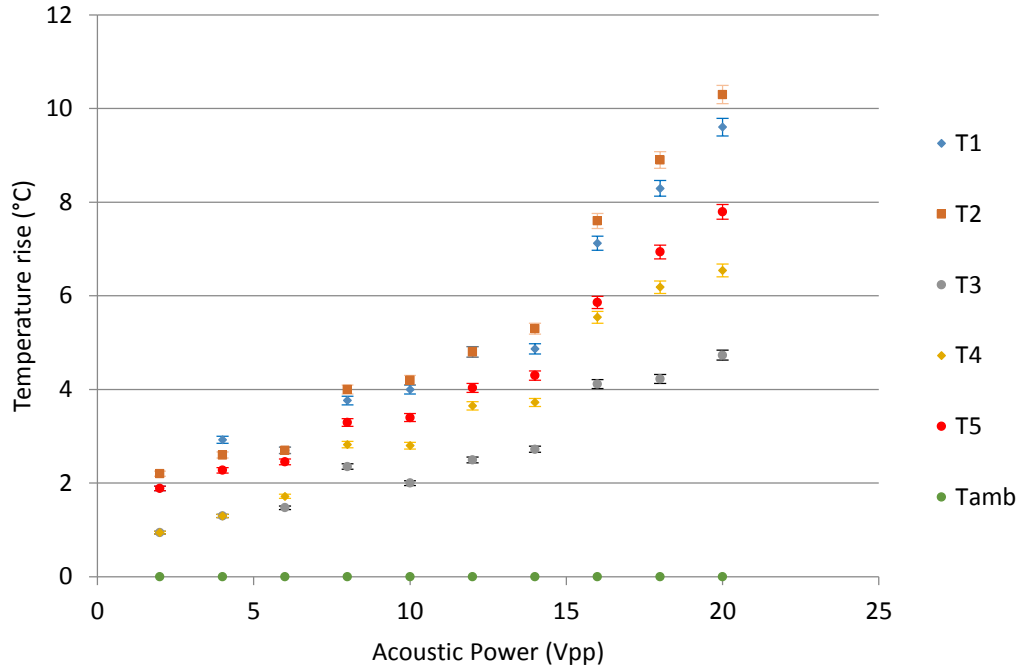

Figure 3-8. Driving the transducer at 2.15 MHz. The temperature rise relative to the ambient temperature is plotted. An exponential trend is noticeable, with points T1 and T2 showing the highest temperatures.

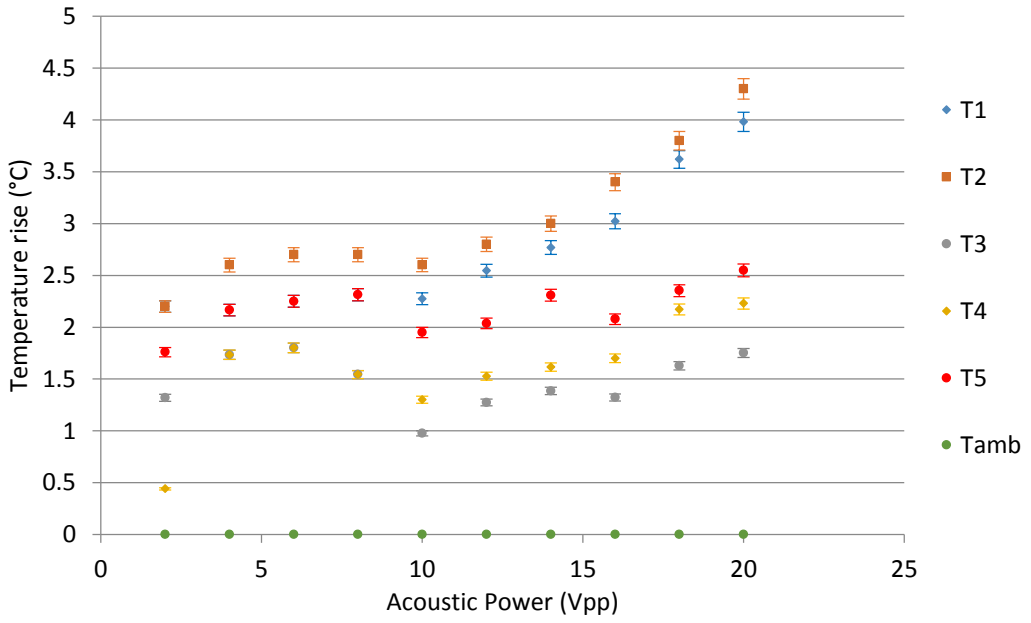

Figure 3-9. Driving the transducer at 6.498 MHz. The temperature rise at the resonant frequency of the transducer. A trend less noticeable in some points, however at T1 and 2 there is a noticeable rise after 10 Vpp.

When driving the transducer at either frequency, a general rise in temperature is noted. As expected, the temperature rises are much less when driving at the resonant frequency of 6.498 MHz. An exponential increase in temperature as the power is increased is expected given the general relationship between power and voltage.

This is best clarified by observing the results shown in Figure 3-8. This proportional relationship is much less pronounced in Figure 3-9, however this is in part due to the small temperature readings and the inherent error in the thermocouple readings.

The hottest readings on the thermocouples are from the thermocouples positioned near the wire contacts, suggesting the heat is generated at the contacts, and is dissipated throughout the rest of the transducer or dissipated into the surrounding air. This would cause a temperature gradient across the device.

For the readings across the capillary when driving at 2.15 MHz, at acoustic powers of 8-12 Vpp there are small temperature differences between the points, as can be seen in Figure 3-8. The maximum difference is apparent at 12 Vpp where there is a temperature difference of 2.3±0.17°C between points T2 and T3. At a more localised level this could cause significant problems, however as the temperature gradient is spread out across the capillary, any heating generated from the transducer itself is considered negligible. In terms of cellular damage to RBCs, such temperature rises are also considered negligible. This experiment was carried out once, however the relative magnitudes of the temperature gradients found do not necessitate further experimentation and are satisfactory for this analysis.

3.2.4 Alternative flow chambers

Throughout this body of work, challenges arose that required some re-thinking of the chip design in some cases. Although generally designed around the same principles, some concessions were made for reasons of clarity or functionality.

One of the biggest challenges encountered when dealing with high-powered lasers in large volumes of fluid is thermophoresis. Caused by the localised heating of fluid, thus creating convection currents, thermophoresis has the potential to overpower optical forces, particularly when working with low NA trapping objectives. This became an issue in both Chapters 4 and 5, when dealing with large area, high power optics. Trying to bring particle manipulation away from the surface in the (300x300) μm capillaries became increasingly challenging due to the effects of thermophoresis. These effects were mitigated by using a smaller capillary due to the reduction in thermal gradients produced by laser absorption in the fluid. As Chapter 4 deals with purely optical force balancing, a transducer was not required, so this allowed for the use of the (100x100) μm capillary as a flow chamber without attaching a transducer, circumventing the fabrication issues discussed previously.

3.3 Acoustic manipulation

Having constructed a simple half-wave resonance design microfluidic chip to meet the requirements as set out in Chapter 3.2, the capabilities of the chip are demonstrated such that its functionality can be better integrated into the designs for a hybrid optical and acoustic sorting system.

3.3.1 2D acoustic trapping

As mentioned in Chapter 3, the frequency of the fundamental resonance of the system can be estimated by using the width of the channel as $\lambda/2$. For the capillaries of (300x300) μm internal cross-section, Table 3-A was constructed showing the theoretical driving frequencies corresponding to different harmonics and reflective surfaces. A chip was filled with a solution of 10 μm polymer microspheres in distilled water, and using the aforementioned values as a guide, different resonant modes within the capillary are demonstrated (Figure 3-10). As stated before, the acoustic resonances are best found by scanning around the theoretical values, and as such may not always exactly correspond with the predicted value.

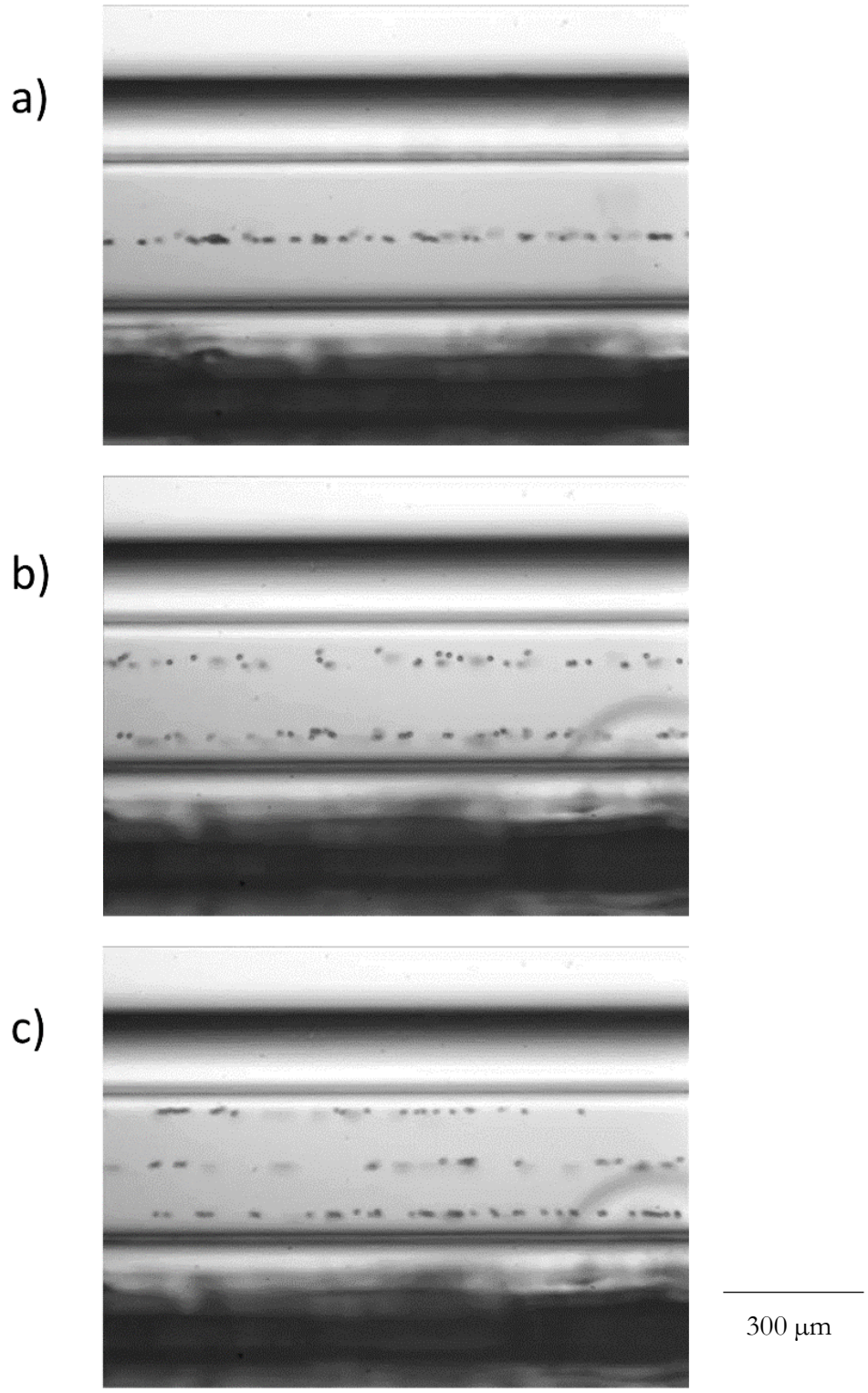

Figure 3-10. Different harmonics are shown by trapping particles in the resultant acoustic fields, with corresponding frequencies of a) 2.43 MHz, b) 5.37 MHz and c) 7.21 MHz.

3.3.2 3D acoustic trapping with bubble-bounded resonance

Standing wave acoustic traps have found success in many different applications, such as cell sorting[108–111], patterning[112] and culture in suspension[113–115]. In order to achieve more localised trapping, usually one must employ an alternative transducer arrangement, for example changing the transducer shape and bonding points to form longitudinal modes in the capillary[116], or by using a multi-element array to manipulate particles along a capillary[85]. While these methods have their own advantages, each serves to increase the complexity of the physical system in order to increase control.

Micro-environments have also been devised previously in different modalities for many different applications, including acoustically levitated droplets for studying enzyme kinetics[117], using surface acoustic waves (SAWs) to create acoustic counter-flow and ultrafast microfluidics[118,119], and high-throughput and low-reaction volume biology[120]. Some of these methods, however, are in open systems, and as such are potentially subject to contamination and evaporation. Others are restricted by geometry and as such can lack in reconfigurability and dexterity. A closed system in which control over particles or cells in a small volume is possible without contamination could be very useful in some biological applications, whilst maintaining adequate control over the particulate.

In the acoustic manipulation devices described in this chapter, the channel walls are used as reflectors that create the standing wave. This is shown in Figure 3-10. It is also possible to use an air-water interface as a reflector. By having a small volume of water in between two air pockets, it is possible to achieve a longitudinal resonance, leading to longitudinal acoustic trapping with respect to the channel. If the geometries of the channel height and

width and the distance between the air pockets match up, discrete acoustic nodes can be formed by the combination of lateral, vertical and longitudinal acoustic trapping.

These bubble-bounded cavities are produced by periodically injecting air bubbles into the fluid flow using a syringe. The fluid flows into the glass capillary, where it is observed with a 5X long working distance (LWD) objective (Mitutoyo). The transducer is driven by a function generator (DG4202, Rigol) at 4.34 MHz, which is empirically found to give the second harmonic across the channel walls. Various lengths of fluid cavities and the resultant acoustic trapping sites are observed. These fluid cavities are shown in Figure 3-11. The particles in these images can be observed in within the red rectangles. Debris is present on the walls of the channel (particularly in the centre) and can be ignored.

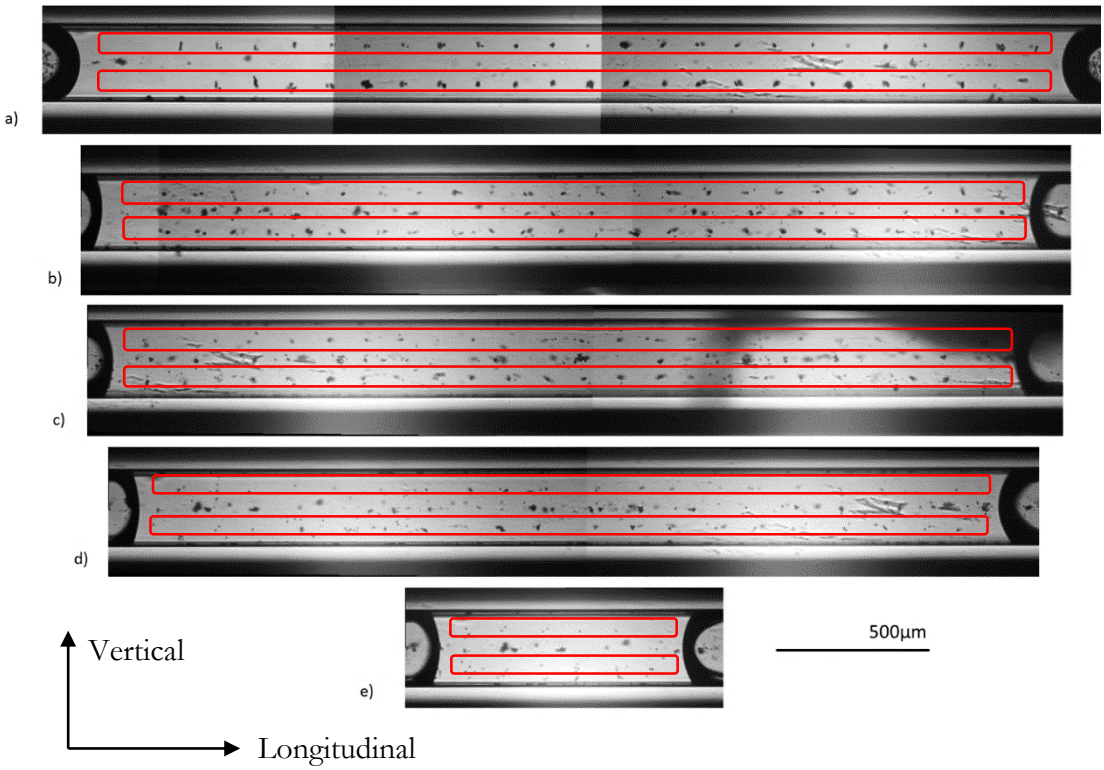

Figure 3-11. Acoustic trapping of 7 and 10 µm microspheres (in red rectangles) in five fluid cavities of lengths a) 3.88 mm, b) 3.72 mm, c) 3.61 mm, d) 3.44 mm and e) 0.97 mm at a driving frequency of 4.34 MHz. Driving the system at the second harmonic produces two acoustic trapping planes across each pair of channel walls, while the air-water interfaces produce a number of nodes across the longitudinal direction, resulting in a 3D acoustic landscape with discrete trapping sites. Debris can be seen across the centre of each image, stuck to the capillary walls. This does not affect the results and can be ignored.

The different lengths of fluidic cavities observed show varying orders of harmonics across the lateral direction. It is seen in Figure 3-11 that alongside the typical resonances found between the channel walls in a square capillary driven in this manner, there are also discrete nodes formed in the longitudinal direction. These nodes are formed between the air-water interfaces at either end of the fluid cavity, demonstrating that it is possible to achieve 3D acoustic trapping in a simple transducer and fluid chamber arrangement.

The longitudinal part of the resonance is bounded by the air-water interfaces at either end of the fluid cavity. The distance between the longitudinal nodes, 140 μm, is consistent across the images in the longitudinal direction (which is consistent with exciting a cavity mode that fits within the bubble defined boundaries).

The resonance in the bubble-bounded cavity is also observed as the channel is instantaneously switched from 4.34 MHz to 2.15 MHz, which is empirically found to give the fundamental mode between the channel walls by scanning the signal generator around the frequency level. The particles are clearly shown to move to the nodes according to the new resonant frequency, shown in Figure 3-12. This shows that the bubble-bounded resonance works as one might expect with different resonances in the same fluid cavity.

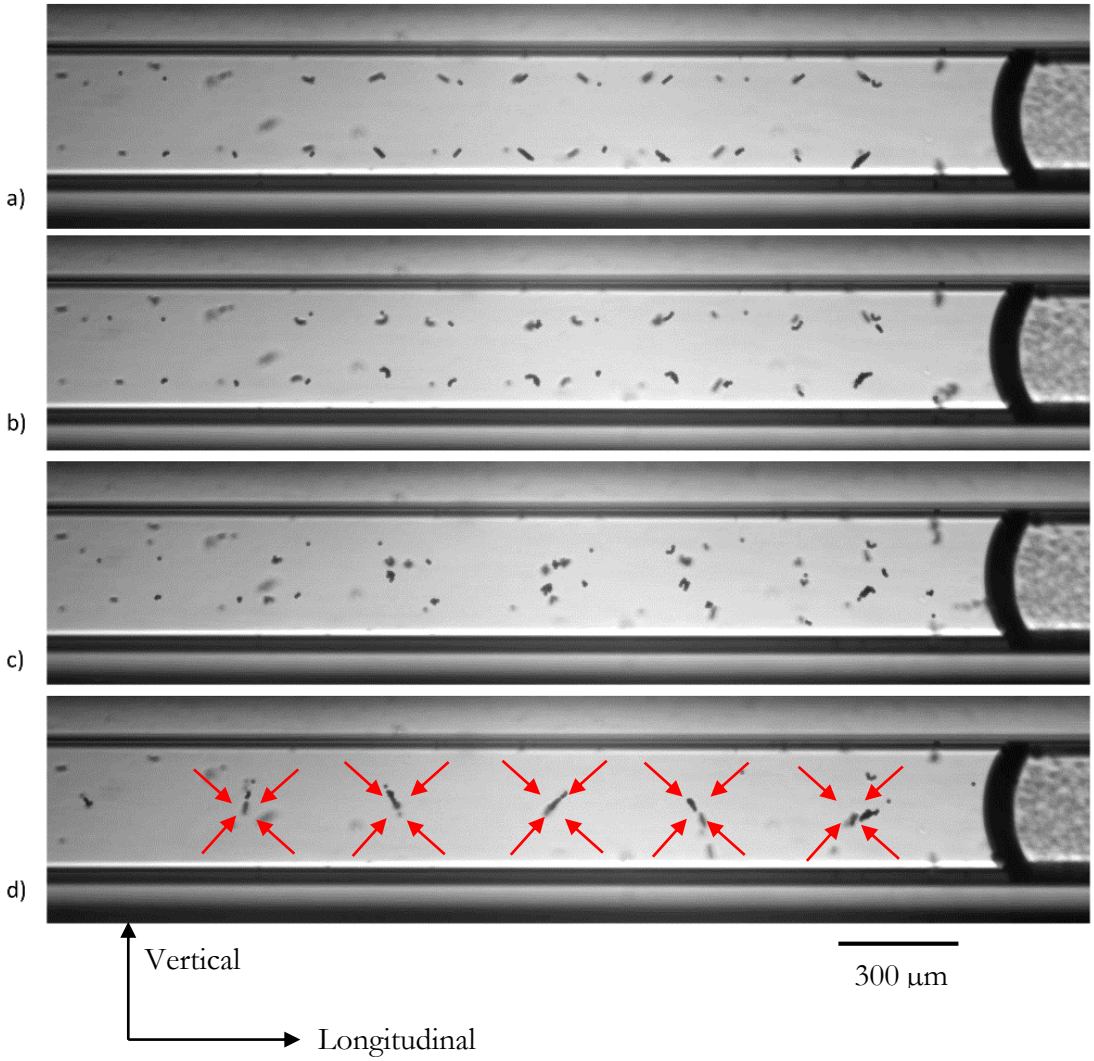

Figure 3-12. a) The transducer is initially driven at 4.34 MHz, and the nodal pattern is observed in the 2nd harmonic according to the vertical direction. The transducer is immediately switched to 2.15 MHz, the fundamental according to the vertical direction, and through b), c) and d) the particles move to the new nodal positions. The red arrows in d) indicate the direction that the particles have travelled, from their original to their final position.

The particles are observed to take different lengths of time to reach a stable longitudinal or vertical position. Ten particles from the video represented in Figure 3-12 are timed to measure the duration they take to move from their initial position to their final resting position. This was timed for both vertical and longitudinal directions, and the results show that the particles took approximately 16.6 (SD = 0.39) and 7.2 (SD = 0.58) seconds to reach a stable horizontal and longitudinal position respectively. This implies that the trapping strength in either direction is not equal, specifically that the strength of the acoustic trapping between the bubble walls is less than the trapping strengths from the resonances between the capillary walls, however this would require further investigation in order to verify.

In order to gain insight into the acoustic field and verify that the air-water interfaces of the bubble walls (in combination with the resonances between the channel walls) were responsible for the observed patter, a simplified model of the system is simulated in COMSOL, in collaboration with Peter Glynne-Jones of Southampton University.

The glass capillary is modelled as linear elastic elements, with Rayleigh damping added to account for losses in the material, and a pressure acoustics domain inside the channel to represent the water. The interest lies in the mode shapes rather than in the precise values given by the simulation, and previous work has shown this method to be a good estimate[121]. The bubble walls are modelled as acoustic free surfaces at either end of the capillary, to simulate a 3.1 mm length fluid cavity. The transducer itself is not modelled, as to reduce the computational load, but is instead represented by a boundary stress on the lower inner channel surface. A range of frequencies are simulated. A number of resonances are then found in the simulation, and the result with the highest energy density in the fluid and best matching the experimentally observed mode shapes is presented in Figure 3-13.

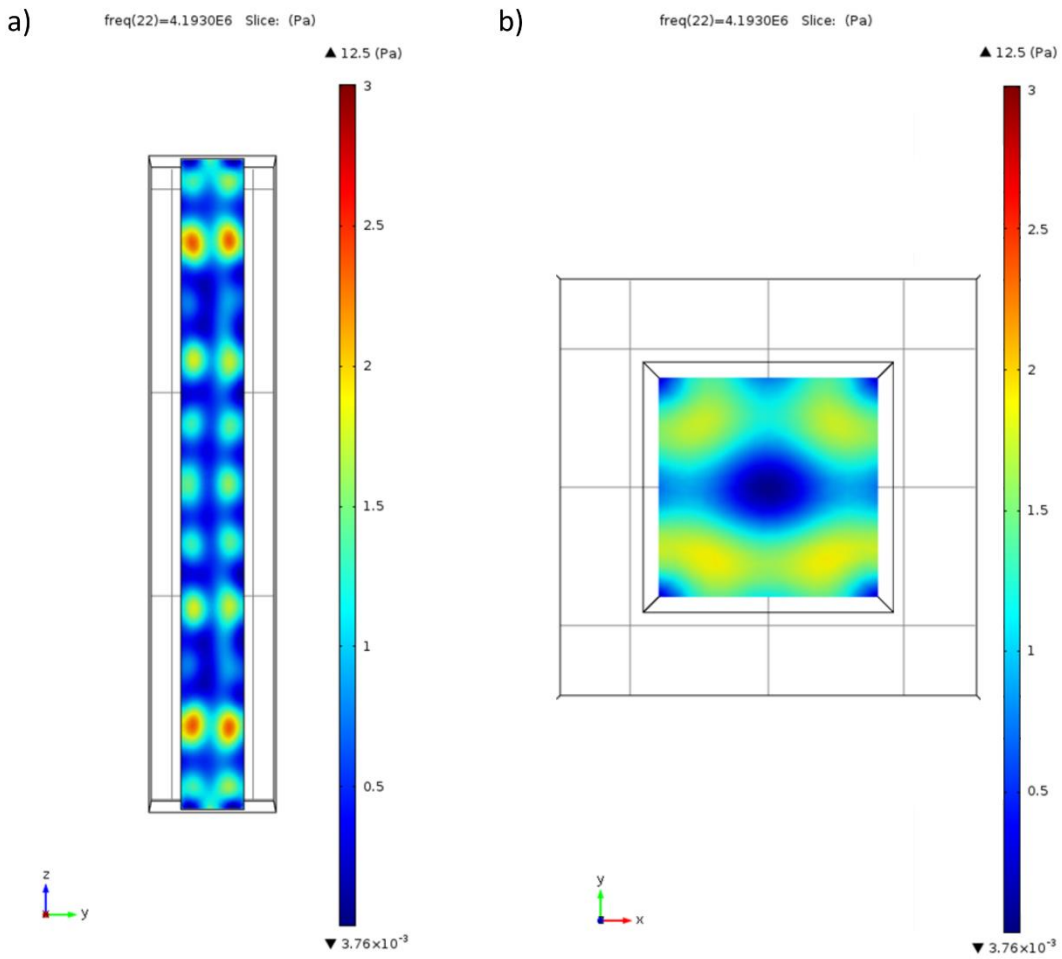

Figure 3-13. a) A top-down view of the capillary shows the discrete nodes formed across the length of the fluid cavity, while b) shows a transverse view through the fluid cavity, and a section of the acoustic field produced across the x-y direction.

The results of the simulation, shown in Figure 3-13, display a similar acoustic landscape to that achieved in the experiments. Although the resonant frequency and the number of modes in the longitudinal direction don't precisely match those of the experimentally obtained results in Figure 3-11, the simulation does give a confirmation that creating an acoustic landscape in such a manner is possible.

A more extensive simulation, involving modelling the bubble walls more closely to their actual properties, i.e. curved soft boundaries, may give further insight into the dynamics of the bubble-bounded resonance.

3.4 Discussion & conclusions

A sample environment has been designed to facilitate hybrid optical and acoustic experiments. The needs outlined in this chapter have been considered, and the end result is a disposable, simple design of a capillary glued to a transparent transducer, held in place with a glass scaffold. The design allows for quick fabrication, and although challenges were met with the small 100 μm glass capillaries, functional systems are realised with the use of a 300 μm inner dimensions capillary. Different harmonic modes are presented, which will prove useful later in the thesis.

The overall design of the microfluidic chip has provided a functional environment for carrying out much of the work in this thesis. It could be further enhanced, however, by improving the process of bonding the capillary and transducer together, and the quality of the wire bonding. Presently, the wires are bonded by application of a silver epoxy to the transducer surface, and the wire fixed in place such that the epoxy sets around the wire contact following the manufacturers recommended curing conditions (20 minutes at

50°C). The quality of electrical conductivity through the epoxy is dependent on the cure time and temperature applied to the epoxy, and as such a comprehensive study characterising the change in the conductive quality of the contacts with respect to the aforementioned variables could add some consistency and reproducibility to the wire bonding process.

The glueing of the capillary to the transducer presents challenges both for the quality of the contact, and hence the transmission of the acoustic waves, and the optical clarity due to the glue adhering to the sides of the capillary walls. Cyanoacrylate based glue is used for this as it is quick, cheap and can be easily cleaned off with acetone if need be. Over the course of the project different brands of glue were used, however through empirical observation no specific brand of glue appeared to perform better than any other in chip fabrication. In practice, the chips were found to vary somewhat in their acoustic characteristics, with some chips performing better acoustically than others. This could be due to the contact between the transducer and the capillary, or equally it could be the quality of the contacts between the transducer and the wires. In future fabrication of these chips, it is recommended to test the transducers in an impedance analyser after connecting the wires to assess the quality of the contacts. Such quality control measurements should be implemented to achieve a more reliable acoustic performance.

A simple method of achieving 3D acoustic trapping in a glass capillary is shown, using the air-water interfaces of two bubbles in the capillary as acoustic reflectors alongside the two pairs of channel walls. The resultant acoustic landscape is demonstrated by the trapping of particles in the fluid cavity, and different lengths of cavity are shown. The system was modelled in COMSOL to verify the general principle of achieving 3D trapping in this arrangement.

The bubble walls were modelled as hard boundaries, whereas in truth they are 'soft' boundaries. This could present some interesting dynamics between the acoustics and the bubble walls, however while such analysis is outside the scope of this work as the interest lay primarily here in demonstrating this effect, and would benefit from further investigation, it can be concluded that the bubble boundaries behave similarly enough to hard boundaries with respect to forming acoustic standing wave patterns between them.

It is proposed that such a technique would find use in applications such as 3D cell patterning for parallelised micro-assays or encapsulation[122]. The addition of a technique like optical tweezers, made trivial by the addition of the transparent transducer, would add an extra level of dexterity to a system that already traps particles in a localised 3D space.

4 Optical Force Balance

4.1 Introduction

As discussed in Chapter 2.3.1, the forces involved in optical trapping can generally be classified as the optical radiation and gradient forces. The radiation force exerts a force on a particle in the direction of beam propagation, while the gradient force acts axially to draw a particle into a potential minimum. For particles of higher refractive index than their surrounding medium, this is typically the beam focus. Depending on their inherent properties, particles will react differently to these forces, and it is this differing response that forms the foundation of label-free, passive optical sorting.

Although the two forces arise from the same source and as such are intrinsically connected, emphasising the effect by choosing the geometry of optical sorting it is possible to broadly classify some techniques as either using the optical radiation or gradient forces as the primary means of separation.

Similarly to acoustic trapping, optics can be used to form a potential energy landscape. In each of these modalities, particles experience a conservative force that brings them to rest at some potential minimum. In optics, the gradient force of a laser beam can serve to guide particles into a potential well, most commonly the centre of a Gaussian beam.

As discussed in Chapter 2.2.2, complex optical landscapes have been used as guides for particle deflection in fluid flow. The differing response of the particles to the optical field can act as a separation mechanism. Previous work on sorting in optical landscapes has primarily utilised a 2D approach, sorting particles or cells along a surface, however these

landscapes could be fully exploited if a means of particle manipulation throughout the three dimensional landscape volume was realised.

The work presented in this chapter will investigate the efficacy of using the optical gradient force as the main driver for separation, and will provide some insight into volumetric particle manipulation within the optical landscape.

4.2 Particle separation with an interference pattern

One way of producing an optical landscape is to use multi-beam interference. The resulting interference patterns have been shown to be useful in sorting biological matter previously[1], and the volumetric nature of the optical landscape could prove powerful when considering the scaling potential of these techniques. Initially, a multi-beam interference system is demonstrated under the premise of building up towards a volumetric approach to optical manipulation.

A multi-beam interference system, shown in Figure 4-1, is designed based on that used by Milne *et al*[123].

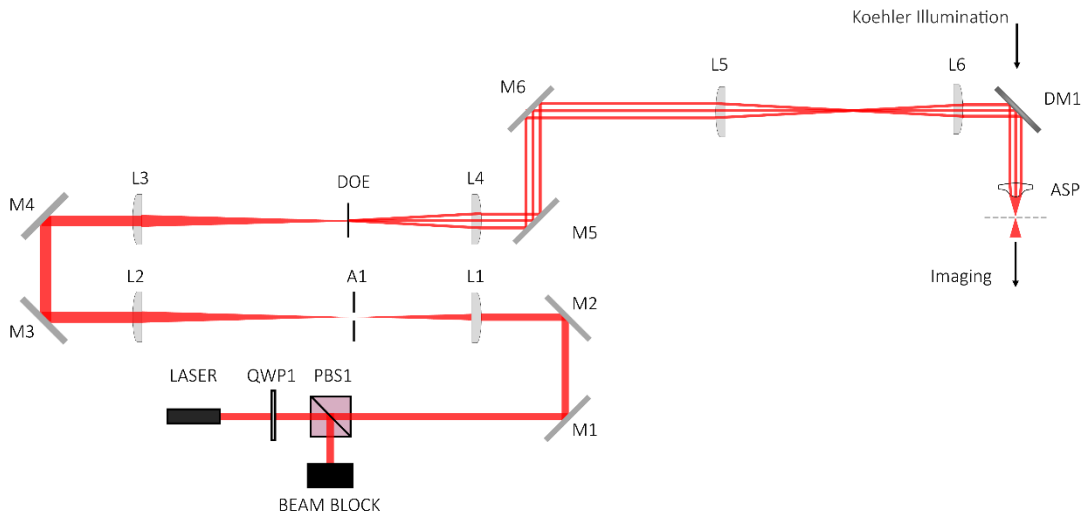

Figure 4-1. The multi-beam interference sorter. Lenses L1 and 2 act as a telescope to expand the beam, before is it focused down on the DOE by L3. L4 collimates the individual beams and the divergence of the pattern, and lenses L5 and 6 relay the beams into the aspheric lens (NA=0.25).

A power attenuator is set up with a 1064nm half wave plate (WPMH05M-1064, Thorlabs) in a rotational mount followed by a polarising beam splitter (PBS232, Thorlabs). Depending on its orientation, the half wave plate will change the linear polarisation of the laser beam to be completely vertical, horizontal, or a mix of both. This allows finer control over the power delivered to the system as opposed to operating the laser amplifier itself. The laser used is a 1064nm Fibre Source ('The Rock', NP Photonics) with a Power Amplifier (ML10-YFA-CW-SLM-P-TKS, Manlight).

A DOE is used to split the laser beam into five separate beams in a cross shape at a divergence angle of 4.3°, with two of the outer beams on opposing sides blocked out. These remaining three beams are then co-aligned, and focused down into the sample plane by a 0.25 NA aspheric lens (C220TMD-C). The beams are rotated such that the optical fringes are aligned at 45° with respect to the direction of fluid flow. Illumination is provided by Köehler illumination, which provides even illumination in the sample

plane, and also ensures that the image of the light source is not imaged in the sample plane. A schematic of Köehler illumination is shown in Figure 4-2.

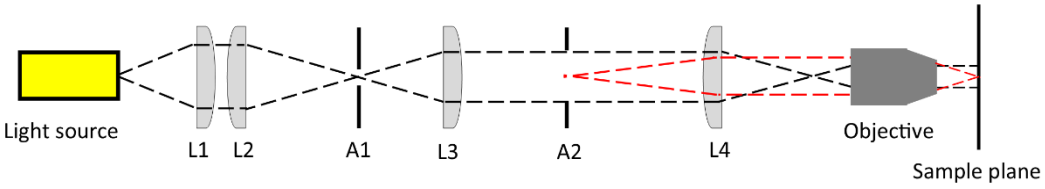

Figure 4-2. Köehler illumination. The image of the light source (black dashed line) is focused down on to the field diaphragm (A1), and collimated by L3. An image of the aperture diaphragm (A2, red dashed lines) is collimated by L4, which also focuses the image of the light source at the back aperture of the objective. The objective then relays the image of A2 to the sample plane while the image of the light source is brought to infinity.

The optical structure resulting from the three-beam interference, shown in Figure 4-3, can be described as a 3D optical landscape with stacks of optical guides layered in the z axis, with each layer being 180° out of phase with the previous. This stacking of optical fringes is shown visually in Figure 4-4, by recording a video whilst scanning through the z axis of the landscape and reconstructing the image stack in a 3D rendering program (VolViewer).

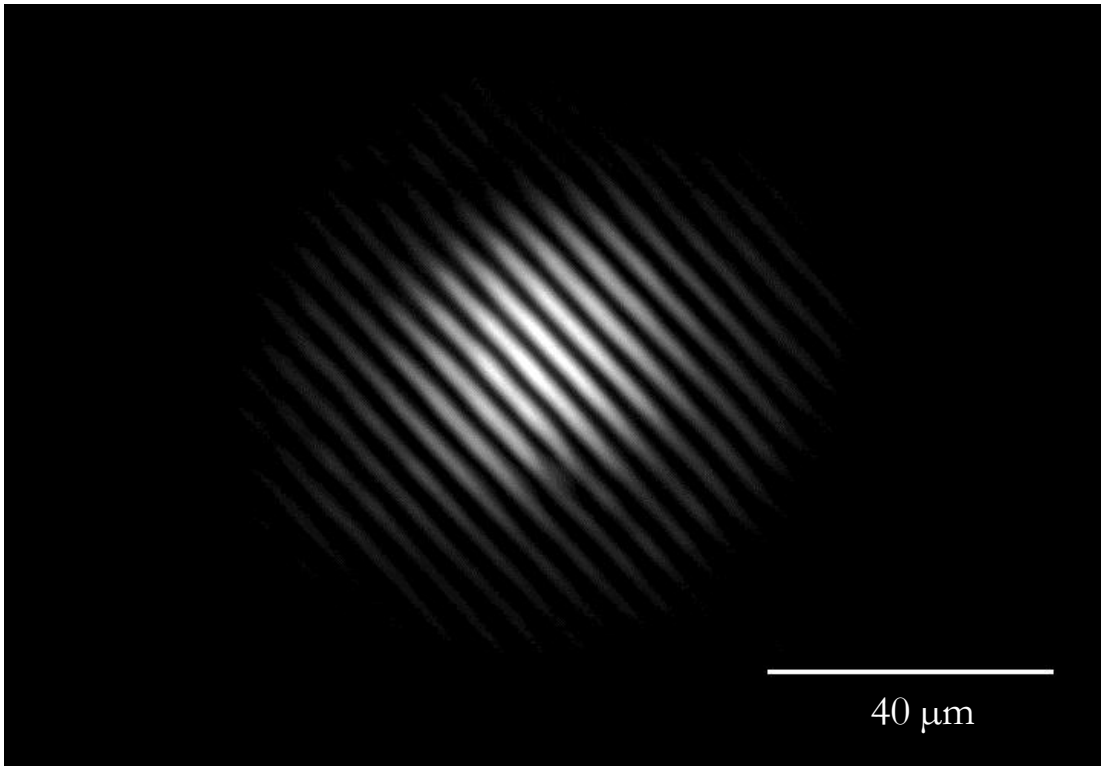

Figure 4-3. A top down view of the 3D optical landscape. The lanscape is comprised of fringes of light stacked on top of each other. The fringes act to guide particles along them by gradient force trapping.

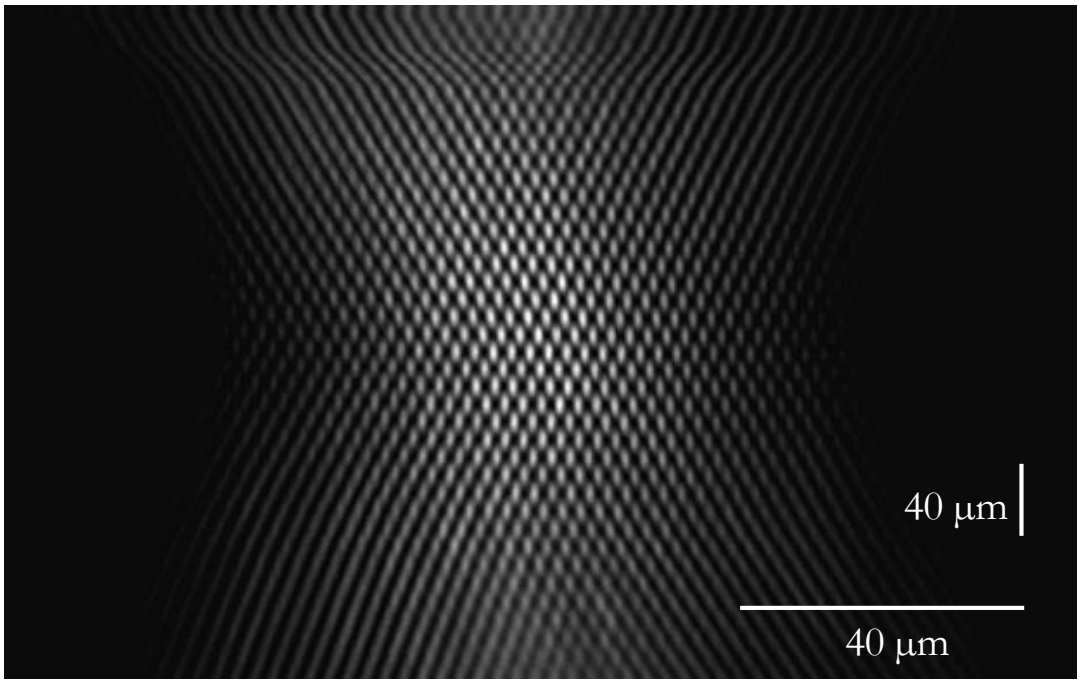

Figure 4-4. A side view of the three beam interference pattern, showing the ordered stacking of the optical fringes. Scale bars are added in both axes.

The optical fringes act as potential wells in which the particles are drawn to via the gradient force. Having the fringes at an angle relative to the direction of fluid flow means that particles that become trapped are directed along the fringes, until the gradient force is no longer strong enough to hold them. Particles' differing response to this effect will be exploited to achieve separation.

Separation of 2 and 5 μm spheres

A sample of 2 and 5 μm polystyrene spheres (Duke Standards, 4202A & 4205A) will be used. This is made up by mixing two and five drops of concentrated 2 and 5 μm solutions respectively in a 2 ml Eppendorf tube with the remainder of the tube filled with distilled water. This gives an approximate concentration of 0.6×10^6 and 1.0×10^6 2 and 5 μm particles respectively per ml of solution. The solution is loaded into a 1 ml syringe. The particles are flowed through the sample chamber. The speed of the particles is calculated using video analysis, as the value given on the syringe pump (PicoPlus, Harvard Instruments) will not be an accurate measurement, particularly for particle motion at the surface. Ten particles of each size are timed as they travel from one edge of the video screen to the other in order to measure an average particle speed at the channel surface. The average speeds of the particles in flow are calculated to be 11.4 μms^{-1} (SD = 0.45) and 17.3 μms^{-1} (SD = 0.4) for the 2 and 5 μm spheres respectively. The difference in particle velocities is to be expected, as due to the Poiseuille flow distribution in the channel, the large 5 μm particles are affected by a higher flow velocity than the smaller 2 μm particles when flowing at the surface.

To characterise the sorting efficiency as a function of laser power, the laser power is increased in 20 mW intervals, from when the particles are barely affected by the optical

landscape, to when most of the particles are deflected – the laser power required for the highest sorting efficiency will lie within this range.

This is a proof of principle experiment, and is carried out to indicate the feasibility of the technique in this particular configuration. Further repetitions of this experiment would indeed contribute towards an increase in accuracy, however a large particle count (Appendix B) confers a level of precision in this particular experiment. Similar work has been carried out previously[1,124], and as such this is satisfactory as a precursor to the work presented further in this chapter.

Analysis of the video recordings is done manually. In analysis of the particles, boundaries are defined, shown in Figure 4-5, where any particle entering at 'A' and exiting the pattern at 'B' are considered 'sorted', while any particle entering 'A' and not exiting at 'B' are considered 'unsorted'. Particles that do not enter at 'A' are not counted. Many of the particles in the fluid flow are not flowing at the surface, i.e. are visually observed to be relatively defocussed and flowing at a higher velocity and hence are less affected by the optical landscape, and as such these particles are not considered in the analysis, but will be discussed later.

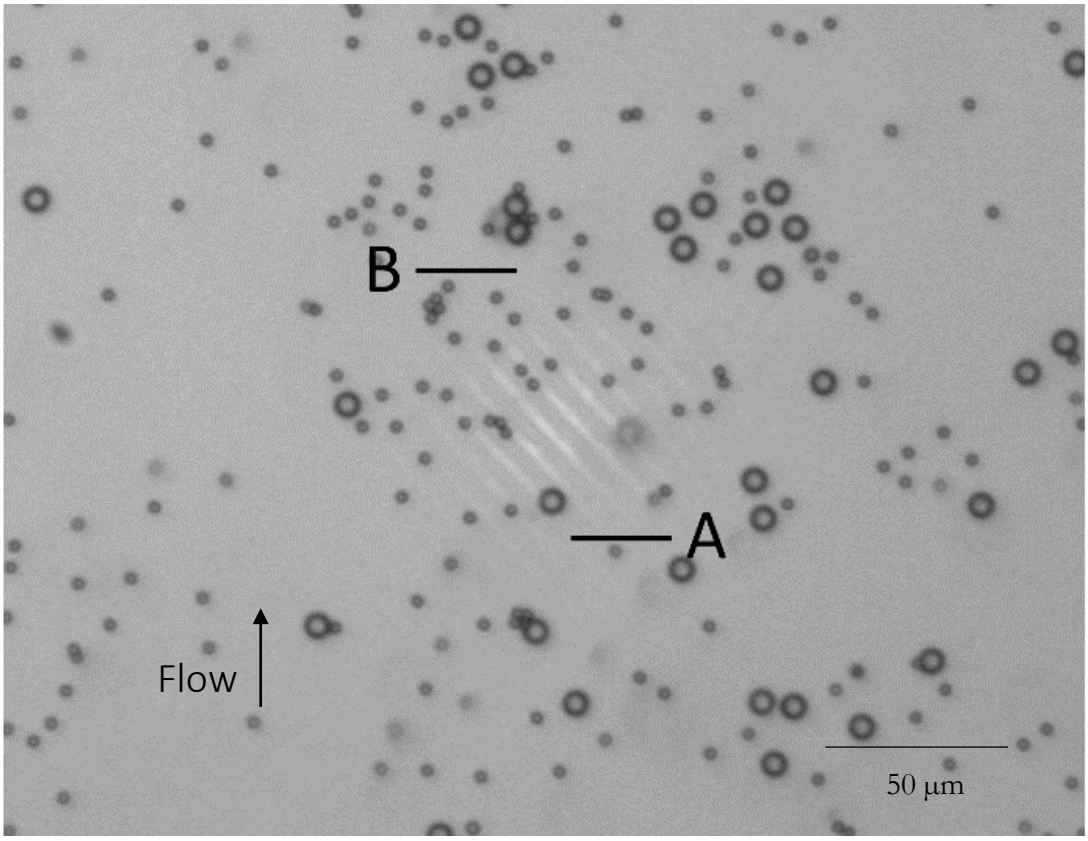

Figure 4-5. The 2 and 5 μm particles shown above are counted as sorted if they enter the inlet region A, and exit the optical landscape at the outlet region B. Particles that enter at A and do not exit at B are counted as unsorted. Particles which do not enter the pattern at A are not considered.

The results are plotted in Figure 4-6. In Figure 4-7, a means of describing the overall functionality of the system, an enrichment rate, is displayed. This is calculated in terms of, out of all of the particles that have been deflected from 'A' to 'B', what percentage are of size 2 μm. This is a useful metric to consider as it relates to how a quality control measure for blood sorting could be described, i.e. how pure is the end mix of cells?

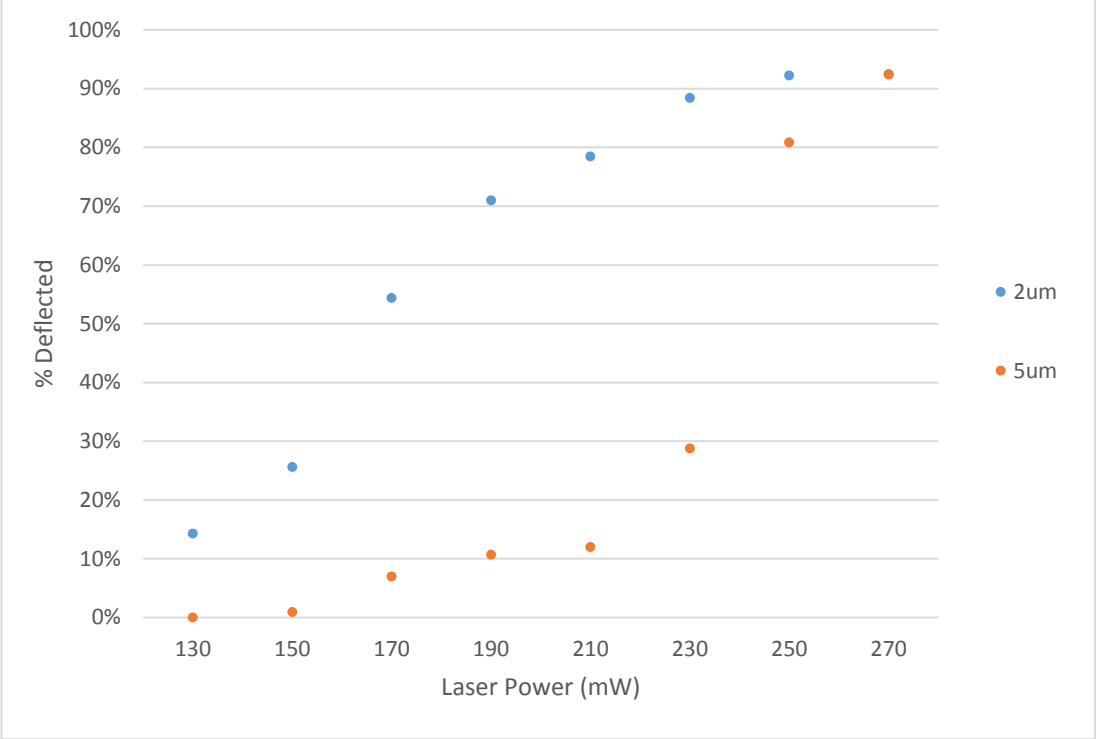

Figure 4-6. The separation efficiencies of 2 and 5 µm spheres with varying laser powers. The graph shows that the 2 µm particles are more readily deflected at lower laser powers than the 5 µm particles, leading to a separation effect of the two particle species.

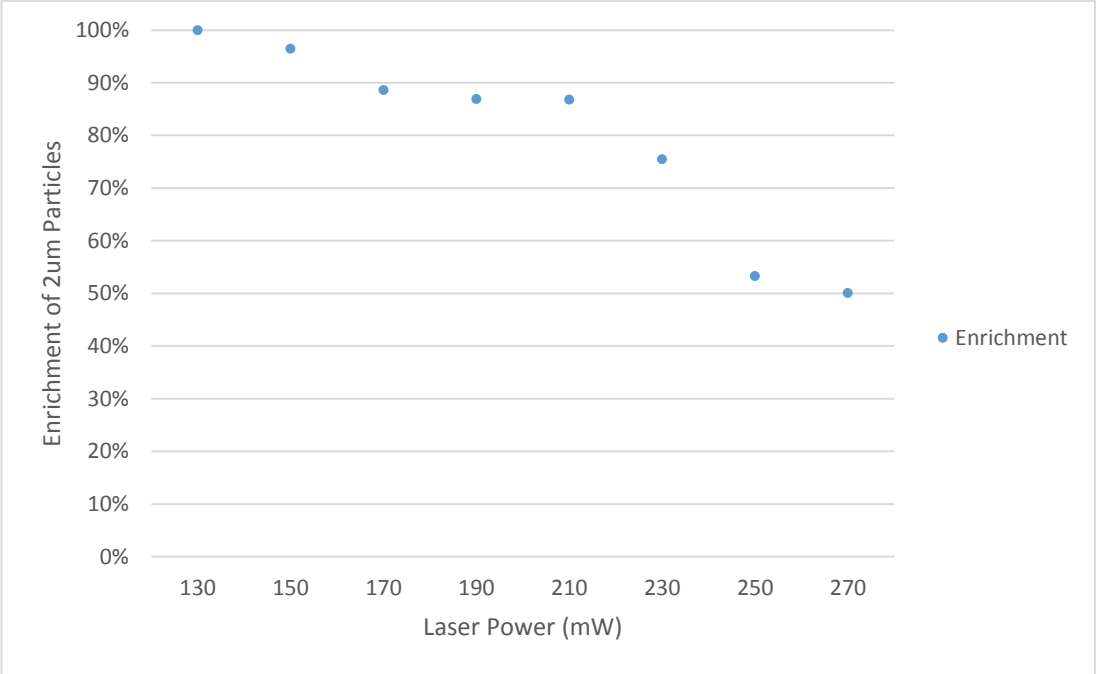

Figure 4-7. The enrichment rate of the 2 µm particles.

There is a peak separation efficiency of the two particle species at a laser power of 210 mW. This gives an enrichment rate of 87%, with a recovery rate of the 2 μm particles at 78%. There is a noticeable drop in the deflection efficiency of the 5 μm particles as the laser power is dropped below 250 mW, however the drop in efficiency for the 2 μm particles is much more gradual. Although there is a high enrichment rate at lower laser powers, the low particle recovery at these data points would limit their practical implementation. Therefore enrichment and recovery rate must both be considered when interpreting the results.

When the particles enter the optical landscape, and are trapped in the fringes, their velocity magnitude changes. This is due to a change in direction relative to their initial trajectory. In the case of this system, the particles are directed 45° counter-clockwise, resulting in a change in their velocity due to the component vector from the Stokes drag acting in that direction. The resultant change in forces is shown diagrammatically in Figure 4-8, where F_D is the Stokes drag and F_g is the gradient force from the optical fringe.

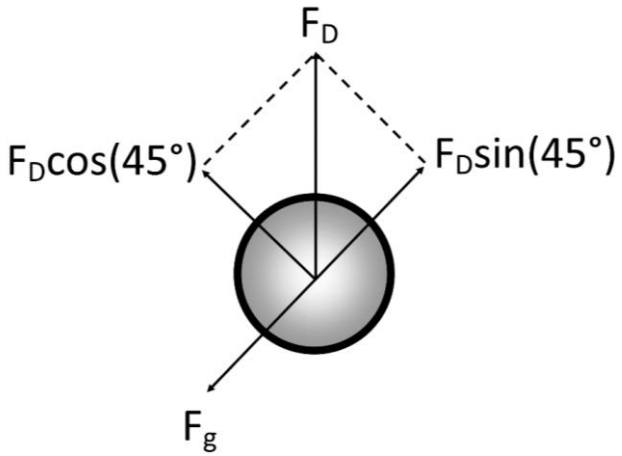

Figure 4-8. A free body diagram of a particle under fluid flow being trapped in an optical fringe. When the particle is trapped in the optical fringes, it experiences an equal force, F_g, in the opposing direction of $F_D\sin(45°)$, resulting in zero net velocity in that direction. The resultant motion of the particle is along the direction of $F_D\cos(45°)$, a smaller force than F_D, resulting in an overall slower particle velocity along the optical fringes.

This can be further explained to represent the resultant velocity of a particle entering and travelling along the optical fringe, as shown below where U_0 and U_1 are the velocities prior to and after entering the optical field:

$$F_D = 6\pi\eta r U_0, and\ F_D \cos(45°) = 6\pi\eta r U_1$$

Substituing F_D, cancelling out common terms and solving for U_1 yields:

$$U_1 = \frac{U_0}{\sqrt{2}}$$

This can also be used to calculate the strength of the gradient forces required to trap the different size particles in the optical fringes. Using the velocity values found previously in this chapter, the forces acting on the spheres are calculated as 0.14 pN and 0.57 pN for the 2 and 5 μm spheres respectively.

This decrease in particle velocity can lead to a build-up of particles in the optical landscape. This build-up can cause particles to be knocked out of the landscape by other incoming particles, before they have time to deflect unimpeded. Although one can imagine that, due to the number of optical fringes present, this is not as prevalent a problem as is possible in single line optical deflection systems, or in single beam radiation force systems as demonstrated in Chapter 5, this effect can serve to reduce the overall efficiency of the system.

One observed advantage in this configuration however, is that the overall radiation force from the three beams can be enough to push particles flowing in a velocity profile just above the surface down to the surface to then be sorted by the interference fringes.

4.3 Optical radiation force balance in an interference pattern

As can be seen from the interference sorter, the radiation forces from the three beams can push the particles down to surface of the channel. To take advantage of the volumetric nature of the potential energy landscape, it is necessary to balance out the radiation forces, such that particles can be sorted throughout the volume of the optical landscape. A first step towards achieving this is to balance out the radiation forces present from propagation of the multiple beams forming the interference pattern, by introducing a single beam from the opposing direction. This is a similar principle to that of a typical counter-propagating optical trap, where two identical beams are aligned in the x and y axes, and the foci offset in the z axis[5]. This produces a balance of the optical radiation forces at the mid-point between the two beam foci, where a particle will come to rest. In the context of optical interference patterns, tuning of the power of this extra beam has been shown to hold particles in place in a 2D interference landscape[125], and could serve to allow choice over which horizontal plane of interference fringes the particles will be deflected along in a 3D interference landscape.

4.3.1 Materials and methods

A system is designed, similar to that in Figure 4-1. In this system, the interference pattern is formed by five beams, as opposed to three beams previously. This is to have an optical landscape of discrete potential wells (discussed later in this section), which keeps particles trapped in localised positions, making any vertical displacement easier to visualise. The five beams enter the sample from above, with a single beam entering the sample from below. This system is detailed in Figure 4-9.

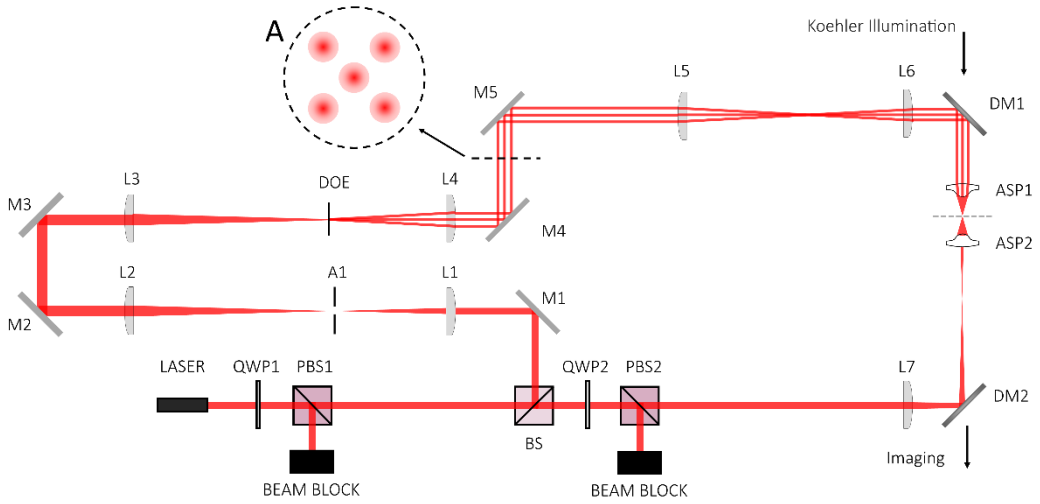

Figure 4-9. A similar system to that in Figure 4-1. A 50:50 beam splitter (BS) is inserted such that a beam can be introduced from the opposing direction of the interference pattern, this time produced by five beams (shown by the cross-section A). The lower beam is attenuated as desired, and L7 is used to purposefully defocus the beam in the sample plane, such that the resultant beam diameter can be configured by moving L7 back and forth. The beam is focused through an identical 0.25NA aspheric lens, which is also used for imaging.

The power of the single beam entering from below can be attenuated, allowing for control over the balance of the optical forces. 2 μm particles are trapped in the potential wells formed by the five beam interference pattern at the surface of the channel. The power of

the lower beam is then increased to the point where the radiation forces become unbalanced, and the particles are pushed upwards. The particles then come to rest in a new lateral plane, determined by the ratios of the powers of the interference pattern and the single laser beam. The lower beam can also be defocused with respect to the sample plane by moving lens L7 along the beam axis. This allows for control over the beam diameter in the sample plane.

4.3.2 Results and discussion

The power of the interference pattern is measured as 750 mW. This is sufficient power to trap 2 μm spheres in the discrete traps formed by the five beam interference. The lower laser beam is then gradually increased in power. At 1.6 W of power, particles are seen to become trapped in a different array of traps. The particles are now located in the array of traps directly above the array used for trapping at the surface. To contextualise the observed motion, it is useful to first visualise the potential energy landscape at the surface, where the particles are initially trapped, and just above the surface, where it is hypothesised that the particles are pushed to. A composite image showing the two layers of potential wells is shown in Figure 4-10, where layers are superimposed over each other, to show that the upper layer of potential wells resides above the interstices of the lower layer.

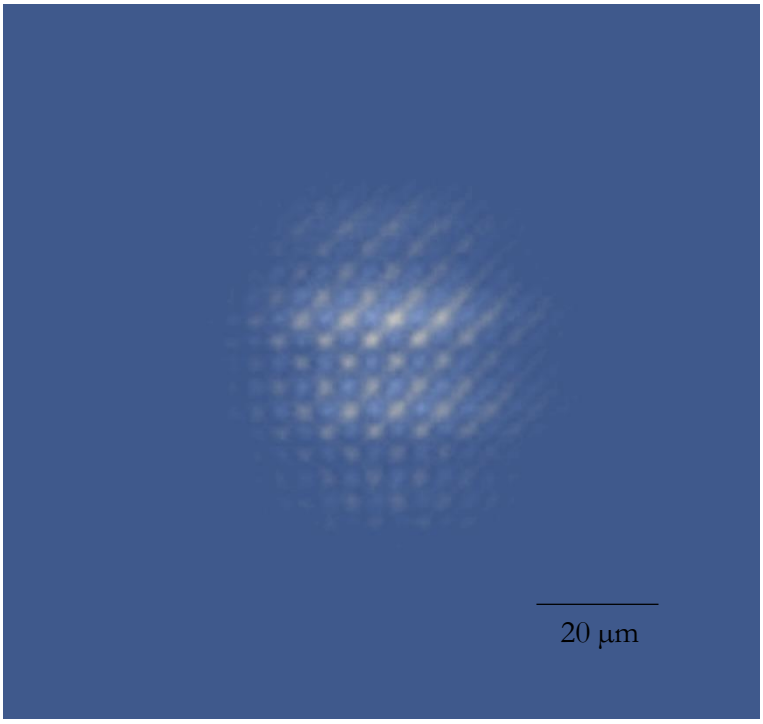

Figure 4-10. The interference pattern shows discrete potential wells in which a particle will be trapped in. The white traps shown are directly below the blue coloured traps, demonstrating the antiphase over lapping of the pattern structure, also visualised in Figure 4-4. Some interlinking due to slight phase mismatch of one of the beams is observed in the upper right of the image, however this has no significant impact upon trapping performance.

This can be further visualised by considering the lattice structure of the potential energy landscape. As shown previously[67], the resultant lattice of a five beam interference configuration takes the form of a b.c.t structure. This structure is visualised in Figure 4-11, with the black circles representing the potential wells in which particles can become trapped in.

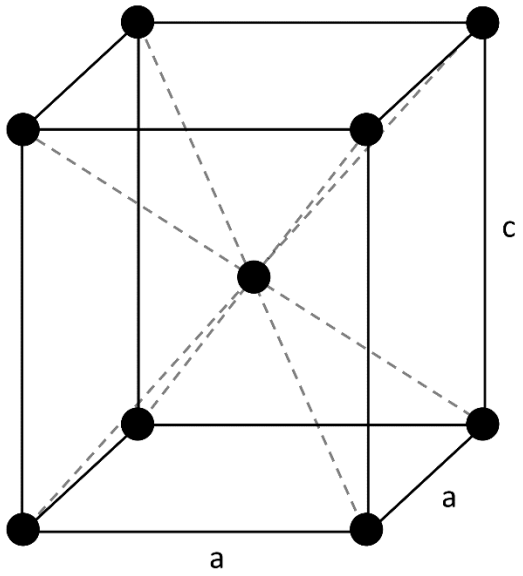

Figure 4-11. The resultant b.c.t structure of the five beam interference, which is repeated throughout the landscape. The black circles represent the discrete potential wells formed by the interference of the five beams. The dimensions are such that a≠c.

With both Figure 4-10 and Figure 4-11 outlined, the results shown in Figure 4-12 where the two particle states are shown can be better understood. First, when the lower laser beam is off, and secondly, when it is set to 1.6 W. The power of the interference pattern is constant at 750 mW throughout. A grid of dots, representing the locations of the potential wells in each layer of the optical landscape, is overlaid on to each image to help clarify the new particle position with respect to their original position.

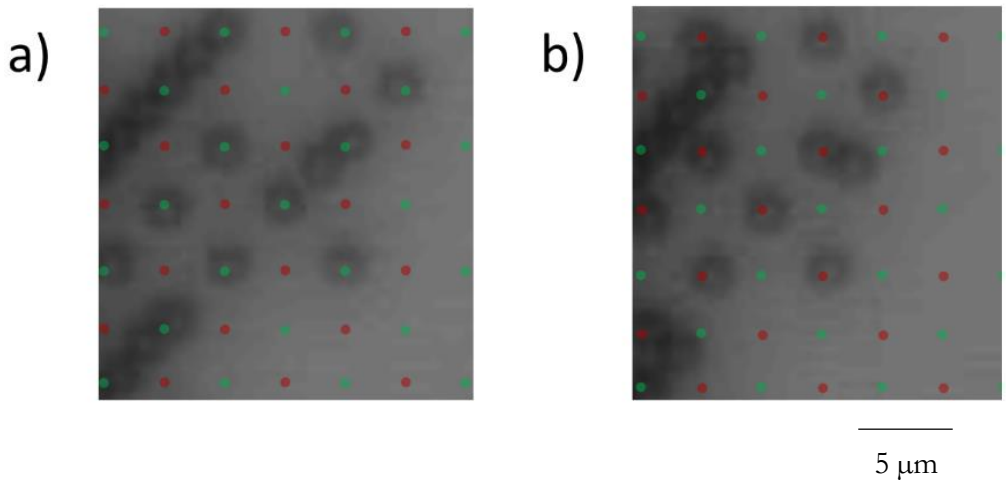

Figure 4-12. a) The 2 μm particles are trapped in the discrete potential wells formed by the five beam interference pattern, with the green array of dots representing the locations of the potential wells in the lower layer, and the red dots the upper layer. b) With the counter-propagating beam increased in power to 1.6 W, the unbalanced radiation forces push the particles into the upper layer of potential wells, where they are stably trapped.

Both the overall interference pattern and the counter propagating beam possess a Gaussian beam profile, meaning that particles at different points in the beam will experience different scattering forces. By overlapping these two Gaussian profiles from the beams, this effect is negated such that all particles will experience the same balance of forces. The particles shown in Figure 4-12 are stable in the upper layer of potential wells, as long as the laser powers are kept constant. In order to verify these findings, the sample stage is connected to a motorised actuator and controller (ESP301, Newport), and the sample moved upwards until the particles became trapped in the next plane of potential wells. The particle motion is compared to that of using solely optical forces, and similar motion and trapping positions is observed. It is also found using this method that the distance between the two planes of interest is approximately 20 μm.

This demonstrates an initial study into selectively manipulating particles in a chosen plane of the interference pattern using purely the balance of optical radiation forces, for

example to bring particles away from the surface in flow, whilst still being affected by the potential energy landscape.

A clear advantage to this force balance would be to achieve the same effect both far away from the channel surface, and in multiple interference planes simultaneously. To better observe particle position in the z axis, an imaging system is mounted such that the capillary can be viewed through the side. The experiment is repeated, with the same laser powers used previously – 750 mW for the interference pattern, and 1.6 W for the counter-propagating beam. It becomes clear, even with the lower beam blocked off, that there are thermophoretic effects on the fluid volume. The effects of thermophoresis will be discussed in more detail in Chapter 5.3. The need for greater vertical deflection is apparent in bringing particles to a much more homogenous part of the laminar flow, i.e. near the centre of the channel. As such, higher laser powers are required to achieve this. With the larger laser powers necessary to achieve this vertical deflection, the next requirement then becomes to reduce the effects of thermophoresis. With thermophoresis overwhelming the forces produced by the optics, particularly away from the surface, it is challenging to achieve a stable force balance throughout the fluid volume.

4.3.3 Overcoming thermophoresis with a smaller capillary

In an attempt to reduce the thermophoretic effects in the fluid, a 100 μm inner diameter square capillary is used instead as the sample chamber as a smaller fluid volume will produce less of a thermal gradient due to laser absorption, hence less thermophoretic effects. The smaller 100 μm capillaries were discussed in Chapter 3, and were ruled out initially as they were quite fragile and had issues with glueing to the transducer. In this case a transducer is not needed, so the 100 μm capillary could be used freely without complication.

Additionally, in order to increase the energy density of the lower beam, the beam diameter is reduced. This allows for greater vertical deflection of the particle(s) due to the resultant increase in force applied. The beam was characterised in terms of its ability to achieve force balancing of particles throughout the height of the capillary, and not in terms of absolute beam diameter. A result of this beam diameter reduction is that less particles are affected by the force balance.

The conditions are recreated – the solution of 2 μm particles is flown through the sample chamber and allowed to come to rest, the interference pattern set to 750 mW, and the particles trapped at the channel surface. The lower beam is gradually increased in power, and the effect on the particle position observed.

The particles are seen to balance at several stable positions in the vertical direction, depending on the power of the lower laser beam. This is shown for some particle locations in Figure 4-13.

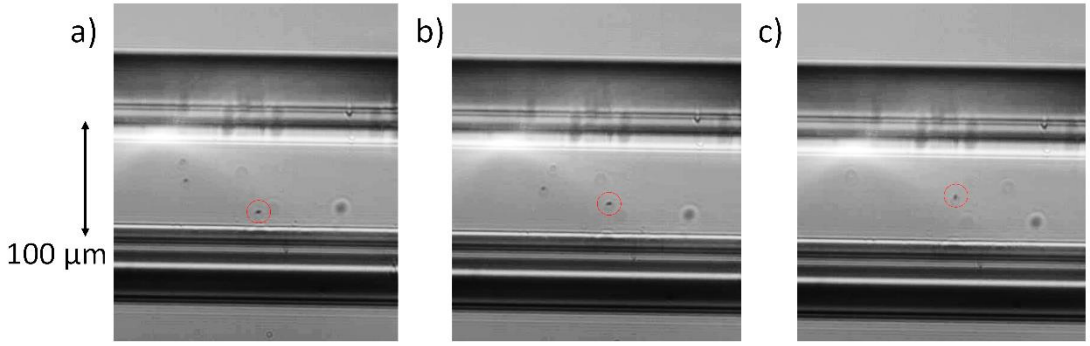

Figure 4-13. Side view of the 100 µm capillary. The particle positions due to the balance of the optical landscape and the counter-propagating beam are shown circled in red, for a) 20 µm, b) 40 µm and c) 60 µm displacements at counter-propagating laser beam powers of 132 mW. 205 mW and 260 mW respectively. Other particles are present in these images however are not integral to this experiment and as such can be ignored.

What is observed through this experiment, is that the particles come to rest at regular vertical intervals. This interval is measured as 20 µm, the value found previously as the distance between the interference planes. A characterisation of the powers of the counter-propagating beam required for a given particle to rest in each interference plane in the 100 µm channel are given in Figure 4-14.

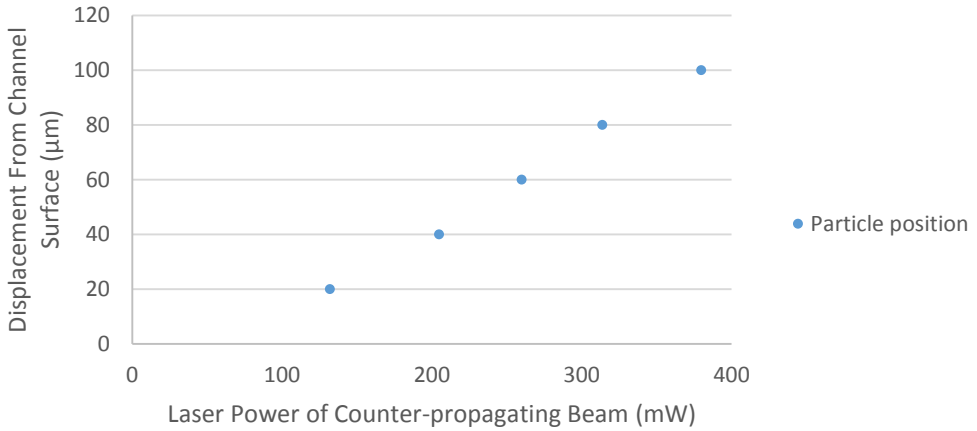

Figure 4-14. The particles come to rest at discrete positions in the optical landscape by varying the power of the counter-propagating laser beam, where the particle is then pinned to the top of the channel when it reaches 100 µm in height. The graph shows a step-wise response of particle motion to the counter-propagating beam.

The particle motion is in a stark contrast to such observed motions as one might find in a typical counter-propagating optical trap. In such a system, varying the power of one of the beams would produce a linear response from the particle in terms of its motion along the axis of beam propagation. In this system, balancing the optical radiation forces in a potential energy landscape, the response is that a particle will still move to the state of least potential energy, however these are located at discrete points throughout the axis of beam propagation, determined by the spacing of the horizontal planes of the interference pattern.

These data point represent one experimental procedure in this case as the experiment was intended to firstly demonstrate a proof of concept: that particles can be optically balanced in the planes of a three dimensional optical landscape. Further experimentation would assist in verifying the accuracy of the presented results, however the principle has been demonstrated in the first instance.

This helps to verify what is observed in Figure 4-12, as it demonstrates that particles can be stably held in the potential wells formed by a multi beam interference pattern via the balancing of the optical radiation pressure from the pattern itself and a counter-propagating beam.

4.4 Discussion & conclusions

In this chapter, particle manipulation via the optical gradient force has been investigated. Initially, this was demonstrated by using a three beam interference system, whereby three beams are interfered in the sample plane to produce a 3D potential energy landscape. The resultant landscape is shown to consist of layers of optical 'rods', in which particles

experience a gradient force. A five beam configuration was also used, which produces discrete trapping sites throughout the optical landscape. The particles' response to these potential wells is the mechanism by which sorting can take place within these optical structures.

A key component in the consideration of using potential energy landscapes as a scalable sorting technique is the ability to affect particles throughout the 3D landscape. This is problematic in this context, as it has been shown that the optical radiation pressure in the direction of beam propagation pushes the particles to the surface of the channel before they can be deflected along the optical fringes. In other words, the optical gradient forces present in the optical fringes are not strong enough, especially with the low NA focusing optics used in the system, to hold the particles against the overall optical radiation force.

Borrowing from the principles of counter-propagating optical trapping, a system is designed to have a single beam directed in the opposite direction to the propagation direction of the interference pattern. This successfully balances the radiation forces from either direction such that particles are trapped in the potential wells in several horizontal planes of the optical landscape. This is useful as it allows for the consideration of affecting particles with the optical landscape away from the surface, e.g. performing particle sorting in multiple interference planes simultaneously.

Optical gradient force sorting has been successfully demonstrated previously[1,38,124,126], however it is almost always carried out at the surface. Attempting to work with the gradient force away from the surface presents a set of challenges that in previous work has been trivial. In viewing the optical force balance effect from the side, it is evident that thermophoretic forces are present when using the 300 μm capillaries. This is remedied by using a smaller 100 μm capillary as the reduction in fluid volume lessened any

thermophoretic effects. Although the issue of thermophoresis can be managed by either using lower laser powers resulting in reduced trapping strength, or by working in smaller fluid cavities, this doesn't pertain to further success in the scale up of these techniques.

Polymer microspheres have been used as a model in these experiments as a means of demonstrating the techniques themselves. However, it is apparent that such developments could improve upon previous applications, such as the separation of red blood cells from other constituents (e.g. white blood cells) using optical landscapes[1], with volumetric manipulation potentially adding greater throughput.

It is clear that further developments are needed to fully realise the scale up of optical gradient force based particle sorting. With initial investigations into the force balancing in optical landscapes however, there is evidence to suggest an optical radiation force balance could hold promise in allowing the sorting of particles to take place in any, or multiple planes of the optical landscape, potentially parallelising the technique of sorting within an optical landscape.

5 Hybrid Optical and Acoustic Force Balance

5.1 Introduction

In this chapter, the force balance between the optical radiation and the acoustic gradient forces is exploited to achieve particle separation. The acoustic forces are also used in part to enhance the hybrid fractionation. By driving the system at the second harmonic, confining particles to different streams after fractionation is a possibility. The acoustic forces also bring the particles away from the channel surfaces and into a higher velocity part of the flow. This method of separation is first demonstrated with a single laser beam, and then potential scale up is considered.

5.2 Separation via the balance of optical radiation and acoustic gradient forces

In this first experiment, the balance of the optical radiation and acoustic gradient forces is tested as a viable method for particle separation. A sample of 7 and 10 μm polystyrene microspheres (Duke Standards, 4K-07 & 4210A) in distilled water are flowed through an acoustic field. The acoustic field, resonating at the second harmonic in the capillary, confines the particles to the four streams produced as a result of the resonance. A single laser beam is used to 'push' particles vertically from one acoustic stream into another. From Chapter 2, it can be seen that the optical radiation force will have a greater effect

on smaller particles, while the acoustic forces scale with the particle radius cubed, exerting a larger force on larger particles. This contrasting response to the applied forces encourages particle separation, while the acoustic streams also act to confine particles after optical manipulation, creating a binary separation system.

5.2.1 Materials and methods

The system is designed to have a weakly focused beam entering the glass capillary in order to deflect particles from the lower to the upper acoustic node. A schematic of the system is detailed in Figure 5-1.

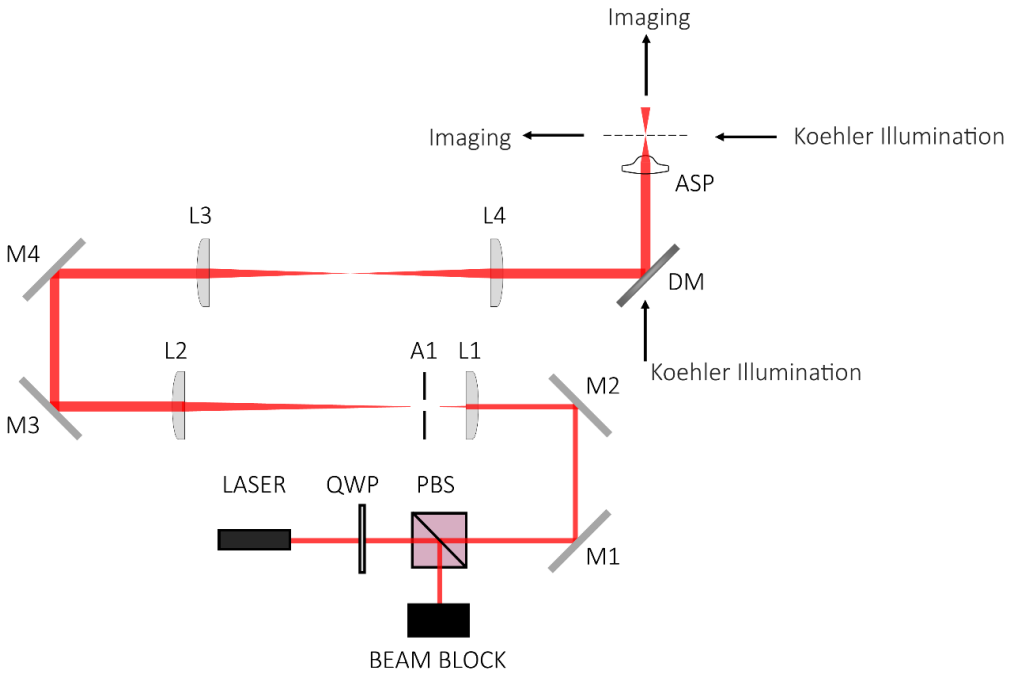

Figure 5-1. The system is designed to relay a single loosely focused beam into the sample plane. Lenses L1 and 2 expand the beam to fill the clear aperture of the aspheric lens. A 4f relay system is formed with lenses L3 and 4 and the back aperture of the aspheric lens. Köehler illumination is used in both imaging axes.

A power attenuator is set up as described in Chapter 4.2. The two lenses L1 and L2 form a beam expansion that fills the back of the aspheric lens (0.25 NA) used to focus the beam down into the sample plane. Lenses L3 and L4 act as a relay in order to make the mirror M4 conjugate to the back focal plane of the aspheric lens. Observation is set up in two axes – from above and from the side. A 20X LWD objective (Mitutoyo) is used to image from above, into a CMOS camera (DCC1545M, Thorlabs). A 5X LWD objective (Mitutoyo) is used to view from the side, into another CMOS camera (GS3-U3-23S6M-C, Point Grey). Illumination in both cases is provided by Köehler illumination.

The LNO-ITO transducer is used to provide acoustic levitation in the (300x300) μm glass capillary. The transducer is driven at 4.34 MHz by a function generator. This value is verified empirically as the 2nd harmonic of the system. Due to the symmetrical nature of the glass capillary, resonance is achieved across the vertical and horizontal walls, resulting in four discrete acoustic streams. In this experiment, only one pair of upper and lower streams is considered.

The top view of the system is used to laterally position the capillary such that the laser is in line with the two acoustic nodes of interest, and also to verify where the location of beam focus, which is positioned halfway between the two acoustic nodes.

A polydisperse sample of 7 and 10 μm polymer microspheres in distilled water is flowed through the glass capillary at a speed of 58 μms^{-1}. As the particles come into contact with the laser beam, they are pushed along the beam axis by the optical radiation force (Figure 5-2). In this set up, they are pushed upwards, towards the upper acoustic node. Varying the power of the laser changes the force balance between the optics and the acoustics, and elicits a changing response in the particle displacement.

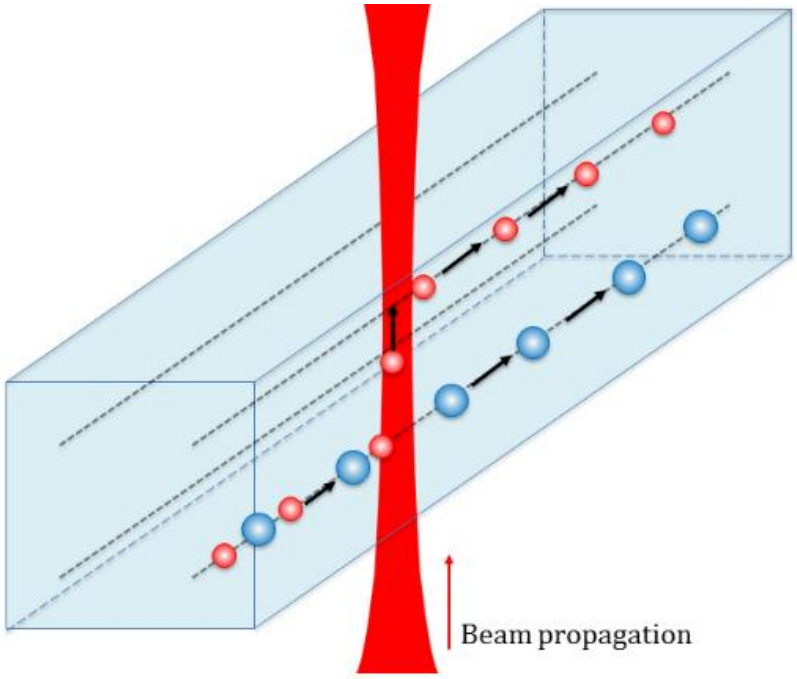

Figure 5-2. At peak efficiency, the system deflects the smaller spheres (red) from the lower stream into the upper stream, whilst leaving behind the larger spheres (blue) in the lower stream. Black arrows denote particle trajectory.

The laser power is set to 93 mW (measured at the back of the aspheric lens) initially. This power is chosen as the lower limit as particles are seen to be shifted vertically slightly, but not enough to move into the upper acoustic node. The experiment is run at several values up to 184 mW, where most particles of both sizes are vertically displaced into the upper stream. The experiment is repeated six times under the same conditions.

5.2.2 Results and discussion

In quantifying the results, particles deflected from the lower to upper acoustic stream are counted as sorted, whereas particles that do not reach the upper stream are counted as unsorted (Figure 5-3). The particles already present in the upper acoustic stream are not considered.

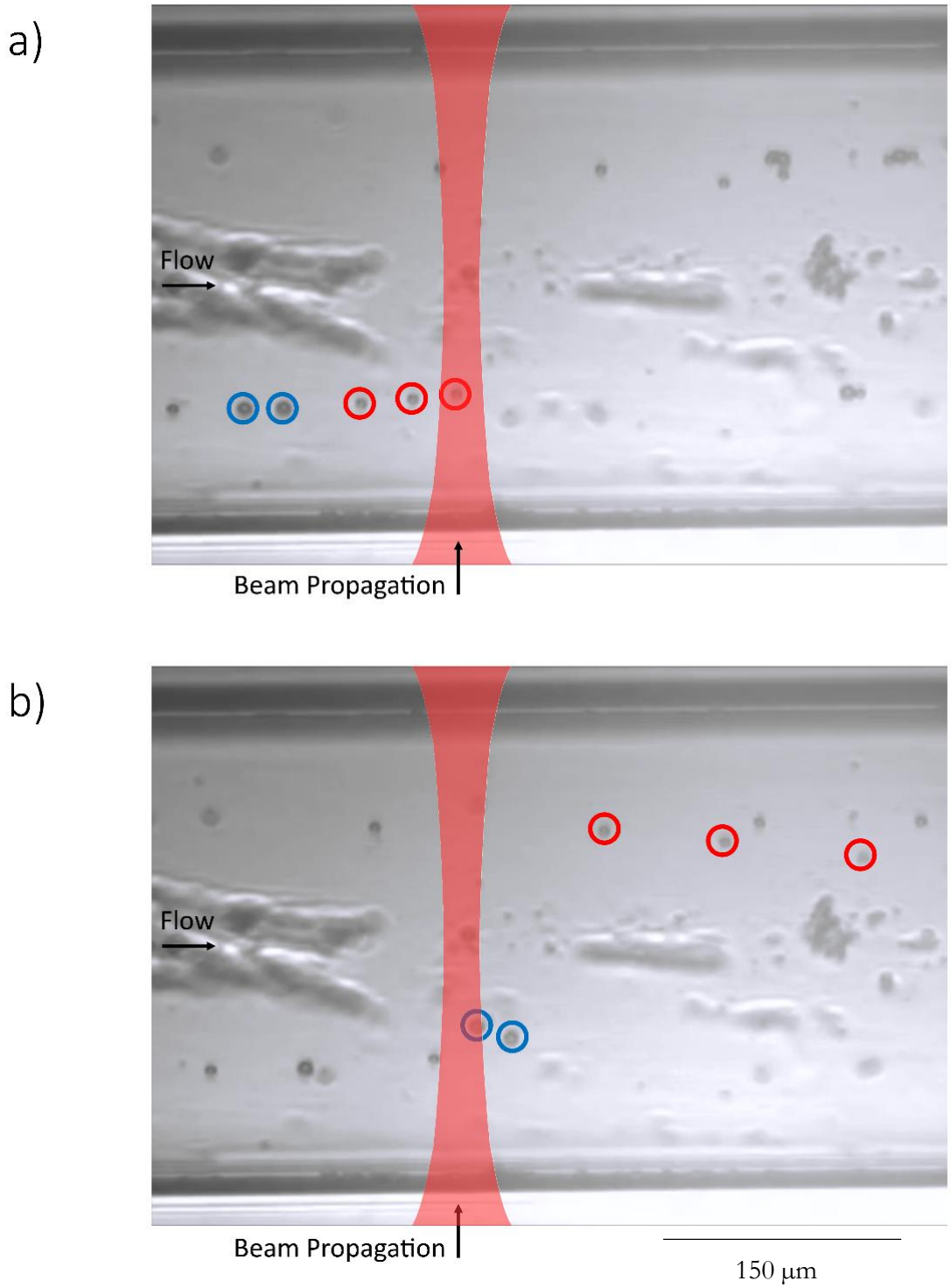

Figure 5-3. a) Particles in the lower acoustic stream approach the laser beam. The 7 µm particles are circled in red, and the 10 µm in blue. b) The 7 µm particles are deflected into the upper acoustic stream by the laser beam, whereas the 10 µm particles remain in the lower stream. Dirt and other artefacts can be observed stuck to the channel walls, however these artefacts have no influence on the device performance.

The results confirm that separation by size in our hybrid optical radiation force and acoustic radiation force system is possible. As the laser power is increased, the deflection efficiencies of both particle sizes increases, with the efficiency of deflecting 7 μm particles increasing at lower laser powers than the 10 μm particles (Figure 5-4). A table of particle numbers and standard deviations is given in Appendix C.

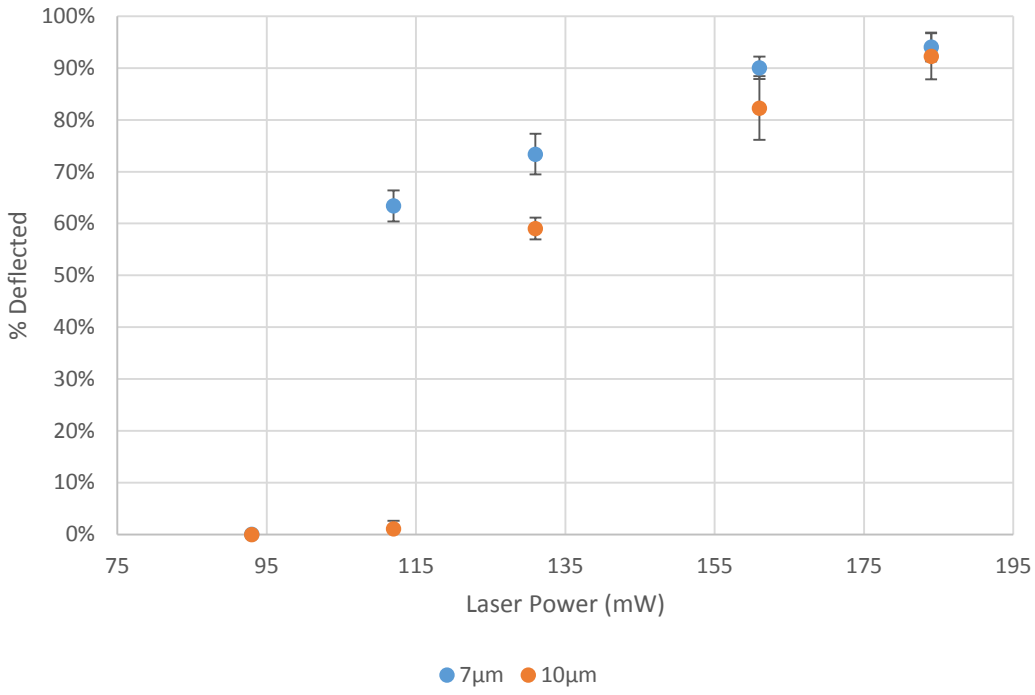

Figure 5-4. The individual deflection efficiencies for each particle size show a marked difference in their response to the laser beam. The smaller 7 μm particles are more readily pushed into the upper node at lower laser powers, while the larger 10 μm particles require more power to be fully deflected

The results show a peak separation at a laser power of 112 mW. At this power, 62% (SD = 2.97%) and 1% (SD = 1.54%) of the 7 and 10 μm particles respectively are deflected from the lower to the upper acoustic stream. This leads to a 98.4% (SD = 4.71%) enrichment of the 7 μm particles in the upper acoustic stream. This enrichment factor

decreases with higher laser powers as each particle size experiences enough force to be deflected from the lower stream.

The hybrid force balance in this method acts as a means of fractionation, where different sizes of particles are deflected to different points in the channel. It is the use of acoustic trapping that allows for these different species of particles to be confined to individual streams, as the particles, given enough time, would sediment at the bottom of the chamber after optical deflection without the acoustics.

The challenges involved with this separation method become clear when considering an ideal system, where if a single particle of a particular species can be pushed to any point above the centre of the channel, the result should be 100% recovery rate for that species as they will then be guided to the upper acoustic stream by the acoustic forces, compared to the 62% recovery rate observed in the experiment presented. However Figure 5-4 shows that this is not the case. This discrepancy is primarily due to the fact that this set up would operate best as a single file sorter, much like FACS does. When particles are close together or agglomerated, the system is less effective at picking out individual particles to push up to the upper stream. Routing errors can also arise from particles being slightly off axis with respect to the beam (and acoustic node). The gradient force of the laser can bring them back in line, but the interaction time with the radiation force is then greatly reduced.

To further increase the efficiency of this hybrid system, it is hypothesised that a means of hydrodynamic focusing, to bring the particles into a single file line in the acoustic streams could help with the effectivity of the optical deflection. This could also bring all the particles into the same lower acoustic plane, such that there are no particles entering in the upper stream, allowing for truly sorted species to be collected at individual sample

outlets. An alternative means of pre-focusing could involve the use of a linear array of electrodes along the length of the capillary, such as the device developed by Démoré *et al.*[96], utilising independent acoustic manipulation regions to direct particles to the required plane.

5.3 Particle deflection from the radiation force of a light sheet

A natural progression from the system in Figure 5-1 is to have the radiation force act at multiple sites, such that each of the lower acoustic streams is affected. Where before only a single stream is affected within the spatial dimensions of the laser beam, with an inverted line optical tweezers, all particles can be affected, even those not fully confined to a lateral acoustic node. A multi-beam method could be employed, e.g. creating multiple traps using an SLM, however one would still experience the aforementioned problems with slightly off-axis particles, and although it would be possible to act on each of the acoustic streams with optical radiation force, similar problems with efficiency would still be present.

5.3.1 Materials and methods

In order to produce a fine light sheet, a Powell lens is used. The Powell lens is a laser line generator that uses spherical aberrations to redistribute light intensity across the line, unlike the more common cylindrical lens, which leaves a larger intensity of laser light near the centre Figure 5-5[127].

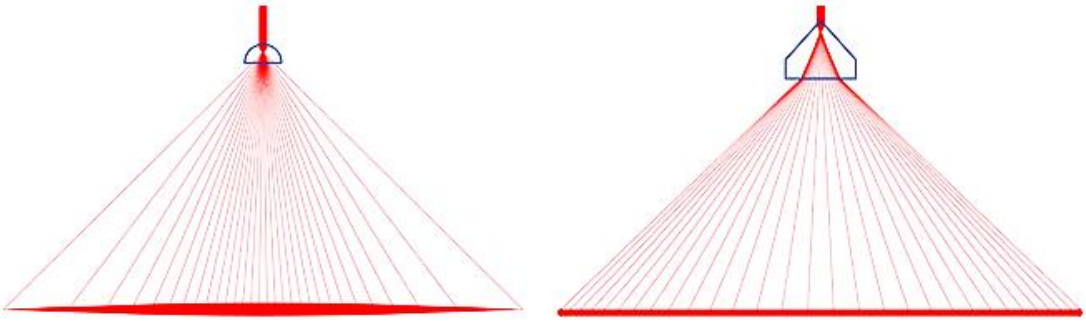

Figure 5-5. Highlighting the differences in the laser intensity distribution of a cylindrical lens (left) and a Powell lens (right) using ray traces. The Powell lens produces a much more even intensity distribution than the cylindrical lens. Image sourced from www.laserlineoptics.com.

A modified version of the system shown in Figure 5-1 is designed, shown in Figure 5-6. The beam expansion L1 and L2 is replaced with a 1:1 collimation, and the Powell lens is placed just over 150 mm back from the lens L3, such that the image just after the Powell lens is relayed into the sample plane. The result is a uniform light sheet in the sample plane. Previous studies have highlighted the characteristics of light sheets from cylindrical lenses and Powell lenses[128].

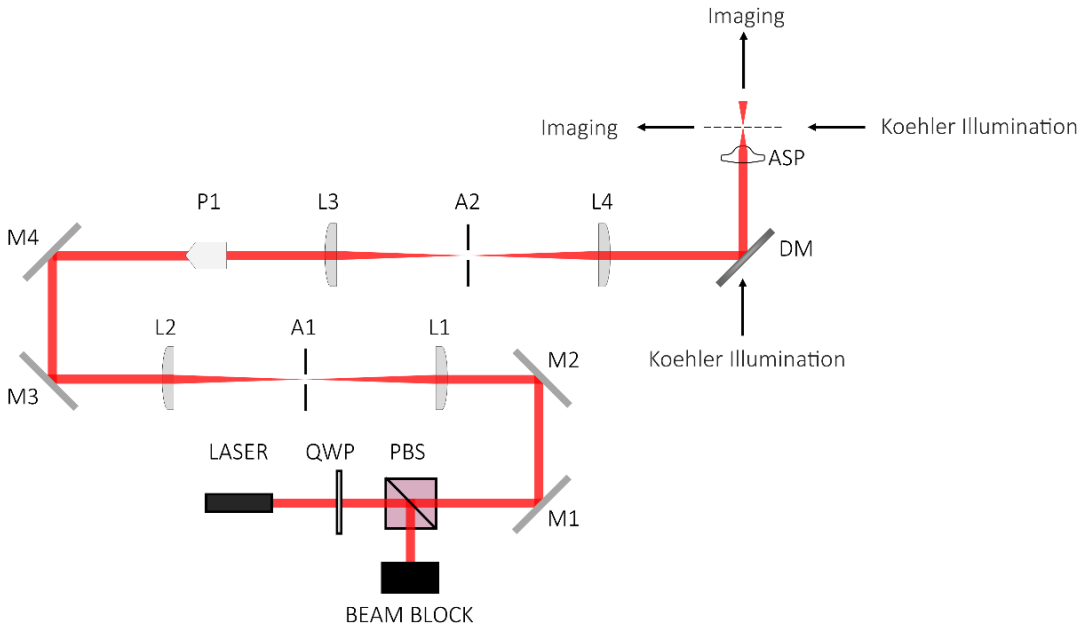

Figure 5-6. A similar system is used to that described in Figure 5-1. A Powell lens is placed in the beam path just over 150 mm back from L3 such that an image of the line produced by the Powell lens is relayed into the sample plane.

The Powell lens is mounted in a rotation mount in order to have fine control over the angle of the light sheet in the sample plane. The light sheet is oriented so that it is perpendicular to the channel walls. Imaging is provided by a 5X LWD objective (Mitutoyo) and a 20X objective (Comar) in the horizontal and vertical axes respectively, into identical CMOS cameras (DCC1545M, Thorlabs).

A sample of 7 and 10 μm polymer microspheres in distilled water is flowed into the (300x300) μm capillary at an average particle velocity of 25 μms^{-1} initially to test the efficacy of the light sheet. Laser power is gradually increased until vertical deflection of the particles is observed. As before, the system is driven at 4.34 MHz to give the second harmonic resonance in the capillary.

5.3.2 Results and discussion

Initial tests show that the light sheet performs poorly at deflecting particles into the upper acoustic streams. Although the power required to push the particles against the force of gravity is relatively low, the Stokes' drag is evidently larger than the gradient forces produced by the light sheet, and the particles are not held in the light sheet long enough to be deflected upwards. Increasing the laser power to strengthen the gradient force results in unwanted thermal effects, at laser powers of 1.4 W, due to heating of the fluid.

A trace of the particle trajectories is obtained using the St. Andrews Tracker[129], shown in Figure 5-7, to give a representation of the particle motion caused by the thermophoretic effects at this laser power. The beam width at the focus is approximately 2 μm using an aspheric lens of 0.25 NA. This also corresponds to the thermophoretic effects mentioned in Chapter 4.3. The exact direction of particle motion is also influenced by the direction of beam propagation[130]. These thermal effects cause a disruption to the intended particle trajectories and no particle sorting takes place. These effects should be minimised.

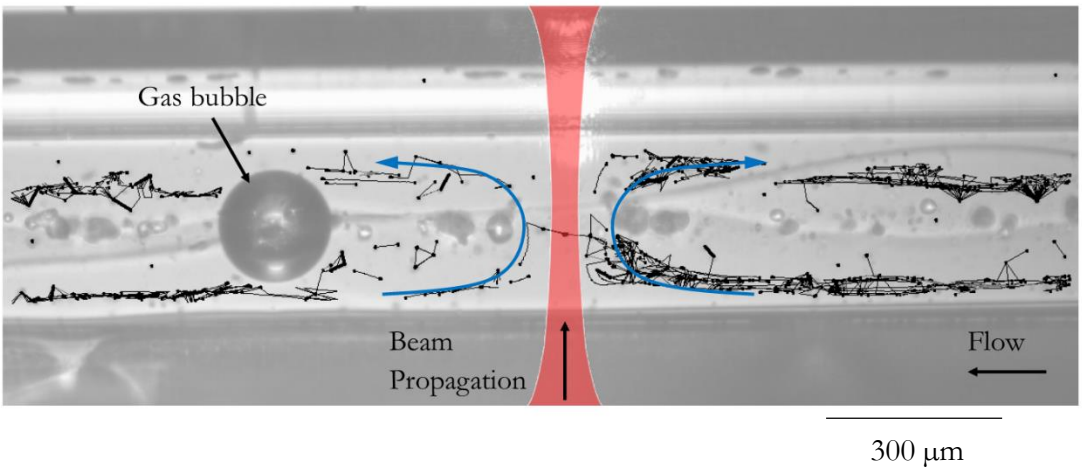

Figure 5-7. The particle motion due to the thermophoresis is represented by the black lines, with the general motion indicated by the blue arrows. Particles generally stay confined to the nodes of the acoustic field, however when they are close to the laser beam they follow the thermal current to the top of the channel, and then away from the laser beam despite the flow direction. A gas bubble is also observed from overheating of the fluid.

Another means of increasing the gradient forces in the focus of the light sheet, other than increasing the laser power, is to use a higher NA aspheric lens for focusing the light sheet. This produces a tighter focus, increasing the effect of the gradient force on the particles. To achieve this increase in gradient force, the 0.25 NA aspheric lens is replaced by a 0.4 NA aspheric (C110TME-C, Thorlabs).

In this configuration, an increase in the gradient force is observed by the resultant increase in vertical deflection of the particles, however the high laser powers required to achieve such deflection result in similar thermophoretic issues as experienced previously. The maximum laser power before thermal effects begin to dominate the flow is observed as 1.15 W.

One final change was made, swapping the 0.4 NA aspheric for a 0.68 NA aspheric lens (C330TME-C, Thorlabs), in order to further increase the stiffness of the trap, and hence increase the gradient force, and the experiment run again. With this configuration, a lower laser power is required to cause the overwhelming thermal effects, 0.8 W, while no reliable vertical deflection of the particles is observed. Gas bubbles caused by the heating of the fluid are also observed in this configuration.

Attempting to increase the gradient forces that the light sheet can exert on the particles in order to hold them against the fluid flow such that there was ample time for the optical radiation force to fractionate the particles has evidently introduced other caveats into the system. By decreasing the focal size of the light sheet, the energy density of laser applied to the sample is increased, facilitating heating of the fluid at lower laser powers. The local

thermal currents are often enough to disrupt the particle trajectory completely, however thermal currents are not the only issue.

Another effect of the local heating is that the speed of sound in the water will increase[131]. This causes the resonant frequency of the cavity to vary locally with the changes in temperature, in line with Equation 3.1. This local disruption of the acoustic field makes stable acoustic levitation and confinement very challenging. The presence of gas bubble formation is also a clear indicator that the sample is being overheated.

In collaboration with Alan McGuinn at Heriot Watt University, a model of the system is simulated in COMSOL to verify the observed effects. To reduce computational load, a 2D model of the capillary-transducer system is constructed, inputting the parameters required for producing the second harmonic across the capillary. The light sheet is modelled as a boundary heat source – a 1D vertical line in the centre of the capillary. Inputting a laser power of 800 mW, a value observed earlier to cause thermophoresis, the simulation is run, the results of which are shown in Figure 5-8.

The simulation, a decent approximation to our experimental conditions, gives a reasonable estimate of the observed particle trajectories.

The temperature plot shows temperatures up to 372 K, which would indicate boiling of the sample fluid. This can be correlated with the gas bubbles seen in the experiments, and gives another affirmation of the reliability of the simulation.

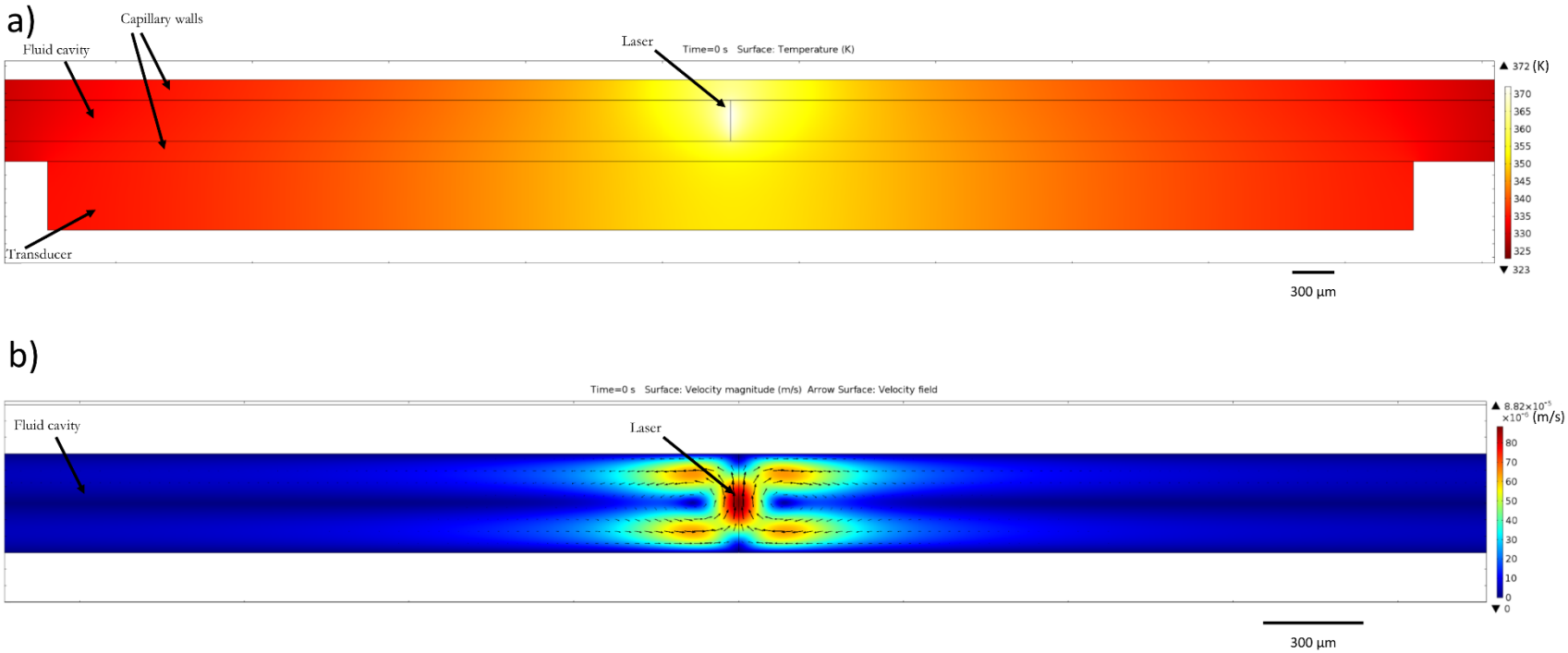

Figure 5-8. The top image a) shows the temperature dissipation throughout the fluid, capillary and transducer when a sheet of light is applied to the centre of the channel, similar to the light sheet system in Figure 5-6 with the system driven at the second harmonic. The resultant effect of the heating is shown in b), where the particle velocities are mapped, both as a colour gradient and as arrows. This model is in general agreement with the observed effects shown previously.

5.4 Discussion & conclusions

The first experiment in this chapter proved a success at sorting microspheres based on size, with an enrichment rate of 98.4% for 7 μm particles at a laser power of 112 mW. Due to the close proximity of the particles and the secondary acoustic forces, the observed recovery rate of the system is lower than is potentially possible. Utilising a method for focusing the particles into single file in the acoustic streams could help improve the recovery rate.

In an attempt to have the optical radiation force act across the width of the channel, a second experiment is designed. In this second radiation force experiment, it has become evident that it is in fact the optical gradient force that often acts as the limiting factor. Although the radiation forces present are capable of deflecting particles vertically, the laser power required to produce gradient forces that can hold particles against the Stokes drag can cause thermophoresis in the fluid. This is observed at decreasing laser powers for increasing the NA of the focusing aspheric lens, due to the subsequent increase in energy density from the laser. This heating effect is also observed in a simulation of the system in COMSOL. The use of two parallel single beams using an SLM, or the light sheet acting along the length of the channel instead are both viable configurations for further experimentation, however due to practical limitations in this case these methods were not attempted.

It is evident from these two configurations for displacing particles with the optical radiation force that minimal application of laser power to the fluid is desirable. However, overcoming these issues could lead to a sorting technique that is easily parallelised, and should be considered for future development.

The force balance between the optics and acoustics could also be exploited to sort between more than two particle species. This could be readily accommodated by increasing the harmonic mode of the system with respect to the acoustics, such that there are three or more acoustic streams to sort between in any one axis. This would allow, for example, separation of three or more particle species into discrete acoustic streams. The separation parameters are not limited to size however, and are only limited by the selective deflection by the optical and acoustic force balance. Deflection can also be introduced in multiple axes, facilitating movement of particles in the horizontal or vertical direction. With the wealth of possibilities in terms of resonant acoustic modes, and bi-axial optical manipulation made possible by the transparent transducer, development of this work has potential to lead to a truly multiplexed hybrid sorting method.

6 Discussions & Conclusion

The use of optical and acoustic forces in a hybrid system has presented a wealth of different configurations and modalities to contend with. The opposing yet complimentary nature of optical and acoustic manipulation has allowed for the investigation of some interesting hybrid separation techniques, and also more generally to investigate the optical and acoustic force balance in such arrangements. Focus has also been placed on the scalability of these techniques, with experimental designs considering how scale up could be achieved. This thesis has explored the manipulation of particles with acoustics, optics and hybrid methods.

6.1 Discussions

6.1.1 Acoustic manipulation

Chapter 3 detailed the reasoning and process for the microfluidic chips that are used throughout the thesis. The glass capillary offered a simple, cheap and disposable fluidic chamber, with good optical access and acoustic properties. The transparent LNO-ITO transducer allowed the chip to feature all planes of optical access, which is useful for combining optical techniques with the acoustic trapping functionality.

The bubble-bounded resonance that was demonstrated facilitates 3D acoustic trapping in a relatively simple capillary-transducer arrangement. The environment could be

considered as 'closed' when compared to some previous work on manipulation in small fluid volumes[117], and as such could benefit in situations where contamination is a potential issue. Such a configuration could be useful in aligning cells in a regular, 3D spacing prior to encapsulation.

The reliability of producing the bubble-bounded cavities could also be vastly improved by implementing a droplet control system such as that demonstrated by Neild *et al*[132], as shown in Figure 6-1. Their device use SAWs focused at the oil-water interface to inject controlled volumes of individual water droplets into the flow of oil. This type of control could equally be applied to delivering the appropriate fluid volume into the capillary such that longitudinal resonance can be assured.

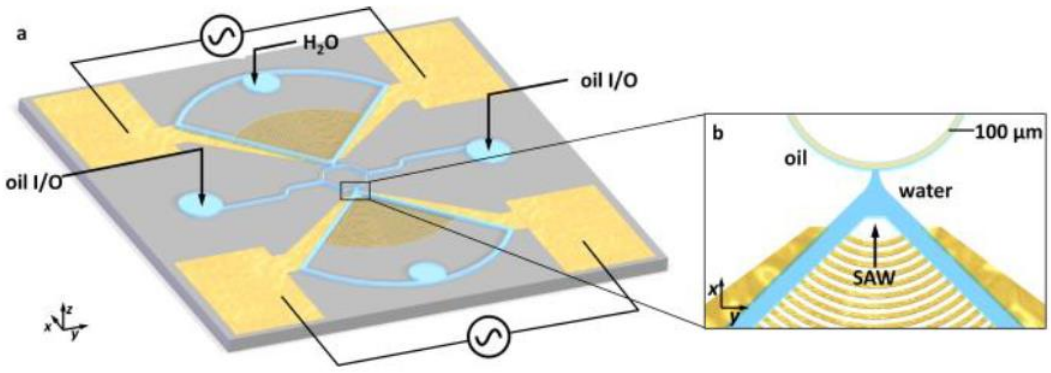

Figure 6-1. Focused SAWs inject water droplets into the flow of oil. This type of microfluidic control would be an ideal addition to the bubble-bounded resonance system as a means of controlling the volume of the fluid cavities. Image sourced from Neild *et al* [132]

As mentioned, another facet of this system is that one retains all planes of optical access, due to the transparency of the LNO-ITO transducer. This would enable the seamless integration of, for example, optical tweezers, further adding to the dexterity of the system.

Considering how acoustics could assist in cell sorting, it is proposed that a device such as ours could facilitate selective cell lysis. Although this runs contrary to much of the '*raison d'être*' of this thesis, it serves as a reminder of the practical transferability of such techniques to other applications. RBCs are bi-concave in shape, meaning that they will orient themselves to potential gradients in a different manner to, for example, WBCs which are spherical in nature. When subjected to a gradient, particles or cells will move or re-orient themselves such that they remain in a low potential energy state. MacDonald *et al* demonstrated this by sorting RBCs and WBCs based on the RBCs' preference to orient along the fringes of a potential energy landscape[1]. This same principle could be applied to an acoustic field, such that depending on the shape of the acoustic landscape, RBCs will orient themselves along a preferred axis, while other cells may not exhibit such behaviour. It is also known that RBCs are susceptible to damage from shear stresses, particularly in non-physiological conditions[133]. By tailoring a changing potential energy landscape, e.g. by rapidly scanning between two resonant acoustic frequencies, either using a single transducer or a bi-axial arrangement, it may be possible to provide enough shear stress on RBCs to lyse them, while leaving other cells intact.

This would also be possible in an optical field. Using the same principles, a sharp change in the optical gradient an RBC experiences could produce enough shear stress to induce lysis. Such a system could take the form of a tightly focused light sheet, acting across a large area to create a parallelised system. A hybrid system is also envisaged, whereby the acoustics could act to orient RBCs such that upon entering an optical field they are disproportionately affected when compared to other cells whose orientation may be less affected by a potential landscape.

6.1.2 Optical force balance

Initially, optical force balance was investigated with respect to particle manipulation in complex 3D potential energy landscapes in Chapter 4. Such landscapes can be formed by interfering multiple laser beams at the sample plane. This has been shown previously to great effect whilst also giving strong evidence for their use in red blood cell sorting[1], however the aim of this section was to study the feasibility of scaling up such a sorting technique, one aspect of which is to bring the sorting away from the surface.

Initially particle manipulation is carried out at the surface in order to provide the framework for developing the technique further. Separation of 2 and 5 μm particles is demonstrated as a model system, with results showing an 87% enrichment rate and 78% recovery rate of the 2 μm particles. By bringing sorting away from the surface and in multiple planes simultaneously, it is thought that enrichment, recovery rate and general throughput of such a device could be improved via the scaling up of sorting. The results are also subject to manual, subjective analysis, and as such would differ depending on how stringent the separation criteria is defined.

The results of the latter half of Chapter 4 are particularly interesting as they point towards a potential method for particle manipulation in an optical landscape away from the surface. There also exists a possibility here that particles could be sorted in multiple planes of potential wells simultaneously. This would be a logical next step in the development of such a system, as parallelisation of the sorting technique could greatly enhance the throughput of sorting, and potentially lead to a scalable, optical cell sorting method. Some developments have been made in this area, however there are not yet enough results to produce a full report.

Thermophoresis in the fluid volume was seen to have a large effect on particle motion within the capillaries. This was remedied by using a smaller capillary in the experiments, however this is something of a step backwards in terms of scale. The laser powers required to achieve volumetric sorting in the optical lattice, combined with the counter-propagating beam, may place a limit on the dimensions of the flow channel, and this would have to be taken into consideration in any future work.

Improvements in trapping stiffness could be made by using a higher NA trapping objective. The NA used in these experiments, 0.25, is considered very low in terms of optical tweezers. One benefit of using the low NA aspheric is the increase in area of effect of the optical landscape, coupled with the longer working distance which helped logistically. Higher NA objectives could be used, however one would have to consider the reduction in pattern size, logistical implementation, and the increase in energy density. The optical landscape itself would also become less uniform through the z axis as the horizontal planes of potential wells would be closer together, which may limit viability in large scale sorting.

It is clear from these conclusions that compromise is necessary when designing a system such as this, and one must choose carefully the parameters necessary to achieve an efficient, functional system.

However, achieving a stable force balance in a potential energy landscape does offer an opportunity to exploit the full potential of a powerful sorting modality. Such a system is envisaged that the full volumetric nature of the optical landscape is used for particle manipulation, leading to a large scale sorting method. Such claims have typically been reserved for inherently scalable techniques such as acoustophoresis or DEP, however achieving a similar effect with an optical configuration would greatly benefit in applications where other techniques may be less suited, for example with particulate of

low acoustic contrast or poor electrical specificity. Previous sorting work based on optical interference has reported sorting at rates of tens of particles per second[1]. By introducing sorting in multiple planes of a 3D optical landscape, such a device could feasibly reach processing speeds of hundreds of particles per second.

6.1.3 Optical and acoustic force balance

The hybridisation of optical and acoustic particle manipulation was explored in Chapter 5. Applying the two fields in parallel required the use of the microfluidic chips designed in Chapter 3, in order to have acoustic manipulation, optical deflection and two imaging axes in the one system.

This system enabled the hybrid force balanced separation of two species of microspheres based on size difference, given that smaller particles will experience a larger radiation force from a laser beam, while larger particles will experience a larger force from the acoustic field. The acoustic localisation of the particles streams is a very useful aspect of the system, and it also helped to improve homogeneity in the sample as particles are localised to similar positions in the velocity profile of the flow. The system could also benefit from having a branched outlet configuration, to achieve genuine sorting of the particle species with the acoustics guiding the separated particles to separate outlets.

One method proposed for improving the system is to have the optical radiation force act across the entire width of the channel, as this could affect all of the particles in the flow. This opens up the potential of hybrid particle separation in multiple acoustic streams

simultaneously. This method was implemented with the use of a light sheet, however issues with thermophoresis limited its application.

A future development may be to try the technique in a smaller capillary, as this has been shown previously in Chapter 4.3.3 to reduce the effects of thermophoresis. If these heating effects can be minimised, and some of the improvements outlined in Chapter 5.2.2 implemented, then this could prove to be an easily scalable technique with the benefits of both optics and acoustic present. Using the smaller 100 μm capillary with this technique would still require the use of a transducer, however, which as discussed in Chapter 3.2, involved challenges in the fabrication process. Improving the process of constructing our devices, by following some of the recommendations outlined in Chapter 3.4, could enable such a configuration.

Such hybrid designs have not yet been widely investigated for sorting applications, and as such there is no baseline for the throughput one might expect from this method. It is however prudent to compare to other passive techniques, and as such throughputs in the region of hundred(s) of particles per second should be sought.

In terms of applying this method to cell sorting, there are several parameters that would need to be taken in to consideration. The optical power required to deflect cells will invariably differ to that of a microsphere, and as such parameter finding will need to be undertaken to obtain a suitable optical power for cell deflection. Furthermore, the acoustic response and contrast of the cells will need to be taken in to account, with characterisation of these optical and acoustic responses vital for sorting in this hybrid system.

The reconfigurability of this technique lends itself well to further enhancements. Changes to the acoustic landscape and number of optical manipulation sites could drastically improve the technique such that the sorting of multiple particle species is a clear possibility. Each optical manipulation point could be dynamically reconfigured to give a multiplexed approach to sorting. One such application could be in sorting between cells at different stages in the differentiation cycle, for example in the differentiation cycle from stem cell to RBC. In our system, utilising the high selectivity of optics, the balance of optical and acoustic forces, and the potential bi-axial transducer arrangement is possible. As such, this type of multi-species sorting could be enhanced by offering improved selectivity over the sorting parameters while retaining the functionality for recovering the separated particle species at a branched outlet configuration.

6.2 Conclusion

The development of optical and acoustic methods for particle separation, with a focus on the potential for scale up of the techniques has led to some interesting developments in the force balance of such systems. Using a balance of forces - optical, acoustic or both - has been shown to provide some benefit to each method explored and has shown that a parallelisation of the particle handling in these methods could serve to increase that capacity of each system.

Further developments of these techniques could yield innovative particle handling methods that may find great use as large scale cell sorting methods, with the work presented in this thesis clearly exhibiting the potential for achieving this goal.

BIBLIOGRAPHY

1. MacDonald, M., Spalding, G. & Dholakia, K. Microfluidic sorting in an optical lattice. *Nature* **426,** 421–424 (2003).

2. Petersson, F., Nilsson, A., Holm, C., Jonsson, H. & Laurell, T. Continuous separation of lipid particles from erythrocytes by means of laminar flow and acoustic standing wave forces. *Lab Chip* **5,** 20–22 (2005).

3. Sun, Y. Y., Yuan, X. C., Ong, L. S., Bu, J., Zhu, S. W. & Liu, R. Large-scale optical traps on a chip for optical sorting. *Appl. Phys. Lett.* **90,** 7–10 (2007).

4. Kuo, S. C. & Sheetz, M. P. Force of single kinesin molecules measured with optical tweezers. *Science* **260,** 232–234 (1993).

5. Ashkin, A. Acceleration and trapping of particles by radiation pressure. *Phys. Rev. Lett.* **24,** 156–159 (1970).

6. Trinh, E. H. Compact acoustic levitation device for studies in fluid dynamics and material science in the laboratory and microgravity. *Rev. Sci. Instrum.* **56,** (1985).

7. Augustsson, P., Magnusson, C., Nordin, M., Lilja, H. & Laurell, T. Microfluidic, Label-Free Enrichment of Prostate Cancer Cells in Blood Based on Acoustophoresis. *Anal. Chem.* **84,** 7954–7962 (2012).

8. Jonás, A. & Zemánek, P. Light at work: the use of optical forces for particle manipulation, sorting, and analysis. *Electrophoresis* **29,** 4813–51 (2008).

9. Lenshof, A., Magnusson, C. & Laurell, T. Acoustofluidics 8: applications of acoustophoresis in continuous flow microsystems. *Lab Chip* **12,** 1210–23 (2012).

10. Radisic, M., Iyer, R. K. & Murthy, S. K. Micro- and nanotechnology in cell separation. *Int. J. Nanomedicine* **1,** 3–14 (2006).

11. Pethig, R. Dielectrophoresis: Status of the theory, technology, and applications. *Biomicrofluidics* **4,** 1–35 (2010).

12. Holmes, D., Whyte, G., Bailey, J., Vergara-irigaray, N., Ekpenyong, A., Guck, J., Duke, T. & Holmes, D. Separation of blood cells with differing deformability using deterministic lateral. (2014).

13. Gossett, D. R., Weaver, W. M., Mach, A. J., Hur, S. C., Tse, H. T. K., Lee, W., Amini, H. & Di Carlo, D. Label-free cell separation and sorting in microfluidic systems. *Anal. Bioanal. Chem.* **397,** 3249–67 (2010).

14. Herzenberg, L. a, Parks, D., Sahaf, B., Perez, O., Roederer, M. & Herzenberg, L. a. The history and future of the fluorescence activated cell sorter and flow cytometry: a view from Stanford. *Clin. Chem.* **48,** 1819–27 (2002).

15. Dholakia, K., MacDonald, M. P., Zemánek, P. & Cizmár, T. Cellular and colloidal separation using optical forces. *Methods Cell Biol.* **82,** 467–495 (2007).

16. Perry, P., Sauer, S., Billon, N., Richardson, W. D., Spivakov, M., Warnes, G., Livesey, F. J., Merkenschlager, M., Fisher, A. G. & Azuara, V. A dynamic switch in the replication timing of key regulator genes in embryonic stem cells upon neural induction. *Cell Cycle* **3,** 1645–1650 (2004).

17. Joyce, E., Al-Hashimi, a. & Mason, T. J. Assessing the effect of different ultrasonic frequencies on bacterial viability using flow cytometry. *J. Appl. Microbiol.* **110,** 862–870 (2011).

18. Hawkins, A. & Schmidt, H. *Handbook of Optofluidics*. (CRC Press, 2010).

19. Wu, T. H., Chen, Y., Park, S. Y., Hong, J., Teslaa, T., Zhong, J. F., Di Carlo, D., Teitell, M. a. & Chiou, P. Y. Pulsed laser triggered high speed microfluidic fluorescence activated cell sorter. *Proc. IEEE Int. Conf. Micro Electro Mech. Syst.* 1097–1100 (2012).

20. Wang, M. M., Tu, E., Raymond, D. E., Yang, J. M., Zhang, H., Hagen, N., Dees, B., Mercer, E. M., Forster, A. H., Kariv, I., Marchand, P. J. & Butler, W. F. Microfluidic sorting of mammalian cells by optical force switching. *Nat. Biotechnol.* **23,** 83–7 (2005).

21. Xia, N., Hunt, T. P., Mayers, B. T., Alsberg, E., Whitesides, G. M., Westervelt, R. M. & Ingber, D. E. Combined microfluidic-micromagnetic separation of living cells in continuous flow. *Biomed. Microdevices* **8,** 299–308 (2006).

22. Inglis, D. W., Riehn, R., Austin, R. H. & Sturm, J. C. Continuous microfluidic immunomagnetic cell separation. *Appl. Phys. Lett.* **85,** 5093–5095 (2004).

23. Klodell, C. T., Richardson, J. D., Bergamini, T. M. & Spain, D. A. Does Cell-Saver Blood Administration and Free Hemoglobin Load Cause Renal Dysfunction? *Am. Surg.* **67,** 44–47 (2001).

24. Mach, A. J., Kim, J. H., Arshi, A., Hur, S. C. & Di Carlo, D. Automated cellular sample preparation using a Centrifuge-on-a-Chip. *Lab Chip* **11,** 2827–2834 (2011).

25. Mohamed, H., McCurdy, L. D., Szarowski, D. H., Duva, S., Turner, J. N. & Caggana, M. Development of a rare cell fractionation device: Application for cancer detection. *IEEE Trans. Nanobioscience* **3,** 251–256 (2004).

26. Inglis, D. W. Efficient microfluidic particle separation arrays. *Appl. Phys. Lett.* **94,** 1–7 (2009).

27. Beech, J. P., Holm, S. H., Adolfsson, K. & Tegenfeldt, J. O. Sorting cells by size, shape and deformability. *Lab Chip* **12,** 1048 (2012).

28. Loutherback, K., D'Silva, J., Liu, L., Wu, A., Austin, R. H. & Sturm, J. C. Deterministic separation of cancer cells from blood at 10 mL/min. *AIP Adv.* **2,** 0–7 (2012).

29. Holm, S. H., Beech, J. P., Barrett, M. P. & Tegenfeldt, J. O. Separation of parasites from human blood using deterministic lateral displacement. *Lab Chip* **11,** 1326–1332 (2011).

30. Huang, R. & Barber, T. A microfluidics approach for the isolation of nucleated red blood cells (NRBCs) from the peripheral blood of pregnant women. *Prenat. Diagn.* 892–899 (2008).

31. Inglis, D. W., Herman, N. & Vesey, G. Highly accurate deterministic lateral displacement device and its application to purification of fungal spores. *Biomicrofluidics* **4,** 1–8 (2010).

32. Pohl, H. A. *Dielectrophoresis: the behavior of neutral matter in nonuniform electric fields*. (Cambridge University Press, 1978).

33. Gascoyne, P., Mahidol, C., Ruchirawat, M., Satayavivad, J., Watcharasit, P. & Becker, F. F. Microsample preparation by dielectrophoresis: isolation of malaria. *Lab Chip* **2,** 70–75 (2002).

34. Hu, X., Bessette, P. H., Qian, J., Meinhart, C. D., Daugherty, P. S. & Soh, H. T. Marker-specific sorting of rare cells using dielectrophoresis. *Proc. Natl. Acad. Sci. U. S. A.* **102,** 15757–61 (2005).

35. Imasaka, T., Kawabata, Y., Kaneta, T. & Ishidzu, Y. Optical Chromatography. *Anal. Chem.* **67,** 1763–1765 (1995).

36. Imasaka, T. Optical chromatography. A new tool for separation of particles. *Analusis* **26,** 53–53 (1998).

37. Terray, A., Taylor, J. D. & Hart, S. J. Cascade optical chromatography for sample fractionation. *Biomicrofluidics* **3,** 44106 (2009).

38. Korda, P. T., Taylor, M. B. & Grier, D. G. Kinetically Locked-In Colloidal Transport in an Array of Optical Tweezers. *Phys. Rev. Lett.* **89,** 128301 (2002).

39. Koss, B. A. & Grier, D. G. Optical peristalsis. *Appl. Phys. Lett.* **82,** 3985 (2003).

40. Petersson, F., Nilsson, A., Holm, C., Jonsson, H. & Laurell, T. Separation of lipids from blood utilizing ultrasonic standing waves in microfluidic channels. *Analyst* **129,** 938–943 (2004).

41. Jönsson, H., Holm, C., Nilsson, A., Petersson, F., Johnsson, P. & Laurell, T. Particle Separation Using Ultrasound Can Radically Reduce Embolic Load to Brain After Cardiac Surgery. *Ann. Thorac. Surg.* **78,** 1572–1577 (2004).

42. Kumar, M., Feke, D. L. & Belovich, J. M. Fractionation of cell mixtures using acoustic and laminar flow fields. *Biotechnol. Bioeng.* **89,** 129–137 (2005).

43. Thevoz, P., Adams, J. D., Shea, H., Bruus, H. & Soh, H. T. Acoustophoretic synchronization of mammalian cells in microchannels. *Anal. Chem.* **82,** 3094–3098 (2010).

44. Nichols, E. & Hull, G. The pressure due to radiation. *Proc. Am. Acad. Arts Sci.* **38,** 559–599 (1903).

45. Maxwell, J. *A treatise on electricity and magnetism*. (MacMillan & Co., 1881).

46. Ashkin, A. & Dziedzic, J. Optical levitation by radiation pressure. *Appl. Phys. Lett.* **19,** 19–21 (1971).

47. Ashkin, A., Dziedzic, J., Bjorkholm, J. . & Chu, S. Observation of a single-beam gradient-force optical trap for dielectric particles. *Opt. Lett.* **11,** 288–290 (1986).

48. Svoboda, K. & Block, S. M. Optical trapping of metallic Rayleigh particles. *Opt. Lett.* **19,** 930–932 (1994).

49. Burns, M. M., Fournier, J. M. & Golovchenko, J. A. Optical binding. *Phys. Rev. Lett.* **63,** 1233–1236 (1989).

50. Singer, W., Frick, M., Bernet, S. & Ritsch-Marte, M. Self-organized array of regularly spaced microbeads in a fiber-optical trap. *Journal of the Optical Society of America B* **20,** 1568 (2003).

51. Tatarkova, S. A., Carruthers, A. E. & Dholakia, K. One-dimensional optically bound arrays of microscopic particles. *Phys. Rev. Lett.* **89,** 283901 (2002).

52. McDougall, C., Stevenson, D. J., Brown, C. T. a, Gunn-Moore, F. & Dholakia, K. Targeted optical injection of gold nanoparticles into single mammalian cells. *J. Biophotonics* **2,** 736–743 (2009).

53. Ogura, Y., Kagawa, K. & Tanida, J. Optical manipulation of microscopic objects by means of vertical-cavity surface-emitting laser array sources. *Appl. Opt.* **40,** 5430–5435 (2001).

54. Sasaki, K., Koshioka, M., Misawa, H., Kitamura, N. & Masuhara, H. Laser-Scanning Micromanipulation and Spatial Patterning of Fine Particles. *Jpn. J. Appl. Phys.* **30,** L907 (1991).

55. Sasaki, K., Koshioka, M., Misawa, H., Kitamura, N. & Masuhara, H. Pattern formation and flow control of fine particles by laser-scanning micromanipulation. *Opt. Lett.* **16,** 1463–1465 (1991).

56. Vossen, D. L. J., van der Horst, A., Dogterom, M. & van Blaaderen, A. Optical tweezers and confocal microscopy for simultaneous three-dimensional manipulation and imaging in concentrated colloidal dispersions. *Rev. Sci. Instrum.* **75,** 2960 (2004).

57. Hoogenboom, J. P., Vossen, D. L. J., Faivre-Moskalenko, C., Dogterom, M. & Van Blaaderen, a. Patterning surfaces with colloidal particles using optical tweezers. *Appl. Phys. Lett.* **80,** 4828–4830 (2002).

58. Dufresne, E. R. & Grier, D. G. Optical tweezer arrays and optical substrates created with diffractive optics. *Rev. Sci. Instrum.* **69,** 1974 (1998).

59. Reicherter, M., Haist, T., Wagemann, E. U. & Tiziani, H. J. Optical particle trapping with computer-generated holograms written on a liquid-crystal display. *Opt. Lett.* **24,** 608–10 (1999).

60. Curtis, J., Koss, B. & Grier, D. G. Dynamic holographic optical tweezers. *Opt. Commun.* **207,** 169–175 (2002).

61. Vettenburg, T., Dalgarno, H. I. C., Nylk, J., Coll-Lladó, C., Ferrier, D. E. K., Čižmár, T., Gunn-Moore, F. J. & Dholakia, K. Light-sheet microscopy using an Airy beam. *Nat. Methods* **11,** 541–4 (2014).

62. Woerdemann, M., Alpmann, C., Esseling, M. & Denz, C. Advanced optical trapping by complex beam shaping. *Laser Photon. Rev.* **7,** 839–854 (2013).

63. Chapin, S. C., Germain, V. & Dufresne, E. R. Automated trapping, assembly, and sorting with holographic optical tweezers. *Opt. Express* **14,** 13095–13100 (2006).

64. Lee, S.-H. & Grier, D. G. Holographic microscopy of holographically trapped three-dimensional structures. *Opt. Express* **15,** 1505–1512 (2007).

65. Glückstad, J. Phase contrast image synthesis. *Opt. Commun.* **130,** 225–230 (1996).

66. Rodrigo, P. J., Perch-Nielsen, I. R. & Glückstad, J. Three-dimensional forces in GPC-based counterpropagating-beam traps. *Opt. Express* **14,** 5812–5822 (2006).

67. MacDonald, M. P., Neale, S. L., Paterson, L., Richies, A., Dholakia, K. & Spalding, G. C. Cell cytometry with a light touch: Sorting microscopic matter with an optical lattice. *J. Biol. Regul. Homeost. Agents* **18,** 200–205 (2004).

68. Jákl, P., Šiler, M. & Zemánek, P. Experimental analysis of multiple-beam interference optical traps. in *Proceedings of SPIE, 19th Polish-Slovak-Czech Optical Conference on Wave and Quantum Aspects of Contemporary Optics* **9441,** 944105 (2014).

69. Ashkin, A. & Dziedzic, J. Optical trapping and manipulation of viruses and bacteria. *Science (80-.).* **235,** 1517–1520 (1987).

70. Ashkin, A., Dziedzic, J. M. & Yamane, T. Optical trapping and manipulation of single cells using infrared laser beams. *Nature* **330,** 769–771 (1987).

71. Ashkin, A. & Dziedzic, J. M. Internal cell manipulation using infrared laser traps. *Proc. Natl. Acad. Sci.* **86,** 7914–8 (1989).

72. Neuman, K. C., Chadd, E. H., Liou, G. F., Bergman, K. & Block, S. M. Characterization of photodamage to Escherichia coli in optical traps. *Biophys. J.* **77,** 2856–2863 (1999).

73. de Oliveira, M. a. S., Smith, Z. J., Knorr, F., de Araujo, R. E. & Wachsmann-Hogiu, S. Long term Raman spectral study of power-dependent photodamage in red blood cells. *Appl. Phys. Lett.* **104,** 103702 (2014).

74. Kuo, S. C., Gelles, J., Steuer, E. & Sheetz, M. P. A model for kinesin movement from nanometer-level movements of kinesin and cytoplasmic dynein and force measurements. *J. Cell Sci. Suppl.* **14,** 135–138 (1991).

75. Gosse, C. & Croquette, V. Magnetic tweezers: micromanipulation and force measurement at the molecular level. *Biophys. J.* **82,** 3314–3329 (2002).

76. Fällman, E., Schedin, S., Jass, J., Andersson, M., Uhlin, B. E. & Axner, O. Optical tweezers based force measurement system for quantitating binding interactions: System design and application for the study of bacterial adhesion. *Biosens. Bioelectron.* **19,** 1429–1437 (2004).

77. Nishizaka, T., Miyata, H., Yoshikawa, H., Ishiwata, S. & Kinosita, K. Unbinding force of a single motor molecule of muscle measured using optical tweezers. *Nature* **377,** 251–254 (1995).

78. Wang, M. D., Yin, H., Landick, R., Gelles, J. & Block, S. M. Stretching DNA with optical tweezers. *Biophys. J.* **72,** 1335–46 (1997).

79. Felgner, H., Frank, R. & Schliwa, M. Flexural rigidity of microtubules measured with the use of optical tweezers. *J. Cell Sci.* **109,** 509–516 (1996).

80. Kundt & Lehman. Longitudinal vibrations and acoustic figures in cylindrical columns of liquids. *Ann. Phys. Chem.* **153,** (1874).

81. Rayleigh, Lord. On the pressure of vibrations. *London, Edinburgh, Dublin Philos. Mag. J. Sci.* **3,** 338–346 (1902).

82. King, L. On the acoustic radiation pressure on spheres. *Proc. R. Soc. Lond. A* **147,** 212–240 (1934).

83. Gor'kov, L. On the forces acting on a small particle in an acoustical field in an ideal fluid. *Sov. Phys. Dokl.* **6,** 773 (1962).

84. Doinikov, A. On the radiation pressure on small spheres. *J. Acoust. Soc. Am.* **100,** 1231 (1996).

85. Glynne-Jones, P., Démoré, C. E. M., Ye, C., Qiu, Y., Cochran, S. & Hill, M. Array-controlled ultrasonic manipulation of particles in planar acoustic resonator. *IEEE Trans. Ultrason. Ferroelectr. Freq. Control* **59,** 1258–1266 (2012).

86. Bjerknes, V. Fields of Force. *Colomb. Univ. Press. New York* (1906).

87. Barnkob, R., Augustsson, P., Laurell, T. & Bruus, H. An automated full-chip micro-PIV setup for measuring microchannel acoustophoresis: Simultaneous determination of forces from acoustic radiation and acoustic streaming. *Proc. MicroTAS 2010* 1247–1249 (2010).

88. Welter, E. & Neidhart, B. Acoustically levitated droplets—a new tool for micro and trace analysis. *Fresenius. J. Anal. Chem.* **357,** 345–350 (1997).

89. Santesson, S. & Nilsson, S. Airborne chemistry: acoustic levitation in chemical analysis. *Anal. Bioanal. Chem.* **378,** 1704–9 (2004).

90. Priego-Capote, F. & de Castro, L. Ultrasound-assisted levitation: Lab-on-a-drop. *TrAC Trends Anal. Chem.* **25,** 856–867 (2006).

91. Hultström, J., Manneberg, O., Dopf, K., Hertz, H. M., Brismar, H. & Wiklund, M. Proliferation and viability of adherent cells manipulated by standing-wave ultrasound in a microfluidic chip. *Ultrasound Med. Biol.* **33,** 145–151 (2007).

92. Vanherberghen, B., Manneberg, O., Christakou, A., Frisk, T., Ohlin, M., Hertz, H. M., Onfelt, B. & Wiklund, M. Ultrasound-controlled cell aggregation in a multi-well chip. *Lab Chip* **10,** 2727–2732 (2010).

93. Christakou, A. E., Ohlin, M., Vanherberghen, B., Khorshidi, M. A., Kadri, N., Frisk, T., Wiklund, M. & Onfelt, B. Live cell imaging in a micro-array of acoustic traps facilitates quantification of natural killer cell heterogeneity. *Integr. Biol.* **5,** 712–719 (2013).

94. Bazou, D., Coakley, W. T., Hayes, a. J. & Jackson, S. K. Long-term viability and proliferation of alginate-encapsulated 3-D HepG2 aggregates formed in an ultrasound trap. *Toxicol. Vitr.* **22,** 1321–1331 (2008).

95. Liu, J., Kuznetsova, L. a., Edwards, G. O., Xu, J., Ma, M., Purcell, W. M., Jackson, S. K. & Coakley, W. T. Functional three-dimensional HepG2 aggregate cultures generated from an ultrasound trap: Comparison with HepG2 spheroids. *J. Cell. Biochem.* **102,** 1180–1189 (2007).

96. Demore, C., Qiu, Y., Cochran, S., Glynne-Jones, P., Ye, C. & Hill, M. Transducer arrays for ultrasonic particle manipulation. *Proc. - IEEE Ultrason. Symp.* 412–415 (2010).

97. Oberti, S., Neild, A., Quach, R. & Dual, J. The use of acoustic radiation forces to position particles within fluid droplets. *Ultrasonics* **49,** 47–52 (2009).

98. Sitters, G., Kamsma, D., Thalhammer, G., Ritsch-Marte, M., Peterman, E. J. G. & Wuite, G. J. L. Acoustic force spectroscopy. *Nat. Methods* (2015).

99. Brodie, G. W. J., Qiu, Y., Cochran, S., Spalding, G. C. & MacDonald, M. P. Optically transparent piezoelectric transducer for ultrasonic particle manipulation. *IEEE Trans. Ultrason. Ferroelectr. Freq. Control* **61,** 389–91 (2014).

100. Chiou, P. Y., Ohta, A. T. & Wu, M. C. Massively parallel manipulation of single cells and microparticles using optical images. *Nature* **436,** 370–2 (2005).

101. Huang, S. Bin, Chen, J., Wang, J., Yang, C. L. & Wu, M. H. A new optically-induced dielectrophoretic (ODEP) force-based scheme for effective cell sorting. *Int. J. Electrochem. Sci.* **7,** 12656–12667 (2012).

102. Kremer, C., Witte, C., Neale, S. L., Reboud, J., Barrett, M. P. & Cooper, J. M. Shape-dependent optoelectronic cell lysis. *Angew. Chemie - Int. Ed.* **53,** 842–846 (2014).

103. Witte, C., Kremer, C., Cooper, J. M. & Neale, S. L. Continuous cell lysis in microfluidics through acoustic and optoelectronic tweezers. *SPIE Photonics West MOEMS-MEMS* 2–7 (2014).

104. Neale, S. L., Witte, C., Bourquin, Y., Kremer, C., Menachery, A., Zhang, Y., Wilson, R., Reboud, J. & Cooper, J. M. New optical, acoustic, and electrical diagnostics for the developing world. in *Proceedings of the SPIE: The International Society for Optical Engineering* **8251,** 1–10 (2012).

105. Thalhammer, G., Steiger, R., Meinschad, M., Hill, M., Bernet, S. & Ritsch-Marte, M. Combined acoustic and optical trapping. *Biomed. Opt. Express* **2,** 2859–70 (2011).

106. Hammarstrom, B., Evander, M., Barbeau, H., Bruzelius, M., Larsson, J., Laurell, T. & Nilsson, J. Non-contact acoustic cell trapping in disposable glass capillaries. *Lab Chip* **10,** 2251–2257 (2010).

107. Utoh, J. & Harasaki, H. Damage to erythrocytes from long-term heat stress. *Clin. Sci. (Lond).* **82,** 9–11 (1992).

108. Franke, T., Braunmüller, S., Schmid, L., Wixforth, a & Weitz, D. a. Surface acoustic wave actuated cell sorting (SAWACS). *Lab Chip* **10,** 789–94 (2010).

109. Ding, X., Lin, S.-C. S., Lapsley, M. I., Li, S., Guo, X., Chan, C. Y., Chiang, I.-K., Wang, L., McCoy, J. P. & Huang, T. J. Standing surface acoustic wave (SSAW) based multichannel cell sorting. *Lab Chip* **12,** 4228–4231 (2012).

110. Dykes, J., Lenshof, A., Åstrand-Grundström, I.-B., Laurell, T. & Scheding, S. Efficient removal of platelets from peripheral blood progenitor cell products using a novel micro-chip based acoustophoretic platform. *PLoS One* **6,** e23074 (2011).

111. Laurell, T., Petersson, F. & Nilsson, A. Chip integrated strategies for acoustic separation and manipulation of cells and particles. *Chem. Soc. Rev.* **36,** 492–506 (2007).

112. Shi, J., Ahmed, D., Mao, X., Lin, S.-C. S., Lawit, A. & Huang, T. J. Acoustic tweezers: patterning cells and microparticles using standing surface acoustic waves (SSAW). *Lab Chip* **9,** 2890–2895 (2009).

113. Doblhoff-Dier, O., Gaida, T., Katinger, H., Burger, W., Gröschl, M. & Benes, E. A novel ultrasonic resonance field device for the retention of animal cells. *Biotechnol. Prog.* **10,** 428–32 (1994).

114. Grösch, M., Burger, W., Handl, B., Doblhoff-Dier, O., Gaida, T. & Schmatz, C. Ultrasonic Separation of Suspended Particles - Part III: Application in Biotechnology. *Acta Acust. united with Acust.* **84,** 815–822 (1998).

115. Castilho, L. R. & Medronho, R. A. in *Tools and Applications of Biochemical Engineering Science* 129–169 (Springer Berlin Heidelberg, 2002).

116. Araz, M. K. & Lal, A. Frequency Addressable Acoustic Collection , Separation and Mixing in a Pzt Driven Glass Capillary Microfluidic Actuator. in *14th International Conference on Miniaturized Systems for Chemistry and Life Sciences* 1919–1921 (2010).

117. Pierre, Z. N., Field, C. R. & Scheeline, A. Sample handling and chemical kinetics in an acoustically levitated drop microreactor. *Anal. Chem.* **81,** 8496–8502 (2009).

118. Cecchini, M., Girardo, S., Pisignano, D., Cingolani, R. & Beltram, F. Acoustic-counterflow microfluidics by surface acoustic waves. *Appl. Phys. Lett.* **92,** (2008).

119. Yeo, L. Y. & Friend, J. R. Ultrafast microfluidics using surface acoustic waves. *Biomicrofluidics* **3,** (2009).

120. Taly, V., Kelly, B. T. & Griffiths, A. D. Droplets as microreactors for high-throughput biology. *ChemBioChem* **8,** 263–272 (2007).

121. Glynne-Jones, P., Boltryk, R. J. & Hill, M. Acoustofluidics 9: Modelling and applications of planar resonant devices for acoustic particle manipulation. *Lab Chip* **12,** 1417–26 (2012).

122. Gherardini, L., Cousins, C. M., Hawkes, J. J., Spengler, J., Radel, S., Lawler, H., Devcic-Kuhar, B., Gröschl, M., Coakley, W. T. & McLoughlin, A. J. A new immobilisation method to arrange particles in a gel matrix by ultrasound standing waves. *Ultrasound Med. Biol.* **31,** 261–272 (2005).

123. Milne, G., Rhodes, D., MacDonald, M. & Dholakia, K. Fractionation of polydisperse colloid with acousto-optically generated potential energy landscapes. *Opt. Lett.* **32,** 1144–6 (2007).

124. Smith, R. L., Spalding, G. C., Dholakia, K. & MacDonald, M. P. Colloidal sorting in dynamic optical lattices. *J. Opt. A Pure Appl. Opt.* **9,** S134–S138 (2007).

125. Casaburi, a., Pesce, G., Zemánek, P. & Sasso, a. Two- and three-beam interferometric optical tweezers. *Opt. Commun.* **251,** 393–404 (2005).

126. Paterson, L., Papagiakoumou, E., Milne, G., Garcés-Chávez, V., Tatarkova, S. a., Sibbett, W., Gunn-Moore, F. J., Bryant, P. E., Riches, a. C. & Dholakia, K. Light-induced cell separation in a tailored optical landscape. *Appl. Phys. Lett.* **87,** 123901 (2005).

127. Laserline Optics Canada, X. Powell Lens - Accessed on 30/05/15. (2015). at <http://laserlineoptics.com/powell_primer.html>

128. Yang, Z. Optical and acoustic beam shaping for imaging and manipulation. (University of Dundee, 2015).

129. Milne, G. Optical Sorting and Manipulation of Microscopic Particles. (University of St. Andrews, 2007).

130. Duhr, S., Arduini, S. & Braun, D. Thermophoresis of DNA determined by microfluidic fluorescence. *Eur. Phys. J. E* **15,** 277–286 (2004).

131. Tschiegg, C. E. Tables of the Speed of Sound in Water. *J. Acoust. Soc. Am.* **31,** 75–76 (1958).

132. Neild, A., Collins, D. J., Sesen, M. & Alan, T. On-Chip Biochemistry : Droplet Generation and Control. in *19th Australian Fluid Mechanics Conference* (2014).

133. Baskurt, O. Red Blood Cell Mechanical Stability. in *2012 world Congress on Engineering and Technology* **2012,** 8–10 (2012).

APPENDIX A

Presented here are the temperature measurements described in Chapter 3.2.3. The raw data is presented, alongside the adjusted values and error margins.

For the frequency = 2.15 MHz;

Voltage (Vpp)	Temperature readings (°C)						
	T1	T2	T3	T4	T5	Tamb	Tcam
2	19.2	19.3	18.9	18.9	19.2	18.6	20.8
4	19.5	19.4	19	19	19.3	18.6	21.2
6	19.8	19.8	19.3	19.4	19.7	18.7	21.4
8	20.3	20.4	19.7	19.9	20.1	18.7	22.7
10	20.7	20.8	19.7	20.1	20.4	18.7	22.9
12	21.3	21.3	20.1	20.7	20.9	18.8	23.6
14	22.3	22.6	20.8	21.5	21.9	18.9	24.2
16	23.4	23.7	21.5	22.4	22.6	18.9	26.5
18	24.5	24.9	21.8	23.1	23.6	19	27.9
20	25.8	26.3	22.3	23.6	24.5	18.9	29.2

Table A-1. Raw temperature data recorded from thermocouples and thermal camera

Voltage (Vpp)	Estimated Surface temperature change (°C)					
	T1	T2	T3	T4	T5	Tamb
2	1.9	2.2	0.9	0.9	1.9	0
4	2.9	2.6	1.3	1.3	2.3	0
6	2.7	2.7	1.5	1.7	2.5	0
8	3.8	4.0	2.4	2.8	3.3	0
10	4.0	4.2	2.0	2.8	3.4	0
12	4.8	4.8	2.5	3.6	4.0	0
14	4.9	5.3	2.7	3.7	4.3	0
16	7.1	7.6	4.1	5.5	5.9	0
18	8.3	8.9	4.2	6.2	6.9	0
20	9.6	10.3	4.7	6.5	7.8	0

Table A-2. Estimated surface change in temperature, adjusted to ambient and thermal camera values

Voltage (Vpp)	Adjusted error values (±°C)					
	T1	T2	T3	T4	T5	Tamb
2	0.05	0.06	0.02	0.02	0.05	0.00
4	0.08	0.07	0.03	0.03	0.06	0.00
6	0.07	0.07	0.04	0.04	0.06	0.00
8	0.09	0.10	0.06	0.07	0.08	0.00
10	0.10	0.10	0.05	0.07	0.08	0.00
12	0.11	0.11	0.06	0.09	0.10	0.00
14	0.11	0.12	0.07	0.09	0.10	0.00
16	0.15	0.16	0.10	0.12	0.13	0.00
18	0.17	0.18	0.10	0.13	0.15	0.00
20	0.19	0.20	0.11	0.14	0.16	0.00

Table A-3. Adjusted error margins for each reading

For the frequency = 6.495 MHz;

Voltage (Vpp)	Temperature readings (°C)						
	T1	T2	T3	T4	T5	Tamb	Tcam
2	19.5	19.5	19.3	19.1	19.4	19	21.2
4	19.5	19.6	19.4	19.4	19.5	19	21.6
6	19.6	19.7	19.5	19.5	19.6	19.1	21.8
8	19.7	19.8	19.5	19.5	19.7	19.1	21.8
10	19.9	20	19.5	19.6	19.8	19.2	21.8
12	20.2	20.3	19.7	19.8	20	19.2	22
14	20.4	20.5	19.8	19.9	20.2	19.2	22.2
16	20.8	21	19.9	20.1	20.3	19.2	22.6
18	21.2	21.3	20.1	20.4	20.5	19.2	23
20	21.7	21.9	20.3	20.6	20.8	19.2	23.5

Table A-4. Raw temperature data recorded from thermocouples and thermal camera

Voltage (Vpp)	Estimated Surface temperature change (°C)					
	T1	T2	T3	T4	T5	Tamb
2	2.2	2.2	1.3	0.4	1.8	0
4	2.2	2.6	1.7	1.7	2.2	0
6	2.3	2.7	1.8	1.8	2.3	0
8	2.3	2.7	1.5	1.5	2.3	0
10	2.3	2.6	1.0	1.3	2.0	0
12	2.5	2.8	1.3	1.5	2.0	0
14	2.8	3.0	1.4	1.6	2.3	0
16	3.0	3.4	1.3	1.7	2.1	0
18	3.6	3.8	1.6	2.2	2.4	0
20	4.0	4.3	1.8	2.2	2.5	0

Table A-5. Estimated surface change in temperature, adjusted to ambient and thermal camera values

Voltage (Vpp)	Adjusted error values (±°C)					
	T1	T2	T3	T4	T5	Tamb
2	0.06	0.06	0.03	0.01	0.05	0.00
4	0.06	0.07	0.04	0.04	0.06	0.00
6	0.06	0.07	0.05	0.05	0.06	0.00
8	0.06	0.07	0.04	0.04	0.06	0.00
10	0.06	0.07	0.03	0.03	0.05	0.00
12	0.06	0.07	0.03	0.04	0.05	0.00
14	0.07	0.07	0.03	0.04	0.06	0.00
16	0.07	0.08	0.03	0.04	0.05	0.00
18	0.09	0.09	0.04	0.05	0.06	0.00
20	0.09	0.10	0.04	0.05	0.06	0.00

Table A-6. Adjusted error margins for each reading

APPENDIX B

Particle count data for the experiment described in Chapter 4.2. Particles were counted manually, and the enrichment rate of 2 μm microspheres is presented in terms of applied laser power;

Laser Power	130mW	
Particle size	2μm	5μm
Sorted	152	0
Un-Sorted	912	179
Deflection %	14%	0%
Enrichment	**100%**	

Laser Power	210mW	
Particle size	2μm	5μm
Sorted	637	28
Un-Sorted	175	206
Deflection %	78%	12%
Enrichment	**87%**	

Laser Power	150mW	
Particle size	2μm	5μm
Sorted	252	2
Un-Sorted	732	211
Deflection %	26%	1%
Enrichment	**96%**	

Laser Power	230mW	
Particle size	2μm	5μm
Sorted	962	80
Un-Sorted	126	198
Deflection %	88%	29%
Enrichment	**75%**	

Laser Power	170mW	
Particle size	2μm	5μm
Sorted	496	20
Un-Sorted	416	266
Deflection %	54%	7%
Enrichment	**89%**	

Laser Power	250mW	
Particle size	2μm	5μm
Sorted	1162	236
Un-Sorted	98	56
Deflection %	92%	81%
Enrichment	**53%**	

Laser Power	190mW	
Particle size	2μm	5μm
Sorted	651	30
Un-Sorted	266	251
Deflection %	71%	11%
Enrichment	**87%**	

Laser Power	270mW	
Particle size	2μm	5μm
Sorted	1462	182
Un-Sorted	119	15
Deflection %	92%	92%
Enrichment	**50%**	

Table B-1. Raw particle numbers, categorised by applied laser power

APPENDIX C

Particle count data for the experiment described in Chapter 5.2. The particles were counted manually, and the enrichment rate of 7 μm microspheres is presented in terms of applied laser power with standard deviations;

Laser Power	93mW						
Particle size	7μm				10μm		
Run	Sorted	Unsorted	Deflection		Sorted	Unsorted	Deflection
1	0	357	0%		0	101	0%
2	0	347	0%		0	89	0%
3	0	617	0%		0	116	0%
4	0	319	0%		0	79	0%
5	0	284	0%		0	31	0%
6	0	308	0%		0	32	0%
Total	**0**	**2232**	**0%**		**0**	**448**	**0%**
Enrichment	0%						
SD	0.00				0.00		

Table C-1. Particle count data for applied laser power of 93 mW

Laser Power	112mW						
Particle size	7μm				10μm		
Run	Sorted	Unsorted	Deflection		Sorted	Unsorted	Deflection
1	161	89	64%		0	37	0%
2	180	108	63%		0	23	0%
3	161	79	67%		0	19	0%
4	121	83	59%		1	40	2%
5	145	74	66%		0	36	0%
6	110	74	60%		1	25	4%
Total	**878**	**507**	**63%**		**2**	**180**	**1%**
Enrichment	98.3%						
SD	2.97				1.86		

Table C-2. Particle count data for applied laser power of 112 mW

Laser Power	131mW						
Particle size	7µm				10µm		
Run	Sorted	Unsorted	Deflection		Sorted	Unsorted	Deflection
1	130	46	74%		20	19	51%
2	146	50	74%		35	22	61%
3	135	71	66%		20	15	57%
4	55	19	74%		29	20	59%
5	131	50	72%		27	18	60%
6	228	70	77%		65	40	62%
Total	**825**	**306**	**73%**		**196**	**134**	**59%**
Enrichment	55.4%						
SD	3.92				2.12		

Table C-3. Particle count data for applied laser power of 131 mW

Laser Power	161mW						
Particle size	7µm				10µm		
Run	Sorted	Unsorted	Deflection		Sorted	Unsorted	Deflection
1	246	22	92%		65	13	83%
2	63	6	91%		18	3	86%
3	144	12	92%		30	3	91%
4	65	7	90%		13	1	93%
5	96	9	91%		19	4	83%
6	310	45	87%		101	30	77%
Total	**924**	**101**	**90%**		**246**	**54**	**82%**
Enrichment	52.3%						
SD	2.18				6.14		

Table C-4. Particle count data for applied laser power of 161 mW

Laser Power	184mW						
Particle size	7µm				10µm		
Run	Sorted	Unsorted	Deflection		Sorted	Unsorted	Deflection
1	149	6	96%		31	5	86%
2	65	4	94%		20	2	91%
3	65	1	98%		14	0	100%
4	56	2	97%		21	1	95%
5	124	7	95%		25	3	89%
6	191	21	90%		56	3	95%
Total	**650**	**41**	**94%**		**167**	**14**	**92%**
Enrichment	50.5%						
SD	2.77				4.45		

Table C-5. Particle count data for applied laser power of 184 mW